RETRIEVAL OF PARAMETERS IN HEAT TRANSFER PROBLEMS INVOLVING THERMAL RADIATION

A Thesis Submitted in

Partial Fulfillment of the Requirements

for the Degree of

DOCTOR OF PHILOSOPHY

By

RANJAN DAS

DEPARTMENT OF MECHANICAL ENGINEERING

INDIAN INSTITUTE OF TECHNOLOGY GUWAHATI

OCTOBER 2009

CERTIFICATE

It is certified that the work contained in this thesis entitled **Retrieval of Parameters in Heat Transfer Problems Involving Thermal Radiation** by Ranjan Das, a student of the Department of Mechanical Engineering, Indian Institute of Technology Guwahati, India, for the award of the degree of Doctor of Philosophy has been carried out under our supervision and that this work has not been submitted elsewhere for a degree.

Dr. Subhash C. Mishra
Professor
Department of Mechanical Engineering
Indian Institute of Technology Guwahati
Assam, India
October 2009

Dr. Ramagopal V.S. Uppaluri
Associate Professor
Department of Chemical Engineering
Indian Institute of Technology Guwahati
Assam, India
October 2009

Acknowledgements

A Ph.D. is not merely study of books, articles and submitting a document. It teaches a method of living, communicating with people, building a team work and management of people, time, resources and many more. It essentially involves a process of transformation of ideas to a conclusive result. Apart from hard work, it requires an effective guidance and a platform to share ideas with many people.

First of all, I would like to express my deepest gratitude to my thesis supervisors, Dr. Subhash C. Mishra and Dr. Ramagopal Uppaluri, for their extraordinary guidance, inspiration and continuous encouragement even at the toughest times of my Ph.D. work. I feel proud to remain associated with them during the Ph.D. program which will certainly help me in a long run to make my life more sound and blissful. As far as the successful completion of the present thesis is concerned, the continuous care, attention, and constructive suggestions given by my supervisors starting right from the formulation of the problem to the final interpretations of the results could made it possible to transform the idea into a reality. To describe their contributions with in such a limited space is next to impossible.

I also express my sincere gratitude to my doctoral committee members: Dr. U.K. Saha, Dr. P. Muthukumar, Dr. A. Singh and Dr. T. Banerjee for providing constructive suggestions to improve the quality of the work and rectifying several errors. Apart from improvement in my communication, their suggestions immensely helped me to enhance my technical skill. I also take this opportunity to thank other faculty members of the Department of Mechanical Engineering for their blessings, encouragement and support.

I am thankful to all staff members of IIT Guwahati who helped me in different ways whenever I had any problem. I specially thank Mr. Amal Kalita for providing me with a very healthy environment in the CAD lab, printer facility and also maintaining other accessories in a very good condition. I also specially thank my seniors Dr. Bittagopal Mondal (Bitta) and Dr. R. Muthukumaran (Muthu), my batchmates Mr. A. Satheesh, Mr. C. Subramanian and my close friends in particular Mr. Vijay Pantangi, Mr. R.P. Chopade, Mr. T. Pavankumar, Mr. M. Ajith, and Mr. D.A. Perumal to have given me a nice company to live in and share my happiness and sorrow.

Last but not the least, I am indebted to my parents and the Almighty whose blessings and moral support have given me the power and helped me to move ahead continuously.

Ranjan Das

October 2009

Synopsis

In the design and analysis of engineering devices, it is essential to have the knowledge of medium properties, initial and/or boundary conditions that yield the desired information which could either be stress/strain fields in a machine element or any of one or more among the velocity, the pressure, the temperature and the heat flux fields in fluid mechanics and heat transfer problems. Depending upon the situation, with known information about the stress/strain/velocity/pressure/temperature field, unknown medium properties and/or initial and boundary conditions need to be retrieved. Problems of such kind fall under the purview of inverse problems. Unlike direct problems whose solutions proceed with known medium properties and initial and/or boundary conditions and thus their solution methods are well established, the analysis of inverse problems are relatively difficult. Inverse problems are ill-posed, and apart from the methods employed in the direct methods, they invariably require a tool for regularization and optimization.

Analyses of inverse problems become essential in the estimation of the medium properties or boundary conditions. In many heat transfer problems, temperature and/or heat flux distributions are known from experiments. However, one or more of the medium properties and/or one or more of the boundary conditions that yield, for example, the desired temperature distribution, remain unknown. The number of unknown parameters to be retrieved depends upon the complexity of the problem. In case of heat transfer problems involving thermal radiation, because of the volumetric nature of radiation, many combinations of parameters need to be retrieved, and thus owing to an increased complexity, they require an efficient solution algorithm.

Heat transfer problems involving volumetric radiation find extensive applications in the thermal analysis of boilers and furnaces, radiant heaters, insulation systems, phase change of semitransparent materials, radiation budget in atmospheric science, medium characterization, etc. Because of the unknown medium properties or the boundary conditions, many such problems require an inverse analysis, and due to the ill-posed nature of the problem, the quality of the estimated unknown parameters depends upon the methods employed in the inverse analysis. From an extensive literature review, it has been observed that many aspects of the inverse transient heat transfer problems involving thermal radiation have not been investigated in detail.

In the recent past, the lattice Boltzmann method (LBM) has gained a considerable momentum in the analysis of a wide range of fluid flow and heat transfer problems. Recently, its application has also been extended to study heat transfer problems involving thermal radiation. However, as far as its usage in the inverse problems is concerned, no work has been reported so far. The finite volume method (FVM) is an elegant method for the computation of the volumetric radiation. Unlike other computational methods, it is less prone to ray effect and is compatible to different solvers that compute other information in fluid flow and heat transfer problems. The genetic algorithm (GA) is a stochastic approach and it works on the evolutionary principle. Unlike deterministic methods which work on the determination of gradients and analyzes only one solution at a time, the GA proceeds with a group of solutions and it refines the solution set gradually in successive iterations. In optimization of a wide range of problems, the GA has received a considerable attention. The objective of the present work is to analyze

different types of combined mode transient conduction and radiation heat transfer problems, and to study the efficacy of the LBM, the FVM and the GA in the retrieval of different types of unknown medium properties and/or boundary conditions. The importance of selecting a right set of optimization parameters is also investigated. Problems in 1-D and 2-D Cartesian and 1-D cylindrical geometry with varying complexities are studied. The thesis is organized in 7 chapters. A brief summary of every chapter is provided in the following pages:

Chapter 1 entitled Introduction provides details on the inverse problems and their applications. A detailed literature review pertinent to the inverse problems in general and heat transfer problems in particular is provided. The optimization methods used in solving an inverse problem are reviewed. The solution methodology and the competent methods applied in inverse heat transfer problems are discussed. The need for a competent and efficient CFD solver for the solution of energy equations and also to evaluate radiative information is highlighted. The advantage of using the stochastic based approach such as the GA for the optimization purpose is supported with relevant explanations. Apart from heat transfer problems, the recent applications of the GA to other branches are also studied. Taking a detailed literature survey into account, objectives of the present work are enumerated at the end of the chapter.

Chapter 2 deals with the formulations involving the LBM - FVM and the LBM-FVM-GA for the direct and the inverse problems, respectively. In the direct as well as in the inverse methods, the energy equation is formulated using the LBM, and the FVM is employed to compute the radiative information. In the inverse method, the GA is used to minimize the

objective function which is formed by squaring the summation of the exact and the guessed temperature fields. The effect of measurement errors is accounted in the objective function. In this case, the minimization is done considering the measured temperature field and the guessed one. Using the error contained in the measured data, the exact temperature field is evaluated and the increased error is added to the guessed field. This way, even, errors of higher magnitudes are minimized using the GA. The optimization and stopping criterion for the inverse algorithm are discussed. The flowchart is provided to highlight the working principle of the GA in the inverse problem. The basic foundation for further analysis is built on the basis of the above mentioned formulations.

Chapter 3 deals with the inverse analysis of a transient conduction-radiation problem in a 1-D planar geometry using the LBM-FVM in conjunction with the GA. A set of two parameters such as (a) the conduction-radiation parameter and the scattering albedo and (b) the conduction-radiation parameter and the hot boundary emissivity are simultaneously estimated. The problem is studied for different genetic parameters and the optimized results are compared. In addition to this, accuracies of the estimated parameters with iterations/generations, comparisons of exact and reconstructed temperature fields and comparisons of the CPU times in the direct and inverse methods are also reported. In order to show the robustness of the algorithm, effects of measurement errors on the estimated parameters are studied, and they are compared with the exact results. The optimization parameters were found to significantly affect the accuracy of the estimated parameters. They were also found to affect the convergence

rate of the objective function. The set of optimization parameters was found to have a significant effect. The LBM-FVM in conjunction with the GA was found to provide a good estimation of unknown parameters.

Chapter 4 extends the usage of the LBM-FVM-GA to an inverse transient conduction-radiation problem in a 2-D Cartesian enclosure. In this chapter, three parameters such as the conduction-radiation parameter, the scattering albedo and the hot boundary emissivity are simultaneously retrieved. Effects of the GA optimization parameters such as the cross-over probability, the mutation probability, the population size and the number of generations on accuracy of results are analyzed and suitable ones are identified. For each of the GA parameters, the accuracy of the estimated parameters is compared with the exact ones and the error analysis is carried out. To study the effects on convergence and computational time, an exclusive test has been carried out by performing an analysis with a high population size of 500. It has been observed that with a higher population size, the convergence is achieved fast, but the CPU time becomes considerably high. In addition to these, effects of the measurement errors on estimated parameters and the required CPU times are carried out. The study reveals that the CPU times vary in direct proportion to the generation as well as the population size. In other words, a linear trend is observed in the variation of the CPU time with the number of generations as well as the population size. Subject to a proper selection of the genetic parameters, the LBM-FVM-GA combination was found to provide good estimates of the unknown parameters.

Chapter 5 analyzes three types of conduction-radiation problems containing different levels of non-linearities and complexities in terms of boundary conditions. The analyses

of inverse problems include consideration of non-Fourier conduction, temperature dependent thermal conductivity and temperature as well as flux (mixed) boundary conditions. The non-Fourier heat conduction finds application in the analysis of many heat transfer problems in which consideration of a finite propagation speed for the conduction wave front becomes important. However, this consideration increases the non-linearity of the energy equation of a conduction-radiation problem. The second problem considers the effect of temperature dependent thermal conductivity. This effect becomes significant in high temperature applications such as that involving radiative heat transfer. In the third problem, we have applied the inverse problem for estimating boundary condition in addition to the unknown parameters. In this study, the boundary condition which in itself produces the thermal disturbance in the medium, is estimated in addition to the unknown parameters.

Problems considered in Chapter 5 are representatives of more realistic situations. The complete analysis of the GA parameters for estimation of different variables such as the medium properties, the boundary properties and conditions, and unknown boundary conditions and CPU times required for the same are presented. Like problems considered in Chapters 1-4, for the three problems considered in Chapter 5, the effects of various optimization parameters such as the cross-over probability, the mutation probability, the population size and the number of generations on estimated parameters are studied. This chapter further establishes the robustness of the chosen methods - the LBM, the FVM and

GA, in simultaneous estimation of unknown parameters in conduction-radiation problems having varying levels of complexities.

In Chapter 6, an inverse analysis is carried out to estimate the properties and to reconstruct the thermal fields involving conduction and radiation problems in a 1-D concentric cylindrical enclosure. The LBM formulation extended to the cylindrical geometry is used to solve the energy equation of the conduction problem, and the discrete transfer method is used for the evaluation of radiative heat flux in the radiation problem. In case of a conduction problem, radius ratio is estimated, and in case of a radiative transfer problem, radius ratio and the extinction coefficient are simultaneously estimated. In both the problems, after the estimation of the unknown parameters, temperature and heat flux fields are reconstructed. For the cylindrical geometry too, subject to the proper selection of optimization parameters, a reasonably good estimates of the unknown parameters are obtained.

Summary of the research work and conclusions are made in Chapter 7. Future scope and recommendations are also made in this chapter.

Contents

List of Figures

List of Tables

Nomenclature

A	-	Area
a	-	anisotropy factor
c_P	-	specific heat, kJ/kg K
$\vec{c}$	-	propagation velocity in the lattice, m/s
f	-	particle distribution function, K
G	-	incident radiation, W/m^2
I	-	intensity, W/m^2
J	-	objective function
k	-	thermal conductivity, W/m K
M	-	number of effective intensities/directions
N	-	conduction-radiation parameter
q_R	-	radiative heat flux, W/m^2
s	-	geometric distance, m
S	-	source term, W/m^2
SS	-	Steady-state

t - time, s

T - temperature, K

w - weight factor in the LBM

x , y - coordinate, m

X, Y - length of the medium and breadth of the medium, m

Greek symbols

α - thermal diffusivity, m^2/s

β - extinction coefficient, m^{-1}

δ - polar angle, rad

ε - Emissivity

θ - non-dimensional temperature

ξ - non-dimensional time

ρ - density, kg/m^3

σ - Stefan-Boltzmann constant = $5.67\times10^{-8}\ W/m^2.K^4$

τ - relaxation time, s

Ψ_R - non-dimensional radiative heat flux

ω - scattering albedo

Ω - solid angle, rad

Subscripts

b - Boundary

E ,W - east, west

i - direction of propagation in a lattice

P - cell center

R - Radiative

Superscripts

j - index for direction

o - Equilibrium

* - non-dimensional

~ - exact

Abbreviations

1-D/2-D/3-D	one/two/three-dimensional
BGK	Bhatanagar -Gross –Krook
CDM	collapsed dimension method
CFD	computational fluid dynamics
DOM	discrete ordinate method
D1Q2	one dimensional and two directions model
D2Q9	two dimensional and nine directions model
D3Q15	three dimensional and fifteen direction model
DTM	discrete transfer method
FDM	finite difference method
FEM	finite element method
FVM	finite volume method
LB	lattice Boltzmann
LBM	lattice Boltzmann method
LHS	left hand side
RHS	right hand side
RTE	radiative transfer equation
SS	steady-state

Chapter 1

Introduction

1.1 Overview of Inverse Problems

An essential task in inverse problems that are often found in many branches of engineering is to retrieve some unknown parameters associated with a mathematical formulation supplemented with process data. Conceptually, inverse problems could be described as those problems in which effects are known, but not the cause. For example, if we know the properties of a star and the intervening atmosphere, we can calculate the amount of radiation received by the earth from the star. This is referred to as the direct problem. However, the inverse problem involves the determination of properties inside the star and/or the atmosphere from the measured radiative information.

Direct problems are characterized by three properties namely existence, uniqueness and stability of the solution [1]. For an inverse problem, one among the above three conditions are violated and the problem becomes mathematically ill-posed in the manner that their solution is highly sensitive to the variation in the input data. Usually, such problems become numerically unstable when the measured data contains significant errors and their solution demands regularization i.e., smoothening of the solution or the minimization of the error and/or efficient optimization.

In the area of heat transfer, the design and characterization of a thermal device requires knowledge of the medium properties, the initial and the boundary conditions to which it remains subjected. In most of the cases, the initial and the boundary conditions along with the medium properties are known, and the objective is to determine distributions of temperature and/or heat flux. Mathematical analyses of such problems are straight forward and their solution methods are well established. These problems fall under the purview of direct problems. However, there are many situations in which the initial condition, the boundary conditions and/or the medium properties are unknown but temperature and/or heat flux distributions are known. These distributions are typically obtained from measurements. On the other hand, especially in the design of radiant enclosures, there may be also instances where a particular heat flux/temperature distribution is desired which may not require any measurement policies. These type of problems may be grouped under the category of inverse problems[2].

1.2 Literature Review on Inverse Problems – Applications and its Solution

Inverse problems [2] find numerous applications in science and engineering. In the area of atmospheric sciences, inverse problems are found in many situations such as parameter estimation [3, 4], study of remote planets [5] and determination of surface properties [6]. Applications of inverse problems further involve determination of many useful parameters such as phase change location in melting process [7], heat transfer coefficient in solidification process [8] and phase front parameters of thermal storage devices [9].

Further, inverse problems are studied in the design of composite materials [10, 11], robotics [12] and many manufacturing processes [13-19]. In thermal analysis, the inverse problems are extensively applied for parameter estimation in a variety of fluid flow and heat transfer problems [20-32].

As described earlier, inverse problems require some kind of regularization/ minimization methodology for their solution. Therefore, in order to obtain an accurate estimation of unknown parameters, an efficient optimization tool along with a robust numerical method is very important for the solution of inverse problems., Many researchers have investigated a wide range of inverse heat transfer problems and they have used various numerical schemes. Reinhardt and Hao [33], Chen *et al.* [34] and Alifanov and Nenarokomov [35] have studied inverse heat conduction problems. From the knowledge of temperature measurements within the conducting solid, Chen *et al.* [34] retrieved temperature and heat flux on a surface. Kalman Filter scheme was used in their inverse analysis. Alifanov and Nenarokomov [35] used iterative regularization method which is based on minimizing the residual function by means of first order gradient methods and spline-approximation of unknown functions. With known transient temperature data of a plate finned-tube heat exchanger, Huang *et al.* [36] estimated thermal contact conductance. They used the conjugate gradient method (CGM) for the minimization. Li [37] estimated thermal parameters in a conduction-radiation heat transfer problem. From the measured exit radiation intensities, he used an iterative process along with the CGM in the inverse analysis. Both for exact and noisy data, with good accuracy, he estimated two parameters viz., single scattering albedo and the optical thickness. The estimation of other two parameters viz., the conduction-radiation parameter and phase function were

not very accurate. Liu [38] and Park and Yoon [39] have studied inverse radiative transfer in 1-D Cartesian and 3-D Cartesian geometry, respectively. Liu used the mixed method (CGM and 1-D search method) and Park and Yoon used the CGM to carry out the inverse analysis. The former estimated the absorption coefficient and the latter estimated two parameters viz., the absorption coefficient and the scattering coefficient.

The inverse radiative transfer using Karhunen-Loeve Galerkin procedure in conjunction with the CGM has been studied by Park and Yoon [40]. Park and Yoon [41] estimated the strength of the heat source using the CGM in conjunction with the discrete ordinate method (DOM). An inverse method to determine time dependent heat source based on S_4-P_1 method along with the CGM was employed by Park and Lee [42]. Erturk *et al.* [43] estimated boundary conditions in a transient radiative enclosure. They used the Monte Carlo method in conjunction with the CGM to solve the problem. Shenefelt *et al.* [44] used the singular value decomposition method and the model reduction method to solve a linear heat conduction problem. A hybrid method involving Laplace transform technique and finite-difference method with the least-squares scheme to predict the unknown surface temperature in a 2-D inverse heat conduction problem was employed by Chen *et al.* [45]. Sarvari *et al.* [46] performed an inverse radiative analysis in an irregular 2-D geometry using the discrete transfer method (DTM) and the CGM and estimated unknown heat flux distribution over heater surfaces. Sarvari *et al.* [47] also studied an inverse problem involving conduction-radiation in a 2-D irregular enclosure. They applied the finite-element method (FEM) and the DTM and determined a set of required heater inputs. The optimization was achieved through the CGM.

A FEM along with a modified Newton-Raphson method to estimate the boundary condition in a non-linear heat conduction problem was used by Yang [48]. Ling *et al.* [49] estimated heat flux profiles in an inverse heat conduction problem using non-iterative finite element based inverse method. Ding and Tao [50] estimated the boundary heat flux in a pipe using proper orthogonal decomposition and the inverse problem was solved by the Fletcher-Reeves CGM. For a 1-D inverse heat conduction problem, a central difference scheme in time having a regularizing effect was used by Xiong *et al.* [51]. An inverse conduction–radiation problem to estimate emissivity in a 2-D Cartesian geometry was investigated by Kim *et al.* [52]. They used the FVM and the hybrid genetic algorithm (GA) in their inverse problem. An inverse analysis to simultaneously estimate the effective thermal conductivity, the effective volumetric heat capacity as well as the heat transfer coefficient between a porous medium and a hot wire was performed by Znaidia *et al.* [53]. They used the Lavenberg-Marquardt method to solve the inverse problem.

For the design of radiative transfer systems using inverse analysis, three different optimization approaches, viz., the conjugate gradient method, Tikhonov's regularization and singular value decomposition method were investigated by Daun and Howell [54]. Reconstruction of an unknown transient heat source in a 3-D radiative transfer problem from the temperature field was conducted by Wang and Zabaras [55]. They used Markov chain Monte Carlo method and Bayesian method in their inverse analysis. Deiveegan *et al.* [56] compared different methodologies for estimation of emissivity and gas properties in a participating media. Deng and Hwang [57] applied neural network in an inverse heat conduction problem. Franca and Howell [58] performed inverse design of radiative

enclosures for thermal processing of materials. Their methodology was based on truncated singular value decomposition method. They estimated heat input to a heater located at the top of a three-dimensional enclosure that can satisfy a prescribed time-dependent temperature curve on a surface located at the base of the enclosure. Kim and Baek [59] performed an inverse analysis in a cylindrical enclosure involving conduction and radiation. They estimated heat flux distribution on the design surface using Lavenberg-Marquardt method for optimization and the FVM for the energy equation. Cheng *et al.* [60] have applied the Tikhonov regularization method to a 3-D inverse conduction problem.

Most recently, stochastic based methods [61-65] have gained considerable attention for inverse heat transfer problems. This is primarily due to the reason that unlike deterministic approaches which progressively provide a single solution at a time, the stochastic based approaches are capable to provide multiple solutions after exhaustive search in the solution space. This increases the probability of obtaining a solution near the global optimum solution.

Stochastic based optimization methodologies have been found to be suitable for problems containing high degree of non-linearities in the mathematical formulation. This is unlike deterministic based methods which fail to provide confidence upon the solution, as they do not involve exhaustive search. The stochastic based approaches are very efficient when the measured data contain considerable uncertainties or randomness which cause the solution to move much away from the global optimum. The deterministic based approaches, on the other hand, may lead to a solution which is only a local optimum.

One of the basic limitations of the deterministic approach is their inability to judge the quality of the optimal solutions. The working nature of some stochastic based methodologies has been derived from the nature and they mimic biological processes. They simultaneously work with a cluster of feasible vectors which upon exhaustive search in the solution space yield optimal solutions. In due course of the search process, they eliminate the local solutions which could be located far away from the global optimal values. In a nutshell, the stochastic based methods are optimization approaches capable to handle randomness and uncertainties that arise due to high degree of non-linearity in the mathematical formulation.

Verma and Balaji [61] used the GA for parameter estimation in a 1-D planar geometry. They estimated conduction-radiation parameter, the optical thickness and the boundary emissivity in a conduction-radiation problem. The direct problem was solved using the FVM. Qi *et al.* [62] have used particle swarm optimization method in a 1-D radiative transfer problem. They investigated three cases in which source term, extinction coefficient, scattering coefficient and absorption coefficient were evaluated using the DOM to solve the direct problem. Liu [63] estimated the unknown heat source in a 1-D heat conduction problem by an inverse method using the GA. Slota [64] estimated the heat transfer coefficient in an inverse Stefan problem. He also used the GA in the inverse analysis. The usage of Bayesian method for parameter estimation has been investigated by Parthasarathy and Balaji [65]. They estimated thermal conductivity and convection heat transfer coefficient in a 2-D unsteady heat conduction problem involving convection and convection-radiation boundary conditions.

The analysis of transient conduction-radiation heat transfer problems are encountered in many physical processes. Depending upon various factors such as the type of geometry considered, the type of non-linearity involved and the existence of unconventional heat transfer modes, the complexity associated with various combination of solution methods varies. This can be corroborated in the following manner. Typically, 1-D transient conduction-radiation heat transfer problems are solved with the assumption of a constant thermal conductivity [66-68]. Therefore, most of the available literature on transient conduction-radiation heat transfer deal with constant thermal conductivity, and its variation with temperature is generally neglected. However, if there is a large temperature difference within a medium, this assumption is not appropriate. Such variations are significant for the case of non-metallic materials subjected to large temperature differences. So far, only a few studies have been available in this area [69-71]. However, it is noticed that an inverse solution involving the effect of variable thermal conductivity type problems have not been reported in the literature. Further, the problem involving conduction-radiation in a 2-D enclosure [72-76] becomes more complex when compared to the 1-D problem. In addition to the complexities in conduction, the solution of the radiative information also becomes difficult due to an increase in the number of discrete directions. In conclusion, it can be inferred that a transient inverse solution of either a 1-D or 2-D Cartesian enclosure has not been presented in literature.

For a conduction problem which follows Fourier's law, effects of any thermal disturbances in the system, in the form of a sudden rise in the boundary temperature or a sudden appearance of a heat source at any location in the medium, propagate with very high speed and hence establishes the thermal disturbances instantaneously. This

assumption is not universally applicable in all situations, and in those cases, the problem becomes unconventional and more complex [77-79]. For example, the validity of the Fourier's law of heat conduction breaks down when we consider heat transport through a processed meat/skin [80-83]. Further, at a very low temperature, heat transport by conduction is not governed by Fourier's law. When any material is subjected to a pulse radiation, at short time levels, a discontinuity in the temperature profile is observed, which can not be explained through the Fourier's law of heat conduction. The governing conduction equation becomes hyperbolic in nature and along with the radiative term, the solution of the problem becomes difficult. Few literature dealing with the involvement of non-Fourier conduction are available [84-86]. However, an inverse analysis dealing with such unconventional heat transport problems has not been reported till date.

Analysis of conduction-radiation heat transfer involving cylindrical enclosures [87-92] find application in many engineering devices such as combustion chambers, rocket propulsion systems, fibrous insulations and many more. The set of equations that formulate radiative heat transfer in cylindrical coordinates require information along the azimuthal direction in addition to the polar direction. Thus, the evaluation of radiative heat transfer in the cylindrical coordinate system is relatively difficult [93-95] than that in the Cartesian geometry. As far as inverse analysis in a cylindrical enclosure is concerned, from the investigations performed by Kim and Baek [59], we find that in a concentric cylindrical enclosure, the governing energy equation corresponds to that in the Cartesian coordinate. In other words, it can be inferred that their work neglected the area effect and the energy equation has been applied between the two lateral surfaces of the cylinder. Also, it can be concluded that the analysis of an inverse transient conduction-radiation

heat transfer problems considering the effect of variable area has not been reported in the literature.

Analysis of heat transfer problem with flux boundary condition [96-98] finds applications in many areas of research such as furnace design, fire protection systems, foam insulations, solidification/melting of semitransparent materials, high temperature porous insulating materials, glass-fluidized bed, electronics chip and power plants, etc. For such cases, the problem is formulated as a mixed boundary condition. The mixed boundary condition typically constitutes the specification of heat flux on one boundary and temperature on the other boundary. Further, it is observed that even though a few literature dealt with such type of direct/well posed problems [99,100], the inverse formulations have not been investigated so far.

A few good number of computational methodologies have been explored to obtain the radiative information in heat transfer problems involving volumetric radiation. These methods enable us to evaluate the information about the radiative transfer in a much simpler and efficient manner which otherwise become too complicated. They include the DTM [101-103], the DOM [104], the spherical harmonics method [105], the Monte-Carlo method [106] and the FVM [107-111]. Among the above mentioned methods, the FVM is most robust and is widely used for the computation of radiative transfer. This is largely due to the reason that the FVM is less prone to the ray effect. However, any of the methods mentioned above can be successfully applied without difficulty. In heat transfer involving conduction along with radiation, in addition to radiative information, the

evaluation of the energy equation is also required. A number of computational methods are available to obtain the solution of the energy equation. They include the finite difference method (FDM) [112], the FEM [113] and the FVM [114].

1.3 Suitability and Selection of Efficient Method for Direct and Inverse Heat Transfer Problems

Since an inverse problem can be analyzed as a direct problem coupled with some kind of regularization/optimization tool, the solution of such problems necessitates the usage of an efficient forward problem solution methodology along with an equally competent optimization tool. In the following pages, we discuss the importance and the competent methodologies used to solve the energy equations for the heat transfer problems in general and to obtain the radiative information in particular.

1.3.1 Selection of Direct Method Required in the Inverse Problem

Conduction and convection are the two important modes of heat transfer. In these two modes, the rate of heat transport is proportional to the temperature difference. On the other hand, the radiative heat transfer rate is proportional to the difference in the absolute temperature to the fourth power. Thus, the analysis of thermal radiation becomes important when the temperature becomes considerably high. Thermal radiation finds extensive applications in the design and analysis of combustion chambers, furnaces, IC engines, re-entry vehicles, etc.

The thermal radiation falls under two categories, viz., surface radiation and gas radiation. In the former case, the radiative intensity does not change as it travels from one point to the other as the intervening medium does not take part during the radiative energy exchange process, and thus is a surface phenomenon. When the intervening medium also takes part in the energy exchange process, it is known as gas radiation and the emitted intensity undergoes a change due to processes such as absorption, emission and scattering by the medium before it reaches the other boundary. In other words, it is a volumetric phenomenon.

In the analysis of radiative transfer through a participating medium, the radiatve transport equation (RTE) is used to analyze the rate of radiative heat transfer through a participating medium, which is third order integro-differntial equation. The RTE in general has seven independent variables such as three space coordinates, two direction coordinates, wavelength and time. Since thermal radiation travels with the speed of light, in most of the engineering applications, even though conduction and convection remain a transient processes, radiative transport is an instantaneous phenomenon. Even with the temporal dimension, compared to conduction and convection, the presence of two extra dimensions, viz., polar angle and azimuthal angle in radiation, brings additional complexity. The analysis becomes further complicated and solution becomes relatively difficult, when apart from radiation, a problem involves conduction and/or convection. Thus, efficient methods are required to analyze combined mode heat transfer problems involving thermal radiation.

Many numerical methods are available for the computation of radiative information either in purely a radiative transport problem or a combined mode problem. Each method has some strong and weak points. Some of the radiative transfer methods found in the literature are the exact analytical method [157], the diffusion approximation [158], the zonal method [159], the multi-flux method [160], the Monte Carlo method [161], the moment method [162], the P_N approximation [163], the DOM [101], the DTM [101], the FEM [157], the FVM [93, 164-166] and the collapsed dimension method [167]. Amongst these methods, the FVM is the most robust and it is less prone to the ray effect. In addition, the method is fully conservative, i.e. the radiative energy remains conserved and in this, the false scattering does not manifest. The method is compatible with other numerical methods. Because of these features, the FVM is a superior method for the computation of radiative information. Therefore, in the present work, the FVM has been used in most of the cases involving radiative heat transfer.

Due to the mesoscopic origin, , the lattice Boltzmann method (LBM) has emerged as an efficient and attractive numerical computational tool to analyze a wide range of heat transfer problems [115-127]. The LBM has many advantages over conventional CFD solvers such as the FDM, the FVM and the FEM. This surge of interest in the usage of the LBM is largely attributed to its ability of handling the complex geometry in a simpler and efficient manner, possession of a clear physical meaning and the ability of parallel computational analysis. The LBM has been successfully used to simulate a wide range of fluid flow and heat transfer problems. These include both single, multiphase and chemically reacting flows as well as phase change phenomena in simple and complex

physical systems. However, the application of the LBM application to the problems involving thermal radiation is very recent [117-119, 166]. Besides this, in the field of inverse problems, its usage has not been explored so far. Therefore, in the present work, both in the direct and the inverse problem, we formulate the energy equations using the LBM. In the next section, we discuss some of the optimization methodologies used for the solution of inverse problems.

1.3.2 Selection of Optimization Method Required in the Inverse Problem

The optimization methodology can be broadly classified under two categories, deterministic based approaches and stochastic approaches. Prominent deterministic methods are the conjugate gradient method, the Newton-Raphson method and the Levenberg-Marquardt method. All these methods involve iterative calculation of the gradient of the function that has to be either minimized or maximized. These methods essentially need an initial feasible point which successively approaches towards the final solution with the concept of function gradients. It has been seen that although most of these methods are useful in attaining a fast convergence, they suffer from many inherent drawbacks. In case of the conjugate gradient method and the Newton Raphson method, solutions mainly depend upon the initial guess, i.e., the global convergence is not guaranteed from any starting point. They require the function to be differentiable, and, they have not been investigated for the problems which are transient in nature. This may be attributed to the reason that the minimization in the inverse method for transient problems needs to be performed at each time level until the steady-state time level is

attained, which results in a large function size. The Lavenberg-Marquardt algorithm provides a fairly good solution for a non-linear function minimization based on least squares curve fitting and non-linear programming. However, in addition to above drawbacks, it is expected to become computationally slower for the problems requiring minimization of large dimensional functions due to the calculations involved in obtaining the gradients at each successive time step. The stochastic based methods, on the other hand, fare well as compared to deterministic methods and the probability of obtaining a solution nearer to a global maximum/minimum is high. This is because, unlike deterministic methods, which work with one solution at a time, the stochastic based approaches work simultaneously and collectively with a group of possible solutions. In successive iterations, the solutions that lie considerably away from the proximity of the global optimal domain are eliminated from the collective groups. However, they demand high CPU times due to exhaustive search performed by them in the solution space.

The concept behind the stochastic method is their heuristic approach. They are evolutionary in nature, i.e., their working is derived from the nature. Besides GA [128-133], other optimization methods based upon evolutionary scheme/stochastic methods include simulated annealing [134-138], particle swarm method [29, 139-145], tabu search [146-152] and ant colony method [153-157]. However, among the above methods, two main methods based upon the stochastic approach which have been investigated for inverse heat transfer problems are the particle swarm optimization and the GA. The main difference between the two is that in the former, only the best particle or solution shares information with other solutions, whereas in the latter, the whole population or groups of

solutions successively move towards the optimality domain. Amongst these two methods, the usage of the GA has been found more applicable than the particle swarm method to the heat transfer problems involving thermal radiation. Apart from heat transfer problems, the GA is one of the optimization tools that has gained considerable attention in other fields of research also. This is due to the reason because the GA offers good flexibility (using crossover operator) to exhaustively search the parametric solution space. This may not exist in a systematic framework for other evolutionary techinques like simulated annealing, particle swarm, Tabu search, etc. Therefore it will be advantageous to rapidly identify solutions with strong parameter dependencies upon one another. Based upon the above discussion, in the present work, in the following pages, we further justify the preference of the GA.

1.4 Selection of the Genetic Algorithm (GA) as an Optimization Tool for the Present Work

It is observed from the literature survey that the application of the GA has not been investigated thoroughly for a variety of inverse transient heat transfer problems involving conduction and thermal radiation. It is also observed from the literature review that there exists a necessity to investigate the effects of optimization algorithm/GA parameters. The inverse problems being dependent upon efficient regularization or optimization method, a simple and convenient implementation of the same becomes an added advantage. The efficiency of the optimization methodology based upon evolutionary approach has been described previously. Many modern commercial packages contain different features

which are useful to solve various kinds of problems. In the same line, MATLAB-7 contains optimization toolboxes based upon gradient or deterministic based method as well as stochastic based tool box involving the GA. Alternatively, the GA can also be easily implemented by the method of calling the function. This requires an objective function to be written and the same can be called by the GA function. Further, in the area of inverse problems, the suitability of a combination involving an efficient set of methods such as the LBM and the FVM/DTM in conjunction with the GA has not been investigated. Therefore, below we set the objectives for the present investigation involving inverse analysis of inverse transient conduction-radiation problems.

1.5 Objectives

From the above discussion, we find that the usage of the LBM and the GA has not been explored in the area of heat transfer problems. Further, in the past studies, the inverse problems involving conduction and radiation heat transfer have been investigated for simple cases where transient effects are ignored, transeint state, variable thermal conductivity, non-Fourier laws, area effect in the cylindrical geometry and mixed boundaru conditions It is well known that the inverse problems are mathematically ill-posed and they pose a tougher challenge when the objective function is highly non-linear and the variables to be determined are interdependent. Moreover, the usage of the GA is subjected to a proper selection of the genetic parameters and thus it requires a careful investigation. Therefore, in the present work, we perform an inverse investigation of different classes of heat transfer problems involving transient conduction and thermal

radiation and we also investigate the implications of different GA parameters The usage of the LBM in conjunction with the GA has been investigated for inverse problems. The FVM or the DTM has been used to obtain the radiative information. To summarize, the objectives of the present work are as mentioned below,

(1) To study the application of the LBM-FVM for the solution of transient conduction-radiation heat transfer problems in participating media under different conditions and in different geometries.

(2) To investigate the application of evolutionary algorithm (GA in the present work) for different inverse problems in participating media and to identify critical optimization parameters for the problems considered in this work.

(3) Subject to proper selection of GA parameters, to establish the suitability of the LBM-FVM-GA in multiparameter retrieval for inverse transient conduction-radiation heat transfer problems in different geometries and under different conditions.

1.6 Organization of the Thesis

This thesis is organized in form of six chapters. In the following pages, we briefly discuss the organization of the thesis and the problems considered for the investigation in the present work.

Chapter 1 summarizes concepts associated to an inverse problem and discusses its application in the area of science and technology. The involvement of thermal radiation mode of heat transfer and the numerical methods are also dealt with. The methodologies

adopted in the past and those gaining recent popularity for solving the inverse problems have also been highlighted to a large extent. The selection of suitable numerical method to solve the direct problem and the selection of competent optimization tool along with the reason for the same are also explained.

Chapter 2 presents the mathematical formulations involved in the present work and the procedure followed for obtaining the solution. The usage of the LBM for the solution of the energy equation and the application of the FVM for computing the radiative information is enumerated in this Chapter. The working procedure of the GA is discussed. The methodology to solve a direct problem and an inverse problem is also presented. The objective function required for optimization is also formulated and the working procedure of the optimization algorithm is also presented in this chapter.

Chapter 3 deals with the application of the LBM-FVM in conjunction with the GA to transient conduction-radiation heat transfer problems in 1-D planar geometry. The formulation of the objective function using the LBM-FVM and the minimization of the same using the GA are studied in detail. An exhaustive study has been conducted to visualize the impact of optimization parameters on the accuracy of the solution. The computational time required in the direct method and the inverse method is also compared. The results are benchmarked with those available in the literature.

In Chapter 4, the usage of the LBM-FVM-GA has been extended to a 2-D Cartesian geometry. The formulation of the objective function is carried out using the LBM-FVM

and the minimization of the same is carried out in the similar manner as for the case of the 1-D problem. Compatible optimization algorithm parameters are identified and tested for different sets of medium properties such as the conduction-radiation parameter, the boundary emissivity and the scattering albedo.

Chapter 5 performs the inverse analysis of three different problems with varying complexities, viz., non-Fourier transient conduction-radiation problem, transient conduction-radiation problem with variable thermal conductivity and transient conduction-radiation problem with mixed boundary condition.. Though the problem has been solved using the same methodology as adopted in Chapters 3 and 4, the efficacy of the LBM-FVM and the GA to solve different kinds of non-linear inverse problems with variant complexities is of relevance in this chapter.

Chapter 6 deals with inverse problems in concentric cylindrical media. The energy equation is modified in the radial direction and the objective function is constructed. The LBM-GA and the DTM-GA are respectively used to solve the conduction and the radiative transfer problem. The effect of various optimization algorithm parameters on the quality of estimated unknown variables is also reported in this chapter.

A summary of the research work conducted in the present study along with the conclusions drawn from the same are provided in Chapter 7. This chapter also presents possible scope for future research direction.

1.7 Summary

In this chapter, inverse problems along with their applications have been summarized. Various methods available for the solution of inverse problems were reported. The methods used for the solution of the direct and the inverse heat transfer problem involving conduction and/or thermal radiation were discussed. The concept to implement the LBM to the field of inverse problem involving transient heat transfer was justified and the need for investigating the effects of optimization parameters was realized. Various shortcomings in the past studies associated with inverse heat transfer analysis have been outlined to justify the usages of the methods in this work. The choice and need for an optimization algorithm based on stochastic or evolutionary approach such as the GA has also been emphasized. Various classes of problems where the computational investigations have been considered were also presented. Finally, objectives of this study and the organization of the thesis were presented.

Chapter 2

Formulation of an Inverse Problem

2.1 Introduction

In a heat transfer problem involving thermal radiation, due to the volumetric nature of radiation, the solution of the energy equation becomes difficult. It has been mentioned in the previous chapter that in the direct problem, the medium properties and the initial and the boundary conditions are known. Determination of either temperature or heat flux may be accomplished using either computationally or experimentally. This is an example of a direct problem. A direct problem is mathematically well-posed. On the other hand, an inverse problem is mathematically ill-posed, and it invariably requires some kind of regularization or optimization. Thus, in addition to an optimization tool, solution of an inverse problem also requires method(s) needed to solve a direct problem.

This chapter deals with the formulations required for the solution of an inverse transient conduction-radiation heat transfer problem. As mentioned in the previous chapter, the LBM has several advantages over other CFD solvers such as the FDM, the FEM and the FVM, in the present work, the LBM is used to formulate the governing energy equation and the FVM is used to compute the radiative information in both direct and inverse

methods. In the inverse method, the GA is used as an optimization tool. The inherent advantages of the GA as an optimization tool have already been mentioned in the previous chapter. In the following pages, first we briefly describe the mathematical formulations of the LBM and the FVM in order to solve the direct problem. Next, we provide the methodology for solving the inverse problem using the GA as an optimization tool. In the present chapter, formulations have been given for 1-D and 2-D Cartesian geometry.

2.2 Energy Equation

The general form of the energy equation, with the assumption of constant thermophysical properties involving transient conduction-radiation problem can be written as [101, 102],

$$\rho c_p \frac{\partial T}{\partial t} = k\nabla^2 T - \nabla \cdot \vec{q}_R \tag{2.1}$$

where ρ is the density, c_p is the specific heat at constant pressure, k is the thermal conductivity and q_R is the radiative heat flux. In the following sections, we briefly describe the methodology of the LBM to solve the energy equation (Eq. (2.1)) and then we deal with the methodology of the FVM to compute the divergence of the radiative heat flux, $\nabla.\vec{q}_R$.

2.3 Lattice Boltzmann Method (LBM)

The usage of the LBM has gained considerable momentum in science and engineering, in general, and it has emerged as an efficient numerical method for fluid flow and heat transfer problems, in particular. Owing to its mesoscopic origin, it presents a clear physical meaning, relatively simple solution procedure especially for complex geometries and its adaptability to parallel computational processing architecture. In the following pages, we describe the derivation of the lattice Boltzmann equation.

2.3.1 Derivation of Lattice Boltzmann Equation

Using the single relaxation time, the Boltzmann equation with Bhatanagar-Gross-Krook approximation can be written as [115, 116]:

$$\frac{\partial f}{\partial t} + c.\nabla f = -\frac{1}{\lambda}\left(f - f^{0}\right) \tag{2.2}$$

Equation 2.2 can be written in the form of an ordinary differential equation [115, 116]

$$D_t f + \frac{1}{\lambda} f = \frac{1}{\lambda} f^{0} \tag{2.3}$$

where $D_t = \frac{\partial}{\partial t} + c.\nabla$ is the Lagrangian derivative along the microscopic velocity vector c, $f = f(x,t)$ is the single-particle distribution function, λ is the relaxation time due to collision and f^{0} is the Maxwell-Boltzmann distribution function given by [115, 116]

$$f^{0} = \frac{\rho}{(2\pi RT)^{D/2}} \exp\left(-\frac{(c-u)^2}{2RT}\right) \tag{2.4}$$

where R, D, ρ, u, T are the ideal gas constant, space dimension, density, velocity vector and temperature, respectively.

The macroscopic variables are the moments of the distribution function f [115, 116]

$$\rho = \int f \, dc, \qquad \rho u = \int cf \, dc, \qquad \rho e = \int \frac{(c-u)^2}{2} f \, dc \tag{2.5}$$

where $e = D_0 RT/2$ and D_0 is number of degree of freedom of a particle.

Multiplying both sides of Eq. (2.3) by the integral factor $e^{\int \frac{1}{\lambda} dt}$, Eq. (2.3) takes the following form [115, 116]

$$\frac{df}{dt} e^{\int \frac{1}{\lambda} dt} + \frac{1}{\lambda} f e^{\int \frac{1}{\lambda} dt} = \frac{1}{\lambda} f^0 e^{\int \frac{1}{\lambda} dt} \tag{2.6}$$

Eq. (2.6) can be rewritten as [115, 116]

$$\frac{d\left(f e^{\int \frac{1}{\lambda} dt} \right)}{dt} = \frac{1}{\lambda} f^0 e^{\int \frac{1}{\lambda} dt} \tag{2.7}$$

Integrating Eq. (2.7) over time Δt, we get [115, 116]

$$\int_0^{\Delta t} d\left(f e^{\int \frac{1}{\lambda} dt} \right) = \frac{1}{\lambda} \int_0^{\Delta t} \left(f^0 e^{\int \frac{1}{\lambda} dt} \right) dt \tag{2.8}$$

Solution of Eq. (2.8) gives the following expression [115, 116]

$$[f(r + c\Delta t, t + \Delta t)] = e^{\frac{-\Delta t}{\lambda}} [f(r,t)] + \frac{1}{\lambda} e^{-\Delta t/\lambda} \int_0^{\Delta t} e^{t'/\lambda} f^0 (r + ct', t + t') dt' \tag{2.9}$$

If Δt is infinitesimally small and f^0 is locally smooth, we can write [115, 116]:

$$f^0(r + ct', t + t') = \left(1 - \frac{t'}{\Delta t}\right) f^0(r,t) + \left(\frac{t'}{\Delta t}\right) f^0(r + c\Delta t, t + c\Delta t) + o(\Delta t^2) \tag{2.10}$$

Subtracting $f(r,t)$ from both sides of the above equation and neglecting the higher order terms [115, 116]

$$\begin{aligned} f(r+c\Delta t,t+\Delta t)-f(r,t) &= e^{-\Delta t/\lambda} f(r,t)-f(r,t) \\ &+\frac{1}{\lambda}e^{-\Delta t/\lambda}\int_0^{\Delta t}\left(e^{t'/\lambda}\right)\left(1-\frac{t'}{\Delta t}\right)f^0(r,t)dt' \\ &+\frac{1}{\lambda}e^{-\Delta t/\lambda}\int_0^{\Delta t}\left(e^{t'/\lambda}\right)\frac{t'}{\Delta t}f^0(r+c\Delta t,t+\Delta t)dt' \end{aligned} \tag{2.11}$$

Simplifying Eq. (2.11) we get [115, 116]

$$\begin{aligned} f(r+c\Delta t,t+\Delta t)-f(r,t) &= \left(e^{-\Delta t/\lambda}-1\right)f(r,t)+\frac{1}{\lambda}e^{-\Delta t/\lambda}\int_0^{\Delta t}\left(e^{t'/\lambda}\,f^0(r,t)\right)dt' \\ &-\frac{1}{\lambda}e^{-\Delta t/\lambda}\int_0^{\Delta t}\left(e^{t'/\lambda}\,\frac{t'}{\Delta t}\,f^0(r,t)\right)dt' \\ &+\frac{1}{\lambda}e^{-\Delta t/\lambda}\int_0^{\Delta t}\left(e^{t'/\lambda}\,\frac{t'}{\Delta t}\,f^0(r+c\Delta t,t+\Delta t)\right)dt' \end{aligned} \tag{2.12}$$

Since,

$$\begin{aligned} \int_0^{\Delta t} e^{t'/\lambda}t'dt' &= \left[\lambda t'e^{t'/\lambda}-\lambda^2 e^{t'/\lambda}\right]_0^{\Delta t} \\ &= \lambda\left[\Delta t e^{t'/\lambda}-\lambda e^{t'/\lambda}+\lambda\right] \end{aligned} \tag{2.13}$$

The Eq. (2.12) can be simplified and after simplification it can be rewritten as [115, 116]

$$\begin{aligned} f(r+c\Delta t,t+\Delta t)-f(r,t) &= \left(e^{-\Delta t/\lambda}-1\right)f(r,t)+e^{-\Delta t/\lambda}f^0(r,t)\left[e^{\Delta t/\lambda}-1\right] \\ &-e^{-\Delta t/\lambda}\,\frac{f^0(r,t)}{\Delta t}\left[\Delta t e^{\Delta t/\lambda}-\lambda e^{\Delta t/\lambda}+\lambda\right] \\ &+e^{-\Delta t/\lambda}\,\frac{f^0(r+c\Delta t,t+\Delta t)}{\Delta t}\left[\Delta t e^{\Delta t/\lambda}-\lambda e^{\Delta t/\lambda}+\lambda\right] \end{aligned} \tag{2.14}$$

Eq. (2.14) can further be simplified and expressed as [115, 116]

$$f(r+c\Delta t,t+\Delta t)-f(r,t)=\left(e^{-\Delta t/\lambda}-1\right)\left\{f(r,t)-f^{0}(r,t)\right\} + \left(1+\frac{\lambda}{\Delta t}\left(e^{-\Delta t/\lambda}-1\right)\right)\left\{f^{0}(r+c\Delta t,t+\Delta t)-f^{0}(r,t)\right\} \tag{2.15}$$

Using Taylor series expansion and neglecting the higher order terms we get

$$1+\frac{\lambda}{\Delta t}\left(e^{-\Delta t/\lambda}-1\right)=1+\frac{\lambda}{\Delta t}\left(-\frac{\Delta t}{\lambda}\right)=0 \tag{2.16}$$

Therefore, Eq. (2.14) gets modified to [115, 116]

$$f(r+c\Delta t,t+\Delta t)-f(r,t)=-\frac{\Delta t}{\lambda}\left\{f(r,t)-f^{0}(r,t)\right\} =-\frac{1}{\tau}\left\{f(r,t)-f^{0}(r,t)\right\} \tag{2.17}$$

where $\tau=\frac{\lambda}{\Delta t}$ is the relaxation time. The Eq. (2.17) represents the evolution equation of the distribution function f with discrete time. Below we provide the usage of the LBM formulation for heat transfer problem.

The discrete Boltzmann equation with BGK approximation for any direction $\vec{r}$, is given as [115-125],

$$\frac{\partial f_i(\vec{r},t)}{\partial t}+\vec{e}_i\cdot\nabla f_i(\vec{r},t)=-\frac{1}{\tau}\left[f_i(\vec{r},t)-f_i^{(0)}(\vec{r},t)\right],\qquad i=0,1,2,\ldots,b \tag{2.18}$$

where f_i is the particle distribution function denoting the number of particles at the lattice node $\vec{r}$ and time t moving in direction i with velocity $\vec{e}_i$ along the lattice link $\Delta r=e_i\Delta t$ connecting the neighbors and f_i^0 is the equilibrium particle distribution function. The selection of lattices used in the LBM depends upon the geometry. For e.g., in a 1-D geometry, we use D1Q2 and D1Q3 lattice, while in a 2-D geometry we use D2Q7 and D2Q9

lattice. In a 3-D geometry, normally D3Q15 and D3Q19 lattices are used. The alphabet D represents the dimension and the number following Q denotes the number of directions

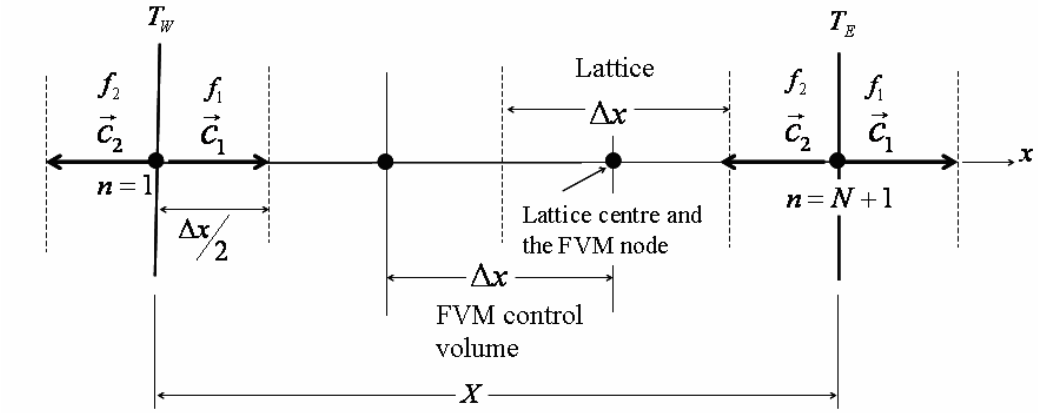

Figure 2.1: D1Q2 lattice of the LBM and control volume of the FVM used in a 1-D planar geometry**.**

through which the particle distribution function f_i propagates, which in the Eq. (2.18) is represented by b. It is to be noted that one particle distribution function always remains at rest at the lattice centre, therefore, $(b+1)$ is the number of particle distribution functions in a lattice. Therefore, for the D2Q9 lattice, $b=8$. In Eq. (2.18), τ is the relaxation time and it is dependent upon the type of lattice selected for the analysis. For D1Q2 lattice (Fig. 2.1), the relaxation time τ is expressed as [115-125]

$$\tau = \frac{\alpha}{\left|\vec{c}_i\right|^2} + \frac{\Delta t}{2} \tag{2.19}$$

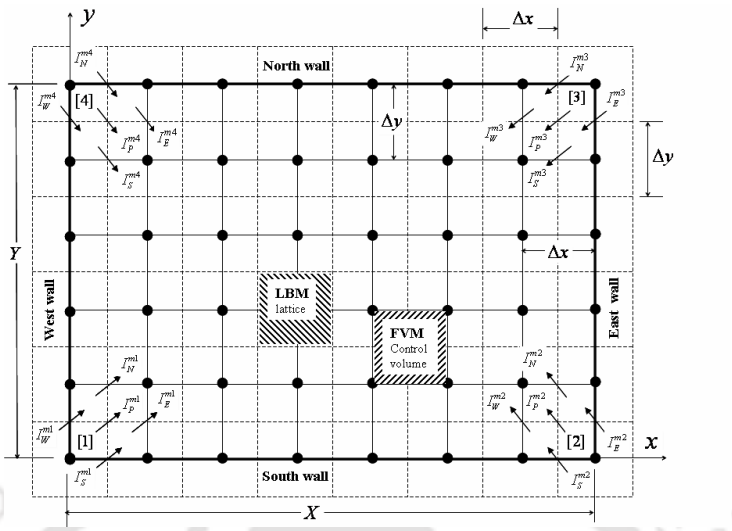

(a)

$$D_x^j = \cos\phi^j \sin\left(\frac{\Delta\phi^j}{2}\right)\left[\Delta\delta^j - \cos 2\delta^j \sin\left(\Delta\delta^j\right)\right]$$

$$D_y^j = \sin\phi^j \sin\left(\frac{\Delta\phi^j}{2}\right)\left[\Delta\delta^j - \cos 2\delta^j \sin\left(\Delta\delta^j\right)\right]$$

Quadrant	$\left(D_x^j, D_y^j\right)$
[1]	(+,+)
[2]	(-,+)
[3]	(-,-)
[4]	(+,-)

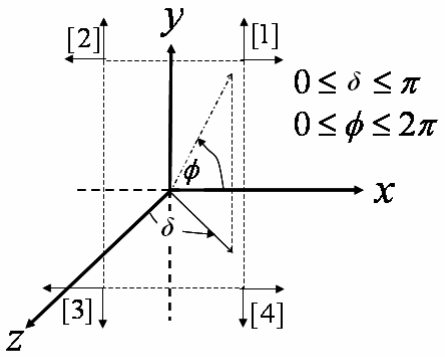

(b)

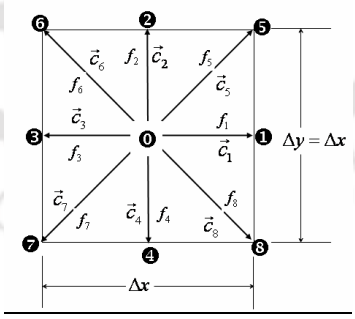

(c)

Figure 2.2: (a) Arrangement of lattices and control volumes in a 2-D rectangular geometry with marching scheme in the FVM for four equally spaced sample directions with one in every quadrant (b) coordinate system for direction in the FVM. (c) D2Q9 lattice.

where α is the thermal diffusivity and Δt is the time-step. For the lattice unc consideration, which is D1Q2, the two velocities c_1 and c_2, and their correspondi weights w_1 and w_2 are evaluated as (2.21)

$$c_1 = \Delta x/\Delta t, \quad c_2 = -\Delta x/\Delta t \tag{2.20}$$

$$w_1 = w_2 = \frac{1}{2}$$

The relaxation time τ for a D2Q9 lattice (Fig. 2.2), which is used in 2-D geometry can be expressed as [115-125],

$$\tau = \frac{3\alpha}{|\vec{c}_i|^2} + \frac{\Delta t}{2} \tag{2.22}$$

The 9 velocities $\vec{c}_i$ and their corresponding weights w_i in the D2Q9 lattice (Fig. 2.2) are the following [115-125],

$$c_0 = (0,0), \quad c_{1,3} = (\pm 1, 0)\cdot U, \quad c_{2,4} = (0, \pm 1)\cdot U, \quad c_{5,6,7,8} = (\pm 1, \pm 1)\cdot U \tag{2.23}$$

$$w_0 = \frac{4}{9}, w_{1,2,3,4} = \frac{1}{9}, w_{5,6,7,8} = \frac{1}{36} \tag{2.24}$$

For any lattice, the weights always satisfy the following relation,

$$\sum_{i=1}^{b} w_i = 1 \tag{2.25}$$

In Eq. (2.23), for a square D2Q9 lattice, $U = \frac{\Delta x}{\Delta t} = \frac{\Delta y}{\Delta t}$. Discretization of Eq. (2.18) leads to the following expression[115-125],

$$f_i\left(\vec{r}+\vec{c}_i\Delta t, t+\Delta t\right)=f_i\left(\vec{r},t\right)-\frac{\Delta t}{\tau}\left[f_i\left(\vec{r},t\right)-f_i^{(0)}\left(\vec{r},t\right)\right] \tag{2.26}$$

Eq. (2.26) is the LB equation with BGK approximation that describes the evolution of the particle distribution function f_i and it represents transient heat conduction problem. The Eq. (2.26) essentially involves two parts,. collision i.e. the calculation of new particle distribution functions, f_i and propagation which involves streaming of the particle distribution functions to the neighboring nodes.

In heat transfer problems, the calculation of the equilibrium particle distribution function and the methodology of obtaining the temperature (by summing f_i over all directions) the following relationship holds good [115-125],

$$\sum_{i=0}^{b} f_i^{(0)}\left(\vec{r},t\right)=\sum_{i=0}^{b} w_i T(\vec{r},t)=T(\vec{r},t)=\sum_{i=0}^{b} f_i\left(\vec{r},t\right) \tag{2.27}$$

For a D1Q2 lattice, $b=2,$ and for a D2Q9 lattice, $b=8.$ To account for the volumetric radiation, the energy equation in the LBM formulation, Eq. (2.26) is modified to the following equation[117-119]

$$f_i\left(\vec{r}+\vec{c}_i\Delta t, t+\Delta t\right)= f_i\left(\vec{r},t\right)-\frac{\Delta t}{\tau}\left[f_i\left(\vec{r},t\right)-f_i^{(0)}\left(\vec{r},t\right)\right]-\left(\frac{\Delta t w_i}{\rho c_p}\right)\nabla\cdot\vec{q}_R \tag{2.28}$$

Equation (2.28) is the equivalent form of the energy equation (Eq. (2.1)) in the LBM formulation. It describes a transient conduction-radiation problem. It is to be noted that using the Chapman-Enskog multi-scale expansion, energy equation (Eq. (2.1)) can be deduced from Eq. (2.28). In Eq. (2.28), since the evaluation of the radiative information

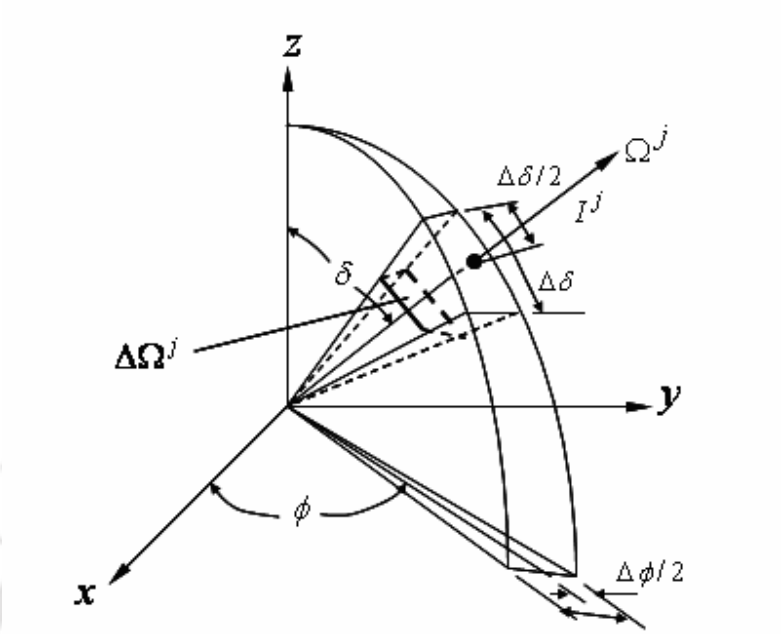

Figure 2.3: Intensity I^j in the direction Ω^j in the center of the elemental sub-solid angle $\Delta\Omega^j$

is direction dependent, Fig. (2.3) shows the discrete angular directions, the polar angle, the azimuthal angle and the concept of elemental solid angle which are used for the calculation of the radiative intensity distribution at any location which in turn is used to evaluate the required radiative information for solving the energy equation (Eq. (2.28)).

In the following pages we describe the methodology of the FVM to calculate the radiative information $\nabla.\vec{q}_R$ required to process the energy equation in the LBM (Eq.(2.28)).

2.4 Finite Volume Method (FVM)

The methodology of computing the radiative information using the FVM was initially formulated by Raithby and Chai [109] and subsequently it was modified and proposed by Chai *et al.* [165]. As described in the previous Chapter, the FVM is less prone to the ray effect and it involves exact integration over both spatial control volume and the solid angle in the angular direction. Because there is no loss of radiative energy, the FVM methodology is fully conservative. In a conduction-radiation problem, the divergence of radiative heat flux $\nabla.q_R$ can be computed using any of the methods such as the discrete transfer method [117, 120], the discrete ordinates method [94, 104], Monte Carlo method [101, 106, 160], spherical harmonics method [101, 102] and the FVM [107-111, 119]. Due to the inherent advantages of the FVM as mentioned earlier, in the present work, the same is used to compute the radiative information in both direct and inverse methods. In the following pages, we provide formulation of the FVM.

The governing radiative transfer equation (RTE) which involves the radiative energy balance for the intensity field in an absorbing, emitting and scattering medium is given by the following relation[101, 102],

$$I\left(s+ds,\Omega\right)-I\left(s,\Omega\right)\equiv\frac{\partial I}{\partial s}ds=\kappa I_b(s)ds-\kappa I(s,\Omega)ds-\sigma_s I_b(s,\Omega)ds + \left(\frac{\sigma_s}{4\pi}\right)\int_{\Omega'=4\pi} I\left(s,\Omega'\right)p\left(\Omega'\rightarrow\Omega\right)d\Omega' \tag{2.29}$$

where, I is the intensity, s is the location, Ω represents direction, κ is the absorption coefficient, I_b is the boundary intensity, σ_s is the scattering coefficient, p is the phase function and $d\Omega'$ is the elemental solid angle.

Eq. (2.29) can be written as [101, 102],

$$\frac{dI(s,\Omega)}{ds} = \kappa I_b(s) - \beta I(s,\Omega) + \left(\frac{\sigma_s}{4\pi}\right) \int_{\Omega'=4\pi} I(s,\Omega') p(\Omega' \to \Omega) d\Omega' \tag{2.30}$$

where $\beta = \kappa + \sigma$, is the extinction coefficient of the medium.

Rewriting Eq. (2.30) in the differential form of the RTE for any direction $\hat{s}$ and for any solid angle Ω about an elemental solid angle $d\Omega$ is given by [107, 109, 120]

$$\frac{dI}{ds} = -\beta I + S \tag{2.31}$$

where S is the source term which is given by the following equation[107, 109, 120]

$$S = \kappa\left(\frac{\sigma T^4}{\pi}\right) + \frac{\sigma_s}{4\pi} \int_{\Omega'=4\pi} I(\Omega')\Phi(\Omega,\Omega') d\Omega' \tag{2.32}$$

Resolving Eq. (2.31) (Fig. 2.3) along the Cartesian coordinate directions and integrating it over the elemental solid-angle $\Delta\Omega^j$, we get the following expression [107, 109, 120]

$$\frac{\partial I^j}{\partial x} D_x^j + \frac{\partial I^j}{\partial y} D_y^j + \frac{\partial I^j}{\partial z} D_z^j = -\beta I^j \Delta\Omega^j + S^j \Delta\Omega^j \tag{2.33}$$

If $\hat{n}$ is the outward normal to a surface, then D^j is given the following

$$D^j = \int_{\Delta\Omega^j} (\hat{n}.\hat{s}^j) d\Omega \tag{2.34}$$

where the direction $\hat{s}^j = (\sin\delta^j \cos\phi^j)\hat{i} + (\sin\delta^j \sin\phi^j)\hat{j} + (\cos\delta^j)\hat{k}$. When $\hat{n}$ is pointing towards one of the positive coordinate directions, D_x^j, D_y^j and D_z^j are given by [107, 109, 120]

$$D_x^j = \int_{\Delta\Omega^j} \sin\delta\cos\phi d\Omega = \int_{\phi^j-\frac{\Delta\phi^j}{2}}^{\phi^j+\frac{\Delta\phi^j}{2}} \int_{\delta^j-\frac{\Delta\delta^j}{2}}^{\delta^j+\frac{\Delta\delta^j}{2}} \cos\phi\sin^2\delta d\delta d\phi$$
$$= \cos\phi^j \sin\left(\frac{\Delta\phi^j}{2}\right)\left[\Delta\delta^j - \cos 2\delta^j \sin(\Delta\delta^j)\right] \quad (2.35a)$$

$$D_y^j = \int_{\Delta\Omega^j} \sin\delta\sin\phi d\Omega = \int_{\phi^j-\frac{\Delta\phi^j}{2}}^{\phi^j+\frac{\Delta\phi^j}{2}} \int_{\delta^j-\frac{\Delta\delta^j}{2}}^{\delta^j+\frac{\Delta\delta^j}{2}} \sin\phi\sin^2\delta d\delta d\phi$$
$$= \sin\phi^j \sin\left(\frac{\Delta\phi^j}{2}\right)\left[\Delta\delta^j - \cos 2\delta^j \sin(\Delta\delta^j)\right] \quad (2.35b)$$

$$D_z^j = \int_{\Delta\Omega^j} \cos\delta d\Omega = \int_{\phi^j-\frac{\Delta\phi^j}{2}}^{\phi^j+\frac{\Delta\phi^j}{2}} \int_{\delta^j-\frac{\Delta\delta^j}{2}}^{\delta^j+\frac{\Delta\delta^j}{2}} \cos\delta\sin\delta d\delta d\phi$$
$$= \sin\delta^j \cos\delta^j \sin\left(\Delta\delta^j\right)\Delta\phi^j \quad (2.35c)$$

For $\hat{n}$ pointing towards the negative coordinate directions, signs of D_x^j, D_y^j and D_z^j are opposite to what are obtained from Eq. (2.35). In Eq. (2.34), $\Delta\Omega^j$ is given the following [107, 109, 120]

$$\Delta\Omega^j = \int_{\Delta\Omega^j} d\Omega = \int_{\phi^j-\frac{\Delta\phi^j}{2}}^{\phi^j+\frac{\Delta\phi^j}{2}} \int_{\delta^j-\frac{\delta^j}{2}}^{\delta^j+\frac{\delta^j}{2}} \sin\delta d\delta d\phi = 2\sin\delta^j \sin\left(\frac{\Delta\delta^j}{2}\right)\Delta\phi^j \quad (2.36)$$

Integrating Eq. (2.35) over control volume and using the concept of the FVM of the CFD, we get the following[107, 109, 120],

$$\left[I_E^j - I_W^j\right]A_{EW}D_x^j + \left[I_N^j - I_S^j\right]A_{NS}D_y^j + \left[I_F^j - I_B^j\right]A_{FB}D_z^j$$
$$= \left[-\beta V I_P^j\right]\Delta\Omega^j \quad (2.37)$$

where A_{EW}, A_{NS} and A_{FB} are the areas of the x-, y- and z- faces of a 3-D control volume, respectively. In Eq. (2.37), I with suffixes E, W, N, S, F and B designate east, west, north, south, front and back control surface average intensities, respectively. On the right-hand side of Eq. (2.37), $V = dx \times dy \times dz$ is the volume of the cell and I_P^j and S_P^j are the intensities and source terms at the cell centre P, respectively.

In any discrete direction Ω^j, if a linear relationship among the two cell-surface intensities and cell-centre intensity I_P^j is assumed, then we can write as[107, 109, 120]

$$I_P^j = \chi_x I_E^j + (1-\chi_x) I_W^j = \chi_y I_N^j + (1-\chi_y) I_S^j = \chi_z I_F^j + (1-\chi_z) I_B^j \tag{2.38}$$

where χ is the finite-difference weighting factor and its value is normally considered to be 0.5. While marching from the first octant of a 3-D enclosure, for which D_x^j, D_y^j and D_z^j are all positive, I_P^j in terms of known cell-surface intensities can be written as below[107, 109, 120]

$$I_P^j = \frac{\frac{D_x^j A_{EW}}{\chi_x} I_W^j + \frac{D_y^j A_{NS}}{\chi_y} I_S^j + \frac{D_z^j A_{FB}}{\chi_z} I_B^j + (V \Delta\Omega^j) S_P^j}{\frac{D_x^j A_E}{\chi_x} + \frac{D_y^j A_N}{\chi_y} + \frac{D_z^j A_F}{\chi_z} + \beta V \Delta\Omega^j} \tag{2.39}$$

where,

$$A_{E,W} = (1-\chi_x) A_E + \chi_x A_W,\ A_{NS} = (1-\chi_y) A_N + \chi_y A_S,\ A_{FB} = (1-\chi_z) A_F + \chi_y A_B \tag{2.40}$$

are the averaged areas. When any one of the D_x^j, D_y^j or D_z^j is negative, marching starts from other corners. In this case, a general expression of I_P^j in terms of known intensities and source term can be written as the following [107, 109, 120],

$$I_P^j = \frac{\frac{\left|D_x^j\right| A_x}{\chi_x} I_{xi}^j + \frac{\left|D_y^j\right| A_y}{\chi_y} I_{yi}^j + \frac{\left|D_z^j\right| A_z}{\chi_z} I_{zi}^j + \left(V \Delta\Omega^j\right) S_P^j}{\frac{\left|D_x^j\right| A_E}{\chi_x} + \frac{\left|D_y^j\right| A_N}{\chi_y} + \frac{\left|D_z^j\right| A_F}{\chi_z} + \beta V \Delta\Omega^j} \tag{2.41}$$

where in Eq.(2.41), x_i, y_i and z_i suffixes over I^j are for the intensities entering the control volume through x-, y- and z-faces, respectively and A_x, A_y and A_z are given the following,

$$A_x = \left(1-\chi_x\right) A_{x_e} + \chi_x A_{x_i}, A_y = \left(1-\chi_y\right) A_{y_e} + \chi_y A_{y_i} = A_z = \left(1-\chi_z\right) A_{z_e} + \chi_z A_{z_i} \tag{2.42}$$

In Eq.(2.42), A with suffixes x_i, y_i and z_i represent control surface areas through which intensities enter the control volume, while A with suffixes x_e, y_e and z_e represent control surface areas through which intensities leave the control volume.

Therefore, for a 1-D control volume, the cell-centre intensity is given the following [120],

$$I_P^j = \begin{cases} \dfrac{2D_x^j I_W^j + S_P^j \Delta\Omega^j dx}{2D_x^j + \beta \Delta\Omega^j dx}, & D_x^j > 0 \\ \dfrac{2\left|D_x^j\right| I_E^j + S_P^j \Delta\Omega^j dx}{2\left|D_x^j\right| + \beta \Delta\Omega^j dx}, & D_x^j < 0 \end{cases} \tag{2.43}$$

Whereas, for a 2-D control volume, the intensities are given by the following [120],

$$I_P^j = \frac{2D_x^j A_x I_W^j + 2D_y^j A_y I_S^j + \left(V \Delta\Omega^j\right) S_P^j}{2D_x^j A_x + 2D_y^j A_y + \beta V \Delta\Omega^j}, \; 1^{\text{st}} \text{ quadrant: } D_x^j > 0, \; D_y^j > 0 \tag{2.44a}$$

$$I_P^j = \frac{2\left|D_x^j\right| A_x I_E^j + 2D_y^j A_y I_N^j + \left(V \Delta\Omega^j\right) S_P^j}{2\left|D_x^j\right| A_x + 2D_y^j A_y + \beta V \Delta\Omega^j}, \; 2^{\text{nd}} \text{ quadrant: } D_x^j < 0, \; D_y^j > 0 \tag{2.44b}$$

$$I_P^j = \frac{2\left|D_x^j\right| A_x I_E^j + 2\left|D_y^j\right| A_y I_N^j + \left(V\Delta\Omega^j\right) S_P^j}{2\left|D_x^j\right| A_x + 2\left|D_y^j\right| A_y + \beta V \Delta\Omega^j}, \text{ 3rd quadrant: } D_x^j < 0,\ D_y^j < 0 \qquad (2.44c)$$

$$I_P^j = \frac{2D_x^j A_x I_W^j + 2\left|D_y^j\right| A_y I_N^j + \left(V\Delta\Omega^j\right) S_P^j}{2D_x^j A_x + 2\left|D_y^j\right| A_y + \beta V \Delta\Omega^j}, \text{ 4th quadrant: } D_x^j > 0,\ D_y^j < 0 \qquad (2.44d)$$

For a linear anisotropic phase function $\Phi\left(\Omega,\Omega'\right) = 1 + a\cos\delta\cos\delta'$, the source term S at any location $\vec{r}$ can be written as [120]

$$S = \kappa_a\left(\frac{\sigma T^4}{\pi}\right) + \left(\frac{\sigma_S}{4\pi}\right)\int_0^{2\pi}\int_0^{\pi} I\left(\delta',\phi'\right)\left(1 + a\cos\delta\cos\delta'\right)\sin\delta' d\delta' d\phi' \qquad (2.45)$$

which in terms of the incident radiation G and net radiative heat flux q_R is written as [120]

$$S = \left(\frac{\sigma_S}{4\pi}\right)\left[G + a\cos\delta q_R\right] \qquad (2.46)$$

In Eq. (2.46), G and q_R computed using the following expressions,

$$\begin{aligned} G &= \int_{\Omega=0}^{4\pi} I\left(\Omega\right) d\Omega = \int_{\phi=0}^{2\pi}\int_{\delta=0}^{\pi} I\left(\delta,\phi\right)\sin\delta d\delta d\phi \\ &\approx \sum_{k=1}^{M_\phi}\sum_{l=1}^{M_\delta} I^j\left(\delta_l^j,\phi_k^j\right) 2\sin\delta_l^j \sin\left(\frac{\Delta\delta}{2}\right)\Delta\phi_k^j \end{aligned} \qquad (2.47)$$

where M_δ and M_ϕ are the number of discrete points considered over the complete span of the polar angle $\left(0 \le \delta \le \pi\right)$ and azimuthal angle $\left(0 \le \phi \le 2\pi\right)$, respectively. Therefore, $M_\delta \times M_\phi$ constitute the number of discrete directions in which intensities are considered at any point. The radiative heat flux is expressed by the following [120],

$$q_R = \int_{\Omega=0}^{4\pi} I(\Omega)\cos\delta d\Omega = \int_{\phi=0}^{2\pi}\int_{\delta=0}^{\pi} I(\delta,\phi)\cos\delta\sin\delta d\delta d\phi \approx \sum_{k=1}^{M_\phi}\sum_{l=1}^{M_\delta} I^j\left(\delta_l^j,\phi_k^j\right)2\sin\delta_l^j\cos\delta_l^j\sin\left(\Delta\delta_l^j\right)\Delta\phi_k^j \quad (2.48)$$

In case of a 1-D planar geometry, radiation is azimuthally symmetric, thus in this case, incident radiation G and net heat flux q_R are given by and computed from the following expressions [120],

$$G = 2\pi\int_{\delta=0}^{\pi} I\sin\delta d\delta \approx 4\pi\sum_{j=1}^{M_\delta} I^j\sin\delta^j\sin\left(\frac{\Delta\delta^j}{2}\right) \quad (2.49)$$

$$q_R = 2\pi\int_{\delta=0}^{\pi} I\cos\delta\sin\delta d\delta \approx 2\pi\sum_{j=1}^{M_\delta} I^j\sin\delta^j\cos\delta^j\sin\left(\Delta\delta^j\right) \quad (2.50)$$

while marching from any of the corners, evaluation of Eq. (2.41) requires knowledge of the boundary intensity. For a diffuse-gray boundary/wall having temperature T_b and emissivity ε_b, the boundary intensity I_b is computed from the following[120]

$$I_b = \frac{\varepsilon_b\sigma T_b^4}{\pi} + \left(\frac{1-\varepsilon_b}{\pi}\right)\sum_{k=1}^{M\phi}\sum_{l=1}^{M_\delta/2} I^j\left(\delta_l^j,\phi_k^j\right)\sin\delta_l^j\cos\delta_l^j\sin\Delta\delta_l^j\Delta\phi_k^j \quad (2.51)$$

In Eq. (2.51), the first and the second terms represent the emitted and the reflected components of the boundary intensity, respectively.

Once the intensity distributions are known, radiative information $\nabla.\vec{q}_R$ required for the energy equation is computed from the following[120],

$$\nabla.\vec{q}_r = \beta(1-\omega)\left(4\pi\frac{\sigma T^4}{\pi} - G\right) \quad (2.52)$$

where in Eq. (2.52), $\omega = \frac{\sigma_s}{\beta}$ is the scattering albedo.

For generalization and ease of computation, the transformation of the dimensional quantities is done in non-dimensional forms. For a 2-D geometry, with non-dimensional distance x^*, y^*, temperature θ, conduction-radiation parameter N, incident radiation G^*, radiative heat flux Ψ_R and time ξ defined in the following way

$$x^* = \frac{x}{L_{\text{ref}}} \quad y^* = \frac{y}{L_{\text{ref}}} \quad \theta = \frac{T}{T_W} \quad N = \frac{k\beta}{4\sigma T_{\text{ref}}^3} \quad G^* = \frac{G}{\left(\sigma T_{\text{ref}}^4 / \pi\right)} \tag{2.53}$$

$$\Psi_R = \left(\frac{1}{4N}\right)\frac{q_R}{\sigma T_{\text{ref}}^4} \quad \xi = \alpha\beta^2 t$$

Therefore, the energy equation in the LBM form as given by Eq. (2.28) and the divergence of radiative flux given by Eq. (2.52), respectively, become as given below,

$$f_i^*\left(\vec{r}^* + \vec{c}_i^*\Delta\xi, \xi + \Delta\xi\right) = f_i^*\left(\vec{x}^*, \xi\right) - \frac{\Delta\xi}{\tau^*}\left[f_i\left(\vec{x}^*, \xi\right) - f_i^{*(0)}\left(\vec{x}^*, \xi\right)\right] - \frac{\Delta\xi w_i}{4N}\frac{\partial\Psi_R}{\partial x^*} \tag{2.54}$$

$$\nabla.\Psi_R = 4(1-\omega)\left(\theta^4 - \frac{G^*}{4\pi}\right) \tag{2.55}$$

In Eq. (2.54), for 1-D planar geometry, the relaxation time τ^* in the non-dimensional form is expressed as,

$$\tau^* = \frac{1}{\left(\Delta x^* / \Delta\xi\right)^2} + \frac{\Delta\xi}{2} \tag{2.56}$$

whereas, for a 2-D geometry, the relaxation time τ^* in the non-dimensional form can be expressed as,

$$\tau^* = \frac{3}{\left|\vec{c}_i^*\right|^2} + \frac{\Delta\xi}{2} \tag{2.57}$$

where c_i^* is the non-dimensional velocity.

Below we describe the steps involved for calculating the temperature field in a transient conduction-radiation problem using the LBM-FVM to solve the direct problem.

2.5 Solution Methodology for the Direct Problem:

1. According to the geometry (1-D or 2-D), select the type of lattice (D1Q2 or D2Q9).
2. Divide the computational domain into finite number of lattices/ control volumes. It should be noted that the number of lattices will be one more than the number pf control volumes.
3. Compute the corresponding relaxation time, τ using Eq. 2.19 or Eq. 2.22.
4. Depending upon the initial temperature condition, evaluate the equilibrium particle distribution function using Eq. 2.27
5. Subject to the same temperature distribution, calculate $\nabla.q_R$ using the Eq. 2.52. For the selected number of discrete directions, use appropriate relationships for computing the intensities (Eq. 2.43 or Eq. 2.44).
6. Evaluate the new particle distribution function using Eq. 2.28 and propagate the particle distribution functions to neighboring lattice centers/ nodes of control volumes.
7. At the next time step, calculate the new temperature field using the Eq. 2.27.

8. Calculate the equilibrium particle distribution function corresponding to the new temperature field.
9. Check the convergence criterion for the attainment of steady state and if so, terminate the process.
10. Modify the particle distribution function locally for the satisfaction of boundary condition.
11. If not converged, go to step 4.

In the direct method, temperature θ distributions are obtained from the given values of the medium properties along with the known initial and boundary conditions. In the inverse method, for known temperature θ distributions, in the present work, simultaneous estimation of unknown parameters has been done. It is assumed that the temperature θ distributions provided by the direct method are accurate and thus assumed to be experimental values. In the inverse method, we minimize the difference between the known temperature distributions and some initially guessed temperature distributions using the GA. In the following pages we present the working procedure of the GA.

2.6 Principle of Genetic Algorithm

It has been mentioned earlier in Chapter 1 that the working principle of the GA is derived from the nature and is based upon the Darwin's theory of evolution. In other words, the evolutionary approach of the GA enables the worst individuals to get eliminated from the population and it ultimately results in a population having better characteristics befitting the imposed condition. This very similar analogy when applied in mathematical mode

gives rise to the GA. The process of the GA is analogous to biological evolution of any species in which successive generations are conceived, born and raised until they themselves become ready to reproduce. Thus a number of different operators as required for the evolution of individual in nature are required in the GA too. The exchange of information in the GA occurs by virtue of the genes. In a binary coded GA, the genes are represented using binary digits 0 and 1 and their different arrangement constitutes different strings. These strings represent an individual and the individuals constitute the

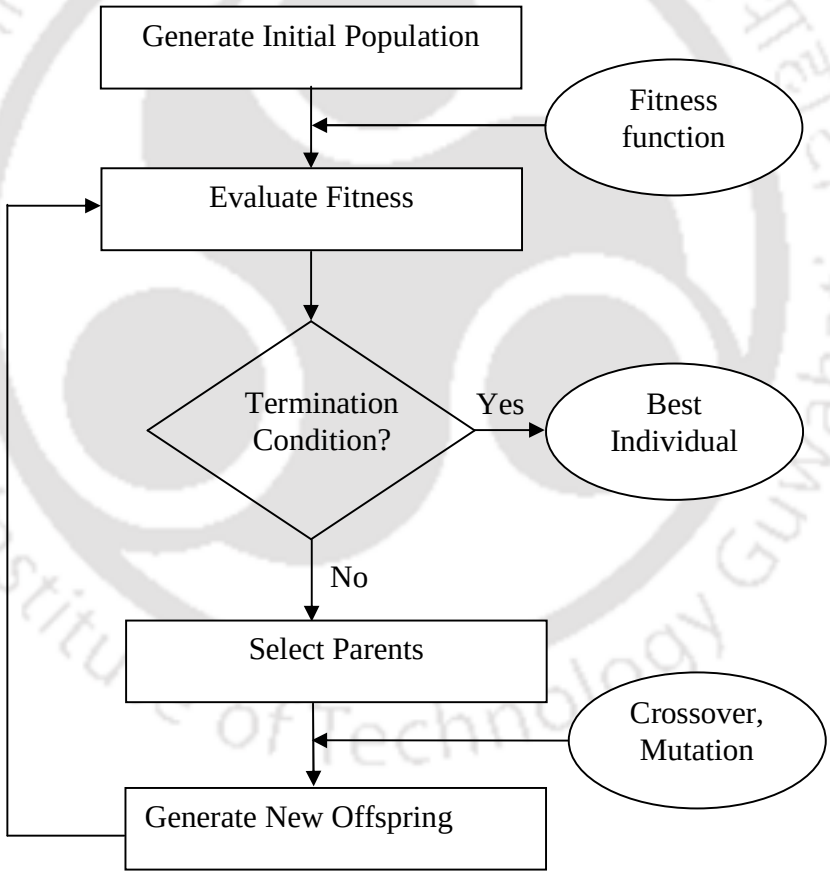

Figure 2.4: Flowchart of the genetic algorithm.

population. Figure 2.4 shows the flowchart of the GA. The following processes with necessary operators are involved in the GA and work together in a sequential order during the operation of the algorithm:

2.6.1 Generation of Initial Population

The very first step of any GA is to generate a group of individuals collectively known as the population. This population represents a group of solutions which give different values of the objective function to be optimized. Population undergoes gradual refinements in successive generations. The generations are mathematically analogous to the iterations. The higher the population size, the more the chance of getting good as well individuals/solution. This has the advantage of obtaining a higher proportion of better individuals/solutions and also, more number of bad individuals to get eliminated in successive generations of evolution.

2.6.2 Evaluation of Fitness

The next step of the algorithm is to obtain the fitness value of the individuals which in turn represent the value of the objective function to be optimized. It should be noted that the objective function may be a representation of cost, efficiency, weight, strength, error and so on. In our present study, the objective function is represented as the sum of square of errors between the measured and the exact temperature fields. The population having good fitness values is replicated in the next generation. Retaining the best individual in the next generation from the previous generation is determined by the elite count operator and the phenomenon is called elitism. Since the optimum or minimum value of the

objective function can not be initially determined in advance, accordingly the appropriate fitness limit too can not be determined in advance. So, a theoretical value of fitness needs to be prescribed and a minimum number of individuals whose fitness lies closer to the prescribed limit are replicated in the next generations. In our present work, the theoretical value of the required objective function is zero.

2.6.3 Reproduction, Crossover and Mutation

The other individuals which are not retained by the elite count operator undergo reproduction among themselves. The reproduction also known as selection is the first operator and it selects good individuals for mating. There are different types of selection schemes such as proportionate selection, ranking selection and tournament selection. In proportionate selection operator alternatively known as roulette-wheel selection, a string in current population is selected with a probability proportional to the string's fitness. In ranking selection scheme, all strings in a population is copied based upon increasing order of their best fitness or objective function value and ranked (1 for the best, 2 for the second best and so on). In tournament selection scheme, two strings are randomly chosen and better of the two is selected and if done systematically, the best string gets two copies in the mating pool.

Since crossover is required for the reproduction and the generation of new offspring, the same is handled by the crossover probability operator in the GA. The crossover can be of

single point, two point and multipoint depending upon the number of sites chosen. The main purpose of the crossover operator is to search the parameter space. Apart from this, the search is required to be carried out in such a manner that the information stored in the parent string is preserved to the maximum extent possible. In uniform crossover, each bit from either parent is selected with a probability of 0.5. However, minimum information is preserved between parent and children strings. In order to preserve some of the previously found good strings, not all strings in the population participate in the crossover operation. The crossover probability represents the number of individuals taking part in the crossover and its value lies from 0 to 1.0. For example, a crossover probability of 0.5 implies that 50% of the selected individuals will undergo crossover operation. A crossover probability of 1.0 or values closer to 1.0 is not preferred because it is better to keep some bad individuals too in the population. This is because these bad individuals can create better offspring in later generations.

The mutation operator maintains the diversity by randomly changing the genes in the string of the generated offspring. Like the crossover probability, the mutation probability also determines the number of individuals undergoing mutation process. In the binary coded GA, the mutation process makes the digit 0 to 1, and vice versa. The difference between the crossover and the mutation is that in the crossover the exchange of genes occurs between two randomly selected individuals and at a randomly selected site whereas in the mutation process, the change occurs within the individual. The main function of the mutation operator is to maintain diversity in the population.

2.6.4 Termination Condition

The fitness value is evaluated for the new population evolved from the processes mentioned in step 2 above. The algorithm is terminated when there is no change of fitness values from one generation to the next generation. A sufficiently good number of generations are needed to be evaluated for the same because the fitness value may get updated at a later stage if the algorithm is terminated at a premature time. The common practice of terminating the GA process is to study the variation of the objective function which in turn represents the fitness for a specified number of generations. The other, but most unlikely mode of termination is the attainment of a global maximum or global minimum of the value of the objective function. In the present work, the theoretically set global minimum value for the objective function is zero. Therefore, the algorithm gets automatically terminated if at any stage, the value of the objective function becomes zero and hence it will fetch out the best individual or solution.

2.7 Formulation of Inverse Problem

In transient conduction-radiation heat transfer problem, from the direct method, the temperature θ distributions are obtained from the knowledge of medium properties, initial condition and the boundary conditions. For the correct value of the unknown parameters, with given initial and boundary conditions, let $\tilde{\theta}_p$, $p=1,2,.....N$ be the known temperature at the west boundary of the p^{th} control volume. For the same initial and boundary conditions, in

the inverse problem, the objective is to estimate the correct values of the unknown parameters for the known temperature $\tilde{\theta}_p$ field. Initially a guessed value of unknown parameters is taken and then the guessed temperature field θ_p is calculated. Since θ_p is based on guess values of unknown parameters, the exact value $\tilde{\theta}_p$ and the estimated value θ_p will not be the same. To minimize the difference between $\tilde{\theta}_p$ and θ_p, an objective function J as given in the following equation is defined.

$$J = \sum_{p=1}^{N} \left(\tilde{\theta}_p - \theta_p \right)^2 \tag{2.58}$$

Similarly for a 2-D geometry the above equation is modified as below;

$$J = \sum_{p}^{N+1} \sum_{q}^{N+1} \left(\tilde{\theta}_{p,q} - \theta_{p,q} \right)^2 \tag{2.59}$$

In the above equation, $\tilde{\theta}_{p,q}$ is the exact temperature and $\theta_{p,q}$ is based on some guessed values of the unknown parameters at any lattice center (p,q) of a lattice in the LBM or a node of the control volume in the FVM (Fig. 2.1 and 2.2 a).

The accuracy of the estimated parameters depends on how accurately the temperature field is measured. If E is the error in the measurement of temperature $\theta_{measured}$ profile, then

$$\theta_{measured} = \tilde{\theta} \pm E \tag{2.60}$$

where $\tilde{\theta}$ is the exact temperature. With $\theta_{measured}$ defined as above in Eq. (2.60), if the measured temperature field contains error $\pm E$, in Eq. (2.58 and 2.59), $\tilde{\theta} = \theta_{measured}$. It

should be noted that a measurement error of $E = 2.0$, means that if the exact temperature is 500 K and the reference temperature is 400 K, then the measured temperature is 1,300 K with an error of 800 K. Therefore, the objective function with the inclusion of the measurement error takes the following form:

$$J = \left[\left(\tilde{\theta} \pm E\right) - \theta\right]^2 \tag{2.61}$$

Rearranging the above equation (Eq. 2.61) we obtain the following:

$$J = \left[\tilde{\theta} - \left(\theta \mp E\right)\right]^2 \tag{2.62}$$

It is clear from the expression Eq. (2.62) that for minimizing the objective function, the optimization algorithm must be robust enough to take care of increased uncertainties due to measurement errors. Below we mention the steps involved in solving the inverse problem.

2.8 Solution Methodology to Solve Inverse Problem

1. Obtain any temperature field from the direct method at all the time levels including the steady state. It is this field corresponding to which unknown parameters need to be obtained.
2. Induce perturbations on the above temperature field. Therefore, this becomes the measured temperature field or experimental data at all time levels.
3. Start with a guessed temperature field. This will correspond to some arbitrary values of the parameters to be determined.

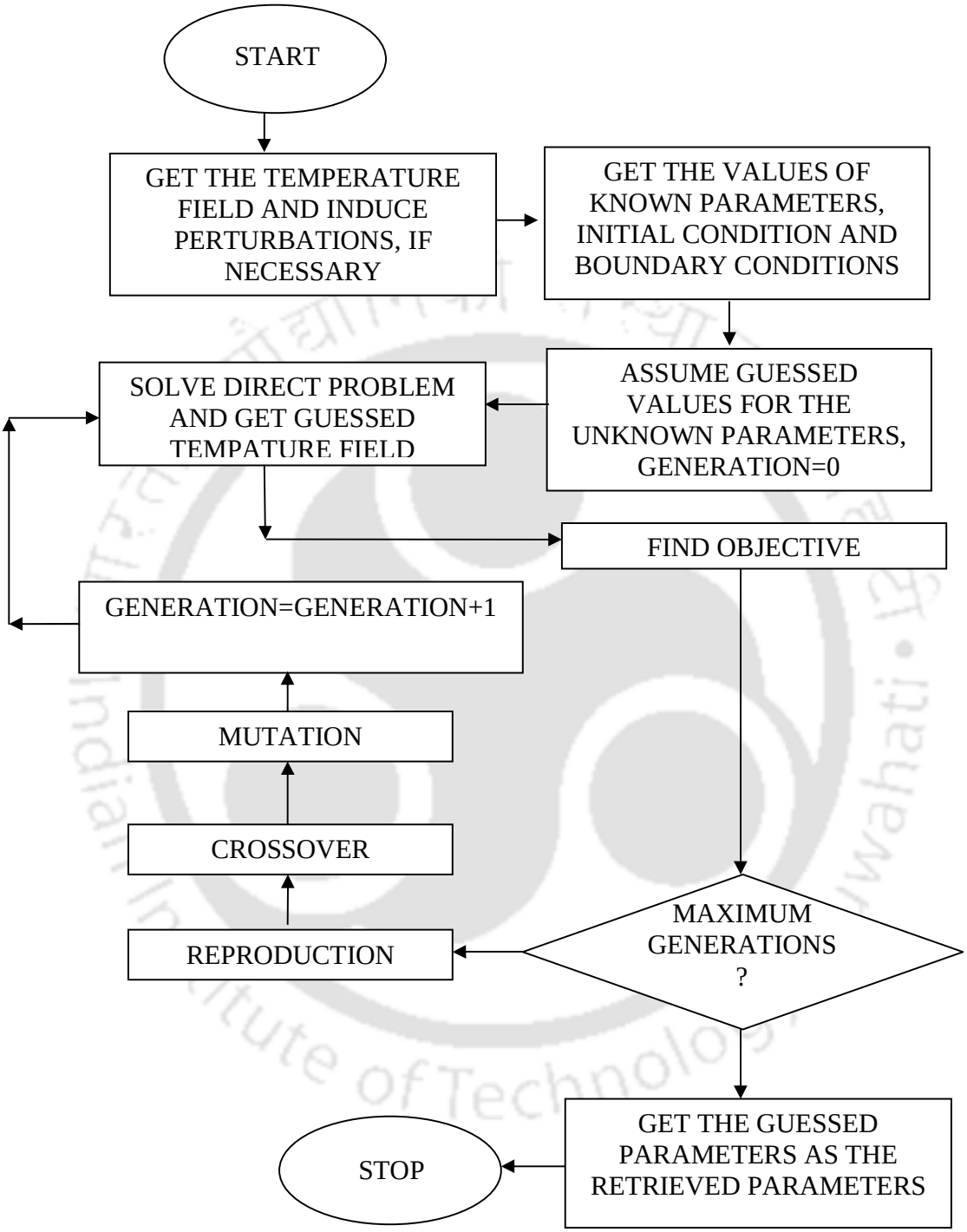

Figure 2.5: Solution methodology to solve the inverse problem.

4. Mininimize/ Regularize/ Optimize the objective function as given by Eq. 2.58 and 2.59.
5. Define the desired value of the objective function.Check if the objective function value changes in successive iterations.If the objective function value remains nearly constant for sufficient finite number of iterations terminate the algorithm.
6. Get the values of the unknown parameters.
7. If the objective function value keeps changing, discard the old values and assume other values of parameters and go to step 2.
8. A flowchart for solving an inverse problem is given in Fig. 2.5.

2.9 Summary

The present chapter comprehensively dealt with complete mathematical formulation of a conduction-radiation problem. It started with the direct problem involving the LBM and the FVM methods respectively to solve the energy equation and the equation of obtaining the radiative information. Then, the formulation of the inverse problem and the construction of the objective function were described for both 1-D and 2-D Cartesian geometries. The methodology of the GA for the optimization and the working nature were discussed. In the next chapter, we study the application of the inverse method to a transient conduction-radiation problem in a 1-D planar medium.

CHAPTER 3

Parameter Retrieval in a 1-D Transient Conduction-Radiation Problem

3.1 Introduction

This chapter deals with the estimation of thermophysical properties in a 1-D transient conduction-radiation problem. This type of problems finds applications in atmospheric science, insulation systems, welding processes, phase change phenomena, etc. [3, 7, 70]. Generally, these problems are transient in nature, and for estimating multiple parameters, their inverse analyses involve varying levels of complexities. Their solutions are generally not unique, as the same output can be obtained with more than one set of estimated parameters. This effect puts a limitation to the number of unknown parameters to be estimated in the inverse method. However, physical insights could guide the inverse formulation for feasible parameter estimation. The analyses of inverse conduction-radiation problems are done by some kind of regularization or optimization of either temperature distribution or radiative intensity distribution.

In the present chapter, simultaneous estimation of a combination of two parameters such as the conduction-radiation parameter, the boundary emissivity and the scattering albedo is done. The temperature field is calculated from the direct method using the LBM-FVM in which the LBM is used to solve the energy equation and the FVM is used to compute the radiative information. This temperature field is taken as the exact or experimental

values and random perturbations are imposed on the same. In the inverse method, the GA is used to minimize the objective function, which is represented by the summation of the square of errors between the exact and the guessed or the measured temperature field. The quality of the estimated parameters is studied for the effects of the optimization algorithm/GA parameters such as the crossover probability, the mutation probability and the numbers of generations. In order to establish the correctness of the estimated parameters in the inverse method using the LBM-FVM-GA, temperature fields are evaluated on the basis of the estimated parameters and compared with that obtained from the direct method. Further, a comparison of the CPU times involved in the direct method and the inverse method is also done. Detailed formulations for the analysis of a transient conduction-radiation problem in the direct and inverse methods have been presented in Chapter 2. In the following pages, we briefly provide the relevant formulations used for the inverse analysis of a 1-D transient conduction-radiation heat transfer problem.

3.2 Formulation

Consider a homogenous conducting-radiating planar participating medium as shown in Fig. 2.1. Initially, the system is at temperature T_E and for time $t > 0$, the west boundary is maintained at temperature $T_W \left(> T_E\right)$. The west and the east boundaries are diffuse-gray with emissivities ε_W and ε_E, respectively. β, ω and N are the extinction coefficient, the scattering albedo and the conduction-radiation parameter, respectively. The variations of the medium and the boundary properties with time are considered negligible. For the problem under consideration, the governing energy equation can be written as,

$$\rho C_p \frac{\partial T}{\partial t} = -\frac{\partial}{\partial x}\left(-k\frac{\partial T}{\partial x}\right) - \left(\frac{\partial q_R}{\partial x}\right) \tag{3.1}$$

The corresponding equation in the LBM-FVM formulation is given by the following

$$f_i\left(\vec{x}+\vec{c}_i\Delta t, t+\Delta t\right) = f_i\left(\vec{x},t\right) - \frac{\Delta t}{\tau}\left[f_i\left(\vec{x},t\right) - f_i^{(0)}\left(\vec{x},t\right)\right] - \frac{\Delta t w_i}{\rho c_p}\frac{\partial q_R}{\partial x} \tag{3.2}$$

where the divergence of radiative heat flux $\frac{\partial q_R}{\partial x}$ is expressed as

$$\frac{\partial q_R}{\partial x} = \beta(1-\omega)\left(4\pi\frac{\sigma T^4}{\pi} - G\right) \tag{3.3}$$

With non-dimensional distance x^*, temperature θ, conduction-radiation parameter N, incident radiation G^*, radiative heat flux Ψ_R and time ξ defined in the following way,

$$x^* = \frac{x}{X} \quad \theta = \frac{T}{T_W} \quad N = \frac{k\beta}{4\sigma T_W^3} \quad G^* = \frac{G}{\left(\sigma T_W^4/\pi\right)} \quad \Psi_R = \left(\frac{1}{4N}\right)\frac{q_R}{\sigma T_W^4} \quad \xi = \alpha\beta^2 t \tag{3.4}$$

in non-dimensional form, Eqs.(3.2) and (3.3) take the following form

$$f_i^*\left(\vec{x}^* + \vec{c}_i^*\Delta\xi, \xi+\Delta\xi\right) = f_i^*\left(\vec{x}^*,\xi\right) - \frac{\Delta\xi}{\tau^*}\left[f_i\left(\vec{x}^*,\xi\right) - f_i^{*(0)}\left(\vec{x}^*,\xi\right)\right] - \frac{\Delta\xi w_i}{4N}\frac{\partial\Psi_R}{\partial x^*} \tag{3.5}$$

$$\frac{\partial\Psi_R}{\partial x^*} = 4(1-\omega)\left(\theta^4 - \frac{G^*}{4\pi}\right) \tag{3.6}$$

For known values of medium properties, using the above formulations, we obtain the temperature θ distributions in the medium using the direct method as explained in the previous chapter. For the correct values of the set of parameters, in this study, first the exact temperature field is obtained by solving the energy equation of the transient conduction-radiation problem using the LBM in which the radiative information is

computed using the FVM. The temperature field which is obtained from the direct method serves as an exact result or experimental values to be used in the inverse analysis and to account for the noise/measurement error, perturbations are also imposed on this temperature field. Therefore, the temperature field becomes a measured temperature field. In order to minimize the difference between the exact temperature $\tilde{\theta}_p$ and the guessed temperature θ_p field, we define an objective function J as given below,

$$J = \sum_{p=1}^{N} \left(\tilde{\theta}_p - \theta_p \right)^2 \tag{3.7}$$

In the present work, based upon the population size, the guessed temperature θ_p field is generated randomly. Henceforth, the initial value of the objective function will be significantly high in comparison with the theoretical minimum value (zero). Further, to visualize the efficacy and robustness of the inverse methodology, we incorporate some measurement error to the exact temperature $\tilde{\theta}_p$ field, so as to evaluate the contribution of measurement error towards retrieved parameters. Also, the concept of measurement error would be also beneficial to provide larger insights upon the sensitivity of retrieved parameters on temperature distribution profiles. If E is the error in the measurement, the measured temperature $\theta_{measured}$ is given by the following,

$$\theta_{measured} = \tilde{\theta} + E \tag{3.8}$$

In order to minimize the objective function (Eq. (3.7)), in the present work, we have used the GA. The working procedure of the GA has been outlined in Chapter 2.

3.3 Results and Discussion

In the following pages, we present the results based on the inverse analysis of a transient conduction-radiation heat transfer problem in a planar medium. In this analysis, we have simultaneously estimated a combination of two properties of the medium such as the scattering albedo ω, the boundary emissivity ε and the conduction-radiation parameter N. In both the direct method and the inverse method, non-dimensional time step $\Delta\xi = 1.0\times10^{-4}$ was considered, and the steady-state condition was assumed to have been achieved when the maximum variation in temperature $\theta = \frac{T}{T_W}$ at any location between two consecutive time levels did not exceed 1.0×10^{-6}. The initial temperature of the system was taken to be $\theta_E = \frac{T_E}{T_W} = 0.5$ and for time $\xi > 0$, the west boundary was raised to a temperature $\theta_W = 1.0 = 2\theta_E$. In the LBM and the FVM, a maximum of 100 equal size lattices/control volumes and in the FVM, 10 equally spaced directions were found sufficient for grid and ray independent solutions. Below we study the effect of the optimization algorithm/ GA parameters on the quality of the estimated results.

Table 3.1: Combination of genetic parameters and measurement errors for different runs used in the inverse method.

Run	Crossover Probability	Mutation Probability	Measurement Error *E*
1	0.20	0.30	0.0
2	0.40	0.60	0.5
3	0.60	0.80	1.0
4	0.20	0.30	1.5
5	0.40	0.60	2.0
6	0.60	0.80	0.0
7	0.20	0.30	0.5
8	0.40	0.60	1.0
9	0.60	0.80	1.5
10	0.80	0.60	2.0

3.3.1 Effect of the GA Parameters

To realize the importance of the genetic parameters, in the present study, in the GA, study was made for three different combinations of crossover and mutation probabilities. For the present investigation, the population size was taken to be 50. For runs 1-10, Table 3.1 shows different combinations of crossover and mutation probabilities along with measurement errors. In the present work, we have studied three different values of the crossover probabilities, viz., 0.20, 0.40 and 0.60. The three values of the mutation probability considered were 0.30, 0.60 and 0.80. The measurement errors *E* introduced was in the range 0.0 to 2.0.

In Figs. 3.1 and 3.2, for runs 1-10 given in Table 3.1, we study the variations of the best fitness against the number of generations. In Figs. 3.1a-c, results are shown for three different combinations of the conduction-radiation parameter *N* and the scattering

albedo ω. In Figs. 3.2a-c, the same are given for three different combinations of N and west boundary emissivity ε_W. It is observed from Figs. 3.1 and 3.2 that beyond 200 generations, no significant change in the best fitness take place, and thus this was taken as one of the stopping criterion. It is to be noted that while presenting the comparisons in Figs. 3.1 and 3.2, for simplicity we have divided the values of the best fitness at each generation by 10^3. It is also observed that, in some cases, no significant change in the best fitness was observed even below 200 generations. Based on these evaluations, it was concluded that 200 generations were sufficient for a population size of 50, and solution near to the global minimum was achieved.

To demonstrate the workability of the LBM-FVM-GA combination in the inverse method, for 10 different runs with crossover and mutation probabilities along with measurement errors as given in Table 3.1, in Table 3.2, we compare the exact and the estimated results for three different combinations of the conduction-radiation parameter N and the scattering albedo ω, viz., (N, ω) = (0.01, 0.1), (0.01, 0.5) and (1.0, 0.1). In Table 3.2, we also compare results for three different combinations of the conduction-radiation parameter N and the emissivity of the west boundary ε_W, viz., (N, ε_W) = (0.01, 0.1), (0.01, 0.5) and (0.01, 0.9). For (N, ω) combinations, we considered extinction coefficient $\beta = 1.0$ and $\varepsilon_W = \varepsilon_E = 1.0$, while for (N, ε_W) combinations, $\beta = 1.0$, $\varepsilon_E = 1.0$ and $\omega = 0.0$ were considered. From Table 3.2, it is

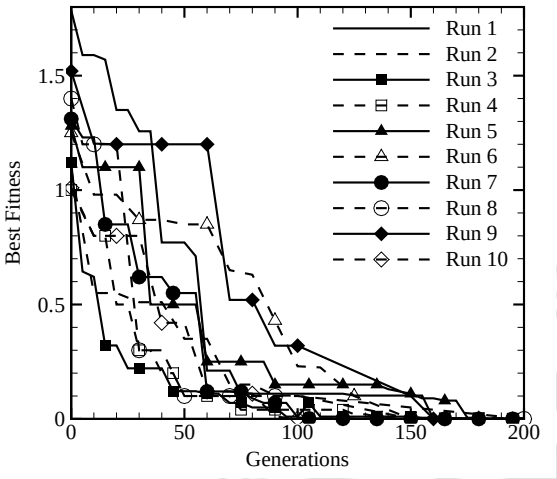

ERROR: undefined
OFFENDING COMMAND: -

STACK:

CHAPTER 4

Parameter Retrieval in a 2-D Transient Conduction-Radiation Problem

4.1 Introduction

In this chapter, an inverse analysis has been done to retrieve unknown parameters in a transient conduction-radiation heat transfer problem in a 2-D rectangular enclosure. Many long enclosures can be mathematically approximated as 2-D rectangular enclosures. The changes in thermal field are found only along two coordinate directions, viz., height and width. Hence, the analysis of such geometry is done as a 2-D problem.

In the present work, an inverse analysis has been done for a 2-D transient conduction-radiation problem. In the direct method, the radiative information has been computed using the FVM and the LBM has been used to solve the energy equation. In the inverse method, the temperature field obtained in the direct method has been used for the simultaneous retrieval of three unknown parameters, viz., the scattering albedo, the boundary emissivity and the conduction-radiation parameter. Effects of measurement errors in the measured temperature field have been accounted. In the inverse analysis, the energy equation has been solved using the LBM in which the FVM has been used to provide the radiative information, and the optimization has been done using the GA. A

detailed study has been done to investigate the effects of the GA parameters, viz., the crossover probability, the mutation probability, the population size and the number of generations. CPU times in the direct and the inverse methods have also been compared.

4.2 Formulation

A 2-D rectangular enclosure (Fig. 4.1) containing an absorbing, emitting and scattering medium is considered. The boundaries of the enclosure are diffuse gray. Initially, the system is at a uniform temperature $T_E = T_W = T_N = T_S = T_0$. For time $t > 0$, the south boundary is maintained at temperature $T_S > T_0$. For the problem under consideration, the energy equation is written as,

$$\rho c_p \frac{\partial T}{\partial t} = k\left(\frac{\partial^2 T}{\partial x^2} + \frac{\partial^2 T}{\partial y^2}\right) - \nabla \cdot \vec{q}_R \tag{4.1}$$

In the LBM with the BGK approximation, the corresponding form of the governing energy equation (Eq. (4.1)) gets modified to the following,

$$f_i\left(\vec{r} + \vec{c}_i \Delta t, t + \Delta t\right) = f_i\left(\vec{r}, t\right) - \frac{\Delta t}{\tau}\left[f_i\left(\vec{r}, t\right) - f_i^{(0)}\left(\vec{r}, t\right)\right] - \left(\frac{\Delta t w_i}{\rho c_p}\right)\nabla \cdot \vec{q}_R \tag{4.2}$$

where, $\vec{r}$ represents position of the lattice node in the 2-D geometry. For a general conduction-radiation problem, development of Eq. (4.2) has been described in Chapter 2. For the present problem, we have used the D2Q9 lattice.

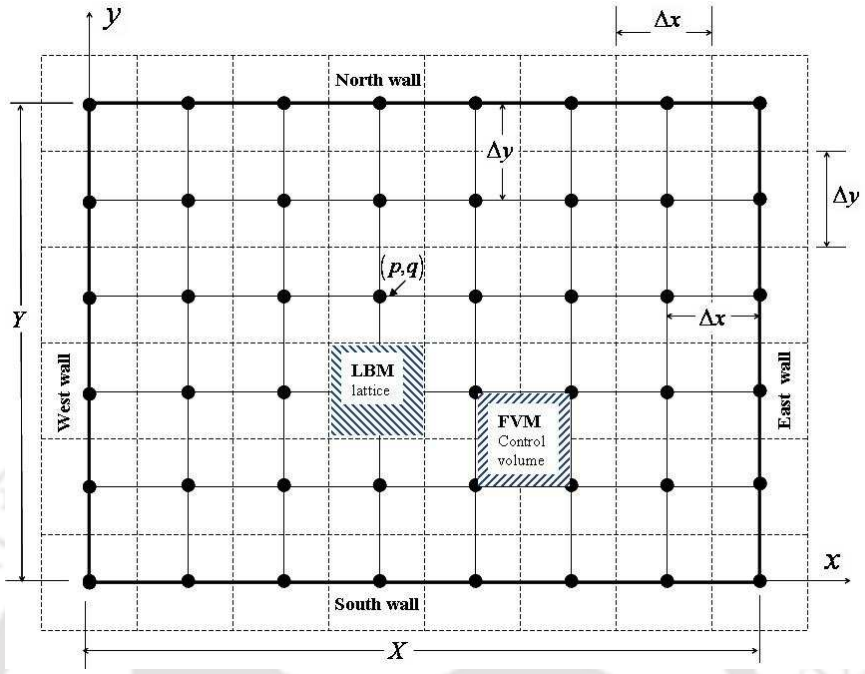

Figure 4.1: Distribution of the lattices in the LBM and the control volumes in the FVM for the 2-D geometry.

For generalization of Eq. (4.2), the non-dimensionalization has been done in the following manner

$$r^* = \frac{r}{L_{\text{ref}}},\quad \theta = \frac{T}{T_{\text{ref}}},\quad N = \frac{k\beta}{4\sigma T_{\text{ref}}^3},\quad G^* = \frac{G}{\left(\sigma T_{\text{ref}}^4 / \pi\right)},\quad \xi = \alpha\beta^2 t,\quad \tau^* = \frac{3}{\left|\vec{e}_i^{\,*}\right|^2} + \frac{\Delta\xi}{2} \tag{4.3}$$

In non-dimensional form, Eq. (4.2) is written as

$$f_i^*\left(\vec{r}^* + \vec{c}_i^*\Delta\xi, \xi + \Delta\xi\right) = f_i^*\left(\vec{r}^*, \xi\right) - \frac{\Delta\xi}{\tau^*}\left[f_i^*\left(\vec{r}^*, \xi\right) - f_i^{*(0)}\left(\vec{r}^*, \xi\right)\right] - \left(\frac{\Delta t w_i}{4N}\right)\nabla\cdot\vec{\Psi}_R \tag{4.4}$$

In the above equation, the divergence of non-dimensional radiative heat flux expressed as

$$\nabla\cdot\vec{\Psi}_{\text{R}} = 4(1-\omega)\left[\theta^4 - \frac{G^*}{4\pi}\right] \tag{4.5}$$

In the present work, the radiative information $\nabla \cdot \vec{\Psi}_R$ has been computed using the FVM. Using the above formulations, the temperature θ field at different time levels ξ can be obtained using the direct method in which the energy equation has been solved by the LBM and the radiative information has been computed using the FVM.

In the inverse method, simultaneous estimation of three parameters, viz., the scattering albedo ω, the south boundary emissivity ε_S and the conduction-radiation parameter N has been done. In this case, the objective function to be minimized using the GA is represented by the following equation

$$J = \sum_{p}^{N+1} \sum_{q}^{N+1} \left(\tilde{\theta}_{p,q} - \theta_{p,q} \right)^2 \tag{4.6}$$

where the subscripts p and q (Fig. 4.1) are the indices for the lattice centre in the LBM and the node in the FVM. With the inclusion of measurement errors (E), the measured temperature profile ($\theta_{measured} = \tilde{\theta} + E$) and the exact one are minimized in the same manner as discussed in Chapter 3. In the following pages, we provide results of the inverse analysis in which three parameters such as the conduction-radiation parameter, the scattering albedo and the boundary emissivity are simultaneously retrieved and the extinction coefficient was fixed.

4.3 Results and Discussion

In heat transfer problems involving transient conduction-radiation, the thermophysical properties of the participating media such as the conduction-radiation parameter, the

scattering albedo, the emissvity, etc., influence the local temperature distributions. As observed earlier in the investigation of a 1-D planar media that the temperatures are generally higher for lower values of the conduction-radiation parameter, scattering albedo and higher values of the boundary emissivity. In this case too, we perform an inverse analysis for the case of a 2-D Cartesian geometry and also study the influence of the thermophysical properties on the temperature field.

In the following pages, we present results of the simultaneous estimation of three parameters, viz., the scattering albedo ω, the conduction-radiation parameter N, and the south boundary emissivity ε_S by the inverse method using the LBM-FVM-GA. To establish the correctness of the estimated values, the centreline temperature distributions at different time levels obtained by the direct method and the inverse method have been compared. Towards this end, some sample results have been also compared with the benchmark results available in the literature [72-74]. Subsequently, effects of the crossover probability, the mutation probability, the number of generations and the population size on the estimated parameters with and without measurement errors have also been investigated. Variation of computational time with increasing the number of generations as well as increasing the population size has also been reported.

In order to study the effect of the population size, in the GA, the population size was varied from 25 to 100, and beyond 200 generations, no significant change in the value of the objective function was observed. Since the genetic parameters, such as the crossover probability, the mutation probability, the population size and the number of generations

significantly affect the accuracy of the estimated parameters, the proper selection of these parameters is important. The following pages provide results which show effects of these genetic parameters on the accuracy of the estimated values along with the computational time.

In the LBM, 21×21 lattices were used and since in the FVM, the number of CVs in every coordinate direction remains one less, in the FVM, this number was 20×20. In the FVM, the number of directions was $M_\delta \times M_\phi = 4\times8$. No significant variation in temperature θ was observed when the numbers of lattices, control volumes and directions were further increased. The steady-state condition was assumed when the maximum variation in temperature $\theta = \dfrac{T}{T_S}$ at any location between two consecutive time levels did not exceed 1.0×10^{-6}. The initial temperature of the system was taken to be $\theta_E = \theta_W = \theta_N = \theta_S = 0.5$ and for time $\xi > 0$, the south boundary was raised to a temperature $\theta_S = 1.0 = 2\theta_E = 2\theta_W = 2\theta_N$.

4.3.1 Retrieval of Parameters without Measurement Error

To investigate the workability of the LBM-FVM-GA combination, 6 sets of different parameters $(\omega, N, \varepsilon_S) = (0.8, 0.03, 0.9), (0.3, 0.01, 0.1), (0.0, 0.01, 0.5), (0.0, 1.0, 1.0), (0.0, 0.1, 1.0)$ and $(0.0, 0.01, 1.0)$ were estimated. For each of the 6 cases, five different runs were taken. The objective function was minimized on the basis of SS temperature field only. In this case, parameters were estimated considering that the measured

Table 4.1: Comparison of exact and estimated values of parameters for (ω, N, ε_S) = (0.8, 0.03, 0.9), (0.3, 0.5, 0.1), (0.0, 0.01, 0.5), (0.0, 1.0, 1.0), (0.0, 0.1, 1.0) and (0.0, 0.01, 1.0).

Runs	Exact values			Inverse Analysis results		
	ω	N	ε_S	ω	N	ε_S
1	0.8	0.03	0.9	0.7657	0.0353	0.7915
2				0.7024	0.0252	0.9209
3				0.8699	0.0338	0.8835
4				0.7910	0.0243	0.8812
5				0.8094	0.0277	0.9303
Average				**0.7876**	**0.0292**	**0.8814**
1	0.3	0.01	0.1	0.3662	0.0093	0.1319
2				0.2533	0.0115	0.0877
3				0.2447	0.0142	0.0971
4				0.3119	0.0088	0.1080
5				0.3125	0.0104	0.0912
Average				**0.2977**	**0.0108**	**0.1031**
1	0.0	0.01	0.5	0.0005	0.0114	0.6024
2				0.0118	0.0168	0.4739
3				0.0021	0.0095	0.4595
4				0.0007	0.0091	0.5311
5				0.0029	0.0108	0.4473
Average				**0.0036**	**0.0115**	**0.5028**
1	0.0	1.0	1.0	0.0066	0.8722	0.8841
2				0.0141	0.7957	0.9336
3				0.0080	0.9638	0.9972
4				0.0110	0.9442	0.8713
5				0.0053	0.8990	0.9008
Average				**0.0090**	**0.8949**	**0.9174**
1	0.0	0.1	1.0	0.0106	0.0739	0.9074
2				0.0009	0.0910	0.8982
3				0.0077	0.0988	0.9914
4				0.0115	0.1266	0.9458
5				0.0038	0.1018	0.9741
Average				**0.0069**	**0.0984**	**0.9433**
1	0.0	0.01	1.0	0.0087	0.0096	0.8861
2				0.0121	0.0092	0.9736
3				0.0038	0.0108	0.9055
4				0.0024	0.0115	0.9972
5				0.0165	0.0133	0.9048
Average				**0.0087**	**0.0108**	**0.9334**

temperature field contained no error $(E = 0.0)$ and the population size was taken to be 50, the number of generations was 100, the crossover probability was 0.8 and the mutation probability was 0.03. Results are shown in Table 4.1. Estimated values of the parameters have been found to vary with runs. In other words, even if the GA parameters remain the same, the solution generated is not unique. Thus, the averages over the 5 runs have been taken. The corresponding averaged estimated values for different parameters are also shown in Table 4.1. It is observed that the averaged estimated values are in good agreement with the exact ones.

Figs. 4.2-4.3 show the comparisons of the centerline temperature distribution at three different time levels including the steady-state (SS) computed from the estimated values of the parameters obtained using the inverse method with that calculated by the direct method. In the inverse method, the genetic parameters used are the same as taken for results in Table 4.1 and the measurement error is $E = 0.0$. It is seen that, at all time levels, the centerline temperature θ and $\tilde{\theta}$ distributions in the medium at different instants ξ are in good agreement. In Figs. 4.2 and 4.3, steady-state times in the direct and the inverse methods are also shown and they are found to be comparable. This indicates that the estimated values of the parameters obtained by the inverse analysis are in good agreement with the exact ones and also the temperature fields agree very well with each

Table 4.2: Comparison of steady-state centerline $\left(x/X = 0.5\right)$ temperature at three locations in a black square enclosure; $\omega = 0.0, \beta = 1.0$ and $\varepsilon_S = 1.0$.

N	Centreline T/T_S at y/Y	Wu and Ou [72]	Yuen and Takara [73]	Mishra *et al.* [74]	Direct method	Inverse method
1.0	0.3	0.733	0.737	0.734	0.739	0.736
	0.5	0.630	0.630	0.630	0.632	0.631
	0.7	0.560	0.560	0.564	0.566	0.563
0.1	0.3	0.760	0.763	0.759	0.761	0.759
	0.5	0.663	0.661	0.663	0.664	0.660
	0.7	0.590	0.589	0.594	0.596	0.592
0.01	0.3	0.791	0.807	0.789	0.789	0.786
	0.5	0.725	0.726	0.725	0.727	0.725
	0.7	0.663	0.653	0.666	0.668	0.664

other. It is also observed from Fig. 4.3 that with a reduction in the value of the conduction-radiation parameter N, the SS is achieved fast due to the dominance of radiation over conduction and thus, the temperature values are higher.

Table 4.2 compares the centreline $\left(\frac{x}{X} = 0.5, \frac{y}{Y}\right)$ temperature $\theta = \frac{T}{T_S}$ at three different locations viz. y/Y = 0.3, 0.5, and 0.7 obtained from the direct method and the inverse method. These values are compared against those of Wu and Ou [72], Yuen and Takara [73] and Mishra *et al.* [74]. For this comparison, in the inverse method, the same set of genetic parameters as used for results in Table 4.1 was used. It is observed that the results of the inverse method are in close agreement with that of the direct method.

To illustrate the variation of the objective function with increase in the number of generations, a comparison has been shown in Figs. 4.4 and 4.5. The analysis has been done for five different runs taken during the inverse analysis. It is to be noted that while making comparison in Figs. 4.4 and 4.5, the fitness value of the objective function is calculated based on the SS temperature distribution. It is observed from the figures that for the selected set of GA parameters, in the inverse analysis, the initial values of the objective function are invariably less than unity. This is due to reason that in the present case study, the exact field $\tilde{\theta}$, which is used in the objective function deviates less from the initially guessed field θ. Therefore, the errors between the initially guessed temperature field θ and the exact temperature field $\tilde{\theta}$ are lesser in magnitude. It is seen that upto 100 generations, the value of the fitness function converges to a satisfactory minimum value. Therefore, compared to the initial population, after approximately 100 generations, a better population has been developed by the GA. This in turn establishes that the temperature field obtained from the estimated values of the parameters and the exact temperature field $\tilde{\theta}$ are in good agreement with each other.

With 100 generations, Fig. 4.6a presents the variation of the CPU time (second) with the population size. In Fig. 4.6b, with population size of 50, the variation of the CPU time with the number of generations has been shown. Results in Figs. 4.6a and 4.6b are shown for $\omega = 0.0, N = 0.01, \varepsilon_S = 1.0$. All runs were taken on Pentium (R) 4, 2.8 GHz, 248 MB RAM at 266 MHz. It is observed from Figs. 4.6a and 4.6b that the CPU time is directly proportional to the number of generations as well as the population size. This is due to the reason that a gradual refinement of the objective function takes place with increase in

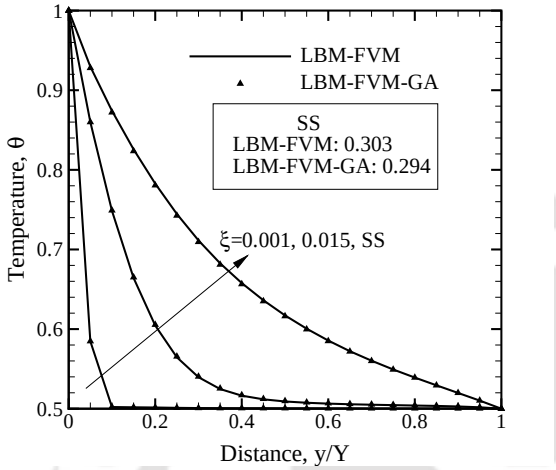

ERROR: undefined
OFFENDING COMMAND:

STACK:

CHAPTER 5

Inverse Analysis of Conduction-Radiation Problems with Varying Complexities

5.1 Introduction

In the previous chapters, estimation of thermophysical properties was done for 1-D and 2-D transient conduction-radiation heat transfer problems involving constant thermal conductivity, Fourier conduction and constant temperature boundary conditions. In this chapter, an inverse analysis is carried out for the estimation of unknown parameters and/or boundary conditions in three different types of transient conduction-radiation heat transfer problems involving varying level of complexities/ non-linearities. The problems considered are non-Fourier conduction-radiation problem, variable thermal conductivity conduction-radiation problem and conduction-radiation problem involving mixed boundary conditions. The consideration of non-Fourier effect incorporates an additional non-linearity in the energy equation appearing in the form of an extra term. Similarly, the incorporation of variable thermal conductivity also induces an extra non-linearity in the energy equation. The mixed boundary condition type problem being different than the previous problems is investigated at the end. Therefore, the trend is to gradually shift the study towards increasing non-lienearities in the chosen problems. In many practical/real

time problems, however, simplifying assumptions are used. In many problems, heat transfer by conduction is governed by the Fourier's law. In Fourier heat conduction, effects of any thermal disturbances in the system which can either be in the form of a sudden rise in boundary temperatures or a sudden appearance of a heat source at any location in the medium, propagate with infinite speed and hence establishes instantaneously. This assumption is not universally applicable in all situations. For example, the validity of the Fourier's law of heat conduction breaks down when we consider heat transport through a processed meat/skin [80]. Further, at a very low temperature, heat transport by conduction is not governed by Fourier's law [77-79]. When any material is subjected to a pulse radiation, at short time levels, a discontinuity in the temperature profile is observed, which cannot be explained through the Fourier's law of heat conduction [82].

In many transient conduction-radiation heat transfer problems, thermal conductivity is assumed constant. However, this assumption is invalid for the heat transfer analysis of metals and the applications involving very high temperatures in which the effect of thermal radiation becomes considerably high. Thus the assumption of constant thermal conductivity can not yield correct temperature field and the effect of variable thermal conductivity needs to be accounted for. Thirdly, many problems involve more than one type of boundary conditions in which the boundaries are maintained under different conditions such as in the heating chambers where heat flux is prescribed at one or more boundaries and the other boundaries remain subjected to some finite temperatures.

In the present chapter, we study three different classes of transient conduction-radiation heat transfer problems, viz., non-Fourier, variable conductivity and mixed boundary condition type. In non-Fourier transient conduction-radiation problem, we have simultaneously estimated two unknown parameters, viz., the extinction coefficient and the conduction-radiation parameter. In the transient conduction-radiation problem involving variable conductivity, we have simultaneously estimated different combinations of two unknown parameters, viz., the extinction coefficient, the scattering albedo and the conduction-radiation parameter. However, in the inverse analysis of transient conduction-radiation with mixed boundary condition, we have simultaneously estimated two unknown boundary conditions, viz., the boundary heat flux and the boundary emissivity. In the following pages, we provide the formulations for three problems considered for the inverse analysis, viz., the transient non-Fourier conduction-radiation heat transfer problem, the transient conduction-radiation heat transfer problem with variable thermal conductivity and the transient conduction-radiation heat transfer problem with mixed boundary condition.

5.2 Formulation of a Non-Fourier Conduction-Radiation Problem

Let us consider a planar participating medium as shown in Fig. 2.1. Its thermophysical and optical properties are constant. The initial temperature of the system is T_{ref}. For time $t > 0$, the west and the east boundaries of the medium are maintained at temperature $T_W \left(> T_{\text{ref}}\right)$ and $T_E \left(= T_{\text{ref}}\right)$, respectively. The boundaries of the medium are

diffuse gray. The thermophysical and optical properties of the conducting-radiating medium are assumed to be constant. For the problem under consideration, the governing energy equation is given by the following equation,

$$\rho c_p \frac{\partial \mathrm{T}}{\partial t} = -\frac{\partial q_C}{\partial x} - \frac{\partial q_R}{\partial x} \tag{5.1}$$

where ρ is the density, c_p is the specific heat, q_C is the conductive heat flux and q_R is the radiative heat flux. In the present analysis, it is assumed that the conduction wave front q_C takes some finite time to establish itself in the medium, and thus the assumption of the infinite propagation speed of the conduction wave as considered in the Fourier heat conduction will not be applicable for the non-Fourier heat conduction. The radiation wave front q_R propagates with the speed of light $\left(3\times10^8\ \mathrm{ms}^{-1}\right)$, and thus for the time-scale considered in the present study, radiative transfer is an instantaneous process.

With finite propagation speed of the conduction wave front, the non-Fourier heat conduction equation can be expressed as below [77, 78]

$$\Gamma \frac{\partial q_{\mathrm{C}}}{\partial t} + q_{\mathrm{C}} = -k \frac{\partial T}{\partial x} \tag{5.2}$$

where $\Gamma = \dfrac{\alpha}{C^2}$, is the thermal relaxation time, α is the thermal diffusivity and C is the speed of the conduction wave front.

Using Eq. (5.2), the energy equation takes the following form [123]

$$\left(\rho c_p\right)\left(\Gamma \frac{\partial^2 T}{\partial t^2} + \frac{\partial T}{\partial t}\right) = k \frac{\partial^2 T}{\partial x^2} - \frac{\partial q_R}{\partial x} - \Gamma\left[\frac{\partial}{\partial t}\left(\frac{\partial q_R}{\partial x}\right)\right] \tag{5.3}$$

In Eq. (5.3), the divergence of radiative heat flux $\frac{\partial q_R}{\partial x}$ is expressed as the following [123]

$$\frac{\partial q_R}{\partial x} = \beta(1-\omega)\left(4\pi\frac{\sigma T^4}{\pi} - G\right) \tag{5.4}$$

where β is the extinction coefficient, ω is the scattering albedo and G is the incident radiation.

In non-dimensional form, defining time ξ, distance x^*, temperature θ, conductive heat flux Ψ_C, radiative heat flux Ψ_R, conduction-radiation parameter N and incident radiation G in the following way,

$$\xi = \frac{Ct}{X} \qquad x^* = \frac{x}{X} \qquad \theta = \frac{T}{T_{\text{ref}}} \qquad \Psi_C = \frac{q_C}{\sigma T_{\text{ref}}^4}$$

$$\Psi_R = \frac{q_R}{\sigma T_{\text{ref}}^4} \qquad N = \frac{kC}{4\alpha\sigma T_{\text{ref}}^3} \qquad G^* = \frac{G}{\sigma T_{\text{ref}}^4/\pi} \tag{5.5}$$

In non-dimensional form, Eq. (5.4) is written as [123]

$$\frac{1}{A}\frac{\partial^2\theta}{\partial\xi^2} + \frac{\partial\theta}{\partial\xi} = \frac{1}{A}\frac{\partial^2\theta}{\partial\xi^2} - \frac{1}{4N}\left[\frac{\partial\Psi_R}{\partial x^*} + \frac{1}{A}\frac{\partial}{\partial\xi}\left(\frac{\partial\Psi_R}{\partial x^*}\right)\right] \tag{5.6}$$

where $A = \frac{XC}{\alpha}$.

In non-dimensional form Eq. (5.4) is written as [123]

$$\frac{\partial\Psi_R}{\partial x^*} = \left(\frac{L\beta(1-\omega)}{\pi}\right)\left(4\pi\theta^4 - G\right) \tag{5.7}$$

In the present work, we compute $\frac{\partial \Psi_R}{\partial x^*}$ using the FVM and the LBM is employed to solve the energy equation.

The formulation of the FVM to compute the information about the volumetric radiation $\frac{\partial \Psi_R}{\partial x^*}$ remains the same as explained in Chapter 2, hence we do not discuss the same in this section. Below the LBM formulation for the solution of the energy equation for a non-Fourier conduction-radiation problem is provided.

In the LBM, in non-dimensional form, equation describing non-Fourier conduction and radiation heat transfer is given by the following [123]

$$f_i^*\left(\vec{x}^* + \vec{c}_i\,\Delta\xi, \xi + \Delta\xi\right) = f_{i\,i}^*\left(\vec{x}^*, \xi\right) - \frac{\Delta\xi}{\tau^*}\left[f_{i\,i}^*\left(\vec{x}^*, \xi\right) - f_i^{*(0)}\left(\vec{x}^*, \xi\right)\right] - 2\Delta\xi\, y_i c_i^* \Psi - \left(\frac{\Delta\xi\, w_i}{4N}\right)\frac{\partial \Psi_R}{\partial x^*} \tag{5.8}$$

where f_i^* is the non-dimensional particle distribution function, $c_i^* = \frac{\Delta x^*}{\Delta\xi}$ is the velocity, τ is the non-dimensional relaxation time and $f_i^{*(0)}$ is the equilibrium distribution function. For a planar medium problem under consideration, with D1Q2 lattice, $b = 2$ and the non-dimensional relaxation time τ^* is computed from the following[119]

$$\tau^* = \frac{1}{\left(\frac{\Delta x^*}{\Delta\xi}\right)^2} + \frac{\Delta\xi}{2} \tag{5.9}$$

To solve Eq. (5.8), an equilibrium distribution function is required, which for the non-Fourier conduction-radiation problem can be written as [119]

$$f_i^{*(0)} = w_i\theta + y_i c_i \Psi \tag{5.10}$$

where,

$$w_1 = w_2 = y_1 = y_2 = \frac{1}{2} \tag{5.11}$$

With known thermophysical properties and the boundary conditions as mentioned above, using the LBM-FVM formulations, the non-dimensional temperature θ distributions at different time levels ξ can be obtained from the direct method. With the known temperature θ field, simultaneous estimation of two unknown parameters is done in the inverse method. The methodology of obtaining the temperature θ distributions, implementation of the measurement errors and the procedure for formulating the objective function to be minimized using the GA remains similar to the case involving conduction-radiation problem with Fourier heat conduction described in the previous chapter, and hence the same are not repeated here. In the following pages we provide the results of the non-Fourier conduction-radiation problem. In the inverse analysis, the two parameters which are retrieved are the conduction-radiation parameter and the extinction coefficient. The scattering albedo and the boundary emissivity are fixed.

5.3 Results and Discussion on Inverse Non-Fourier Transient Conduction Radiation Problem

In the following pages, we present results of the inverse analysis. The boundaries of the planar medium (Fig. 2.1) are assumed black. Initially, the entire system is at a finite temperature $T_{\text{ref}} = T_E$. With this, the non-dimensional initial temperature is $\theta(x^*, 0) = \theta_E$. For time $t > 0$, the west boundary is maintained at a higher temperature $T_W = 2T_E$. In non-dimensional form, at time $\xi > 0.0$, the east and the west boundaries are at temperatures θ_E and $\theta_W = 2\theta_E$, respectively. The non-dimensional velocity $c_i = \dfrac{\Delta x^*}{\Delta \xi}$ is considered to be unity. Therefore, the non-dimensional time step $\Delta\xi = \Delta x^*$ is taken for the analysis. In Table 5.1, we present results of grid and ray independency tests. For this, at time $\xi > 0.0$, we set the non-dimensional temperatures of the west and the east boundaries at $\theta_W = 1.0$ and $\theta_E = 0.5$, respectively. We test the temperature θ distributions at time $\xi = 0.60$ and at three different locations viz. $x^* = 0.20, 0.40$ and 0.80. It is observed from Table 5.1 that beyond 100 control volumes and 12 rays, there is no significant change in the temperature θ distributions. Therefore, in the present work, we have provided the results considering 100 control volumes and 12 rays.

Table 5.1: The effect of the number of lattices in the LBM and control volumes in the FVM and number of discrete directions on temperature distribution at three different locations; $\xi = 0.60$, $\beta = 0.5$, $\omega = 0.8$, N=0.01 and $\varepsilon_1 = \varepsilon_2 = 1.0$; $T_1 = 1.0$ and $T_2 = 0.5$.

Control volumes / lattices	Number of directions M_δ	$x/X = 0.20$	$x/X = 0.40$	$x/X = 0.80$
		LBM-FVM	LBM-FVM	LBM-FVM
Effect of control volumes/lattices				
25	12	0.8706	0.8434	0.7191
50		0.8812	0.8451	0.7164
100		0.8862	0.8465	0.7154
200		0.8886	0.8473	0.7150
Effect of number of directions M_δ				
100	6	0.8682	0.8286	0.7041
	12	0.8862	0.8465	0.7154
	24	0.8913	0.8500	0.7174

To check the accuracy of the direct problem involving the LBM and the FVM, in Fig. 5.1, we compare the temperature θ distributions with that of Chu *et al*. [85]. In this case, for time $\xi > 0.0$, the non-dimensional temperatures of the west and the east boundaries are kept at $\theta_W = 1.0$ and $\theta_E = 0.0$, respectively. For extinction coefficient $\beta = 1.0$ and scattering albedo $\omega = 0.50$, this comparison has been carried out at two different time steps, viz., $\xi = 0.30$ and 0.60. Three different cases for conduction-radiation parameter, viz., $N = 2.5, 0.25$ and 0.025 have been investigated. It is observed from Fig. 5.1 that the temperature θ distributions obtained from the direct method compare very well with

those given by Chu *et al*. who have solved the same problem using the McCormack explicit predictor-corrector scheme and P_3 approximation.

In the following pages, we present the results for the inverse analysis using the LBM-FVM in conjunction with the GA. For this analysis, at time $\xi > 0.0$, we maintain the non-dimensional temperatures of the west and the east boundaries at $\theta_W = 1.0$ and $\theta_E = 0.5,$ respectively. In the direct method involving the LBM and the FVM, for extinction coefficient $\beta = 0.50,$ scattering albedo $\omega = 0.80$ and conduction-radiation parameter $N = 0.01,$ we obtain the temperature θ distributions at two different time levels, viz., $\xi = 0.30$ and 0.60. With the temperature θ distributions available from the direct method in the inverse method, we simultaneously estimate two parameters, viz., the extinction coefficient β and the conduction-radiation parameter N.

5.3.1 Effects of GA Parameters for Inverse Non-Fourier Conduction-Radiation Problem

To demonstrate the workability of the LBM-FVM-GA in the inverse method, for a population size of 100, in Table 5.2, we study the effects of the crossover probability P_c and the mutation probability P_m. For scattering albedo $\omega = 0.80,$ this study has been done for four different cases of P_c and P_m, viz., $(P_c, P_m) = (0.3, 0.03), (0.8, 0.03), (0.8, 0.3)$ and $(0.3, 0.3)$. The exact values of the parameters which were simultaneously estimated in the inverse method are $\beta = 0.50$ and $N = 0.01$. This investigation is done for four different measurement errors, viz., E= 0.0, 0.5, 1.0 and 2.0.

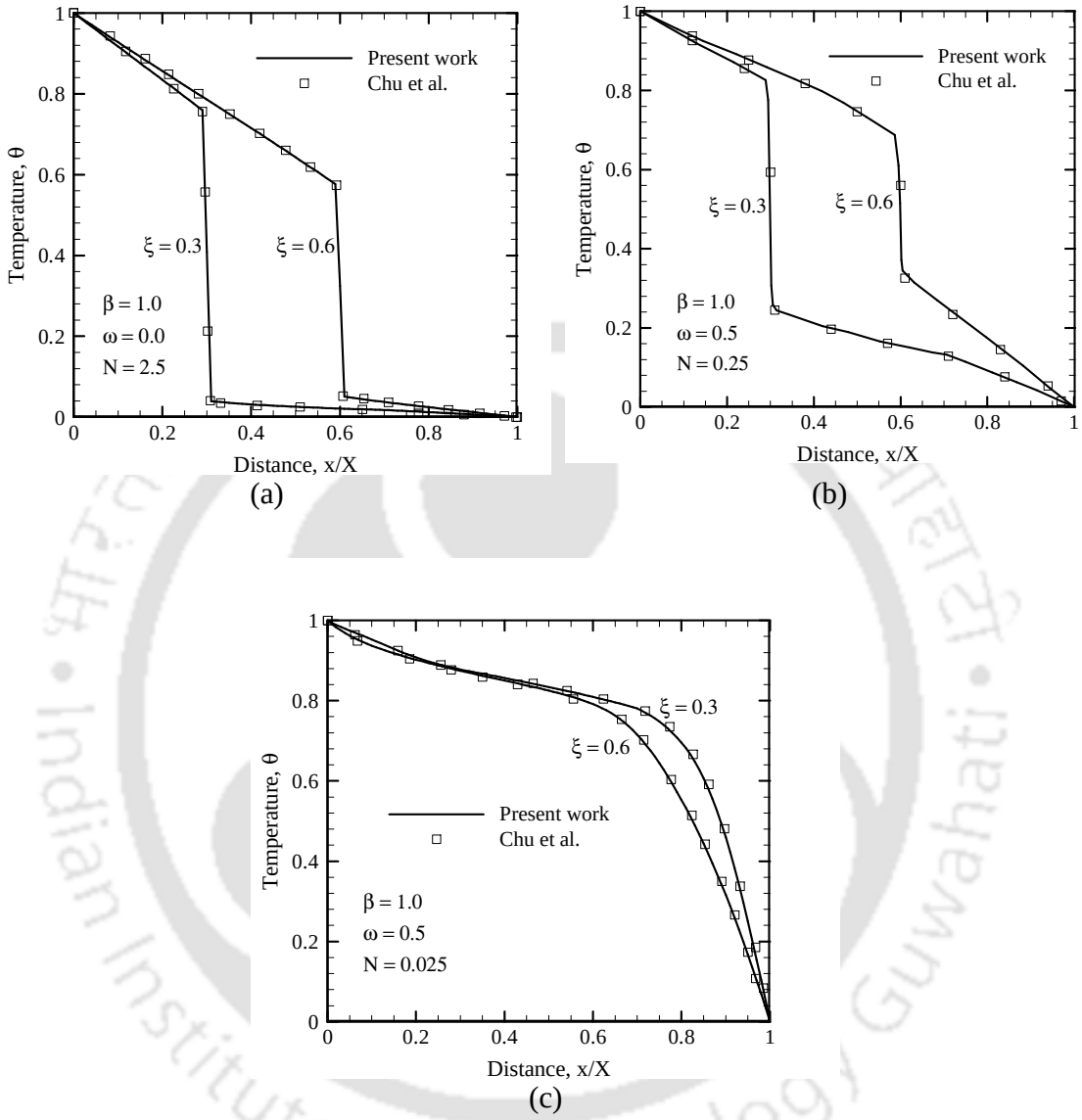

Figure 5.1: Validation of the Direct Problem with Chu *et al.* [85].

Table 5.2: Comparison of exact and estimated value of the parameters for different combinations of P_c and P_m (Range: $(N,\beta)=(0.0-5.0)$).

Exact Value (N,β)	E	P_c	P_m	Estimated Value (N,β)	% Error (N,β)
(0.01, 0.50)	0.0	0.3	0.03	(0.0111, 0.4777)	(11.0, -4.46)
		0.8	0.03	(0.0097, 0.5175)	(3.0, 3.50)
		0.8	0.3	(0.0107, 0.5703)	(7.0, 14.06)
		0.3	0.3	(0.0092, 0.4289)	(-8.0, -14.22)
	0.5	0.3	0.03	(0.0106, 0.5611)	(6.0, 12.22)
		0.8	0.03	(0.0103, 0.4794)	(3.0, -4.12)
		0.8	0.3	(0.0109, 0.5240)	(9.0, 4.80)
		0.3	0.3	(0.0079, 0.4032)	(-21.0, -19.36)
	1.0	0.3	0.03	(0.0119, 0.3982)	(19.0, -20.36)
		0.8	0.03	(0.0106, 0.4749)	(6.0, -5.02)
		0.8	0.3	(0.0111, 0.4148)	(11.0, -17.04)
		0.3	0.3	(0.0075, 0.4207)	(-25.0, -15.86)
	2.0	0.3	0.03	(0.0142, 0.6311)	(42.0, 26.22)
		0.8	0.03	(0.0114, 0.5264)	(-14.0, 5.28)
		0.8	0.3	(0.0074, 0.4113)	(-26.0, -17.74)
		0.3	0.3	(0.0153, 0.6193)	(53.0, 23.86)

It can be observed that for all measurement errors, a crossover probability $P_c=0.8$ and a mutation probability $P_m=0.03$ yields a minimum error in the estimated value of the parameters. This result is in line with that of the 2-D transient conduction-radiation problem.

For the good combination of crossover and mutation probability $(P_c=0.80; P_m=0.03)$, it is also noticed that at lower measurement errors $(E=0.0:1.50)$, the estimation accuracy of the unknown parameters, viz., the conduction-radiation parameter N and the extinction coefficient β are almost similar. However, at large measurement error $E=2.0$,

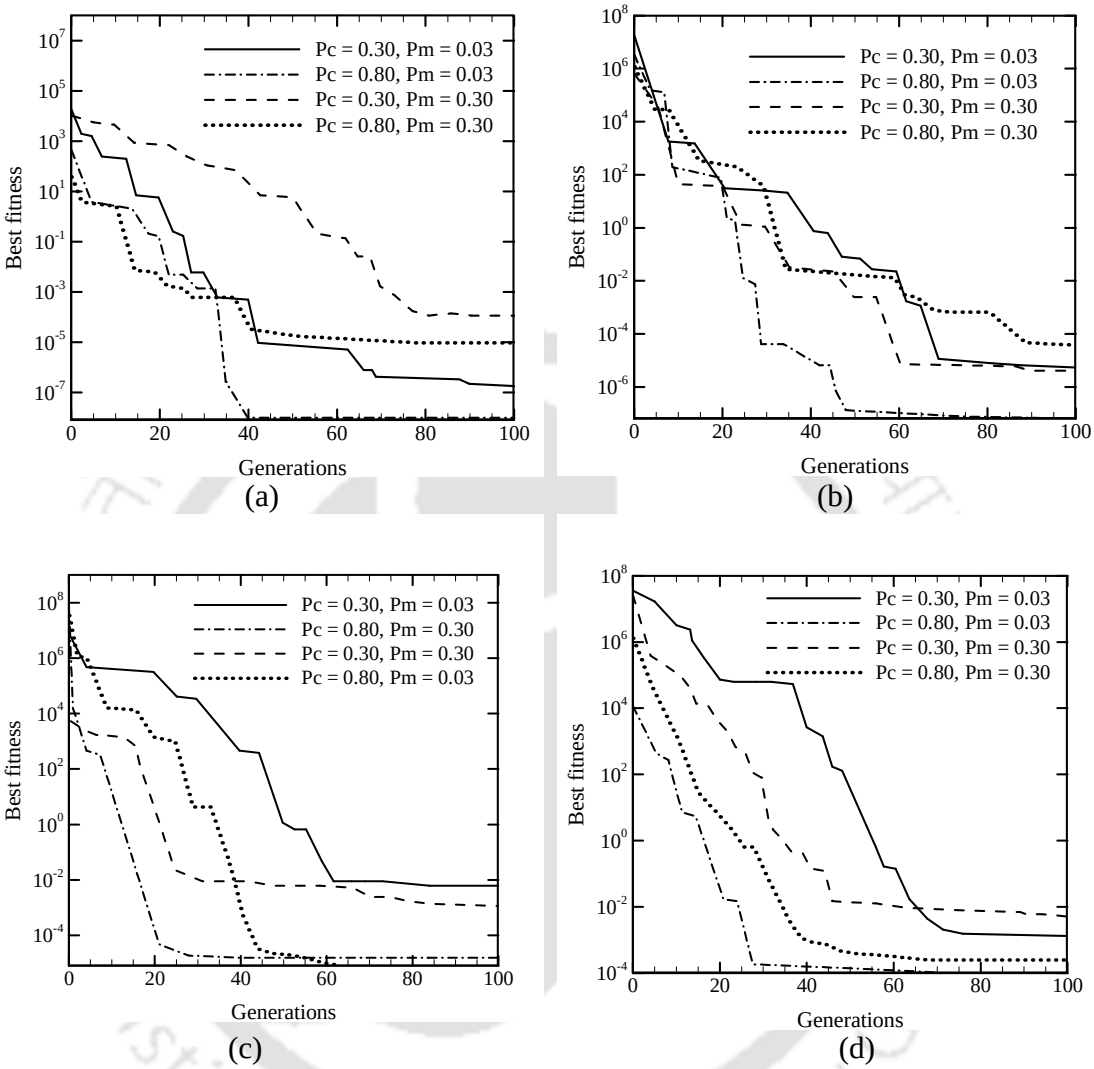

Figure. 5.2: Effect of different cross over probability and mutation probability on the best fitness (a) E = 0.0, (b) E = 0.5, (c) E = 1.0 and (d) E = 2.0.

the estimation of the conduction-radiation parameter N is difficult for all values of the crossover and the mutation probabilities.

For the parameters considered in Table 5.2, to study the effects of the crossover probability P_c and the mutation probability P_m on the convergence rate of the best fitness and their effects on the required number of generations for the convergence, we present a comparison in Fig. 5.2. It can be observed that the crossover probability $P_c = 0.8$ and the mutation probability $P_m = 0.03$ provide a minimum value of the best fitness as compared to other combinations of the crossover and the mutation probabilities. In the previous paragraph it has been observed that the crossover probability $P_c = 0.8$ and the mutation probability $P_m = 0.03$ yield the estimated values of the parameters with least error. Therefore, in the present two-parameter estimation problem, the minimum the value of the objective function, the better is the accuracy of the estimated parameters. Further, it can be noticed that in case of $(P_c, P_m) = (0.8, 0.03)$, the attainment of the convergence is faster. This is due to the reason that the solution or the populations are tuned towards the optimality domain in the earlier generations itself and further refinements do not occur in the successive generations. However, for all combinations of P_c and P_m, it is also observed that there is no significant change in the variation of the best fitness between 60-100 generations. Thus, in the present work, the analysis has been done for a maximum of 100 generations.

From Table 5.2 and Fig. 5.2, it has been observed that $(P_c, P_m) = (0.8, 0.03)$ provide the estimated values with least errors and for the convergence, they also require less number of generations. Thus with $(P_c, P_m) = (0.8, 0.03)$, in Table 5.3, we study the effect of the population size on the accuracy of the estimated values of the parameters. For this comparison, three different population sizes, viz., 25, 50 and 100 have been investigated. For all values of the measurement errors, it is seen that the estimation accuracy deteriorates for small population numbers and as the population size increases, the accuracy also improves. This result is in accordance with the inverse analysis in the 2-D geometry (Chapter 4) and a similar justification holds good in this case too.

Table 5.3: Comparison of the exact and the estimated values of the parameters for different population size, (Range: $(N, \beta) = (0.0 - 5.0)$)

Exact Value N, β	E	Population size	Estimated Value N, β	% Error N, β
(0.01, 0.50)	0.0	25	(0.0072, 0.6681)	(-27.0, 33.62)
		50	(0.0118, 0.4459)	(18.0, -10.82)
		100	(0.0097, 0.5175)	(3.0, 3.50)
	0.5	25	(0.0146, 0.7408)	(46.0, 48.16)
		50	(0.0071, 0.5657)	(-29.0, 13.14)
		100	(0.0103, 0.4794)	(3.0, -4.12)
	1.0	25	(0.0046, 0.3470)	(-54.0, -30.6)
		50	(0.0068, 0.6019)	(-32.0, 20.38)
		100	(0.0106, 0.4749)	(6.0, -5.02)
	2.0	25	(0.0031, 0.3605)	(-69.0,-27.90)
		50	(0.0135, 0.3513)	(35.0, -29.74)
		100	(0.0114, 0.5264)	(-14.0, 5.28)

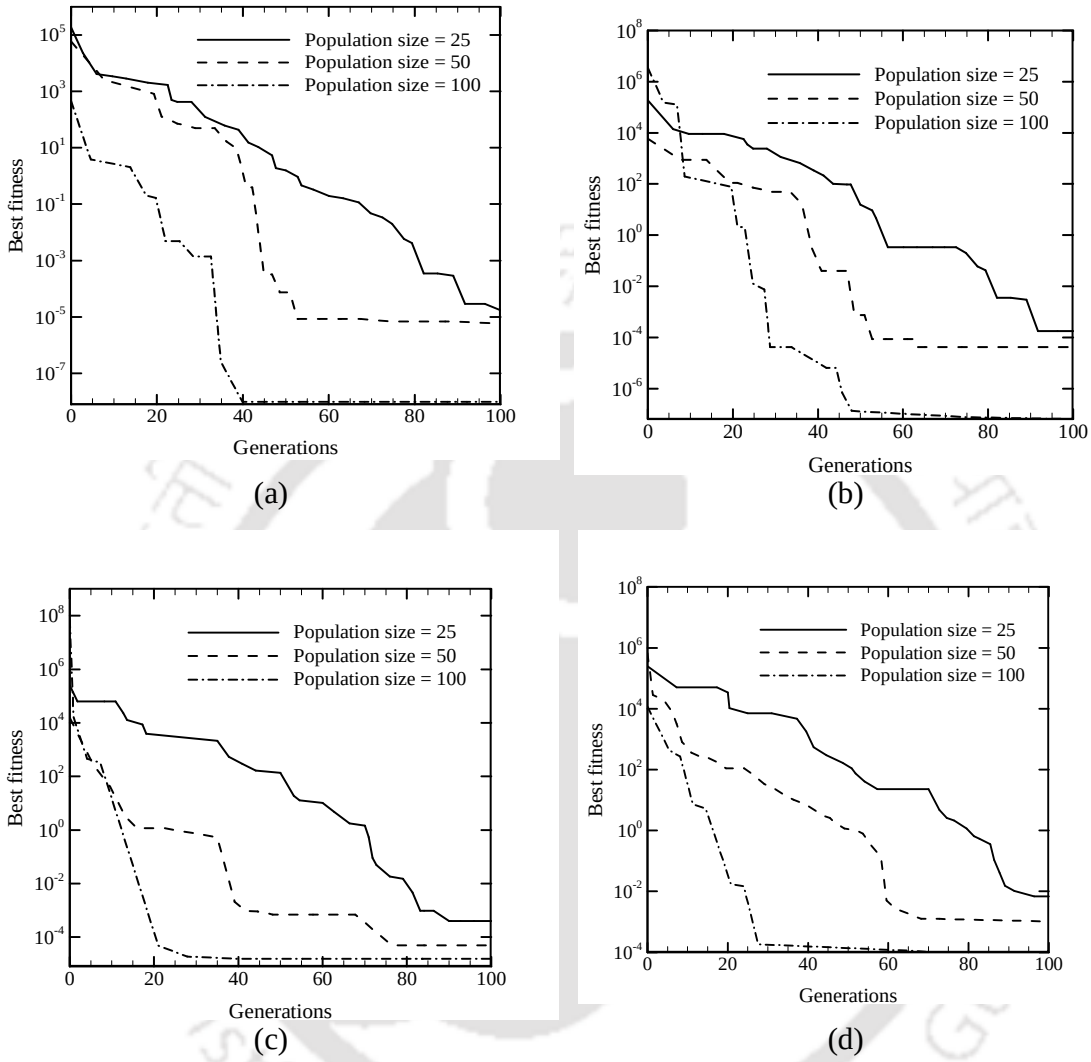

Figure 5.3: Effect of different population sizes on the best fitness (a) E = 0.0, (b) E = 0.5, (c) E = 1.0 and (d) E = 2.0.

In Fig. 5.3, we compare the effect of the population size on the variation of best fitness with the number of generations required for the convergence. In this case too, $(P_c, P_m) = (0.8, 0.03)$ is taken. It is observed from Fig. 5.3 that for all measurement errors

the attainment of convergence is faster for a higher population size. It is also observed that the converged values are low for a population size of 100. Thus, in the present study, a higher value of the population size provides a better result for the estimated parameters. This can be explained in the following manner. A small population number means that in the population, few individuals are present. Hence, the probability of obtaining an individual of desired fitness at a particular generation is also less. So, the number of generations required for the convergence is more and the presence of fitter individuals is also less and hence the estimation accuracy reduces. On the other hand, the presence of more individuals in the population contains more individuals with better fitness and hence require less generations to attain the convergence.

5.3.2 Comparison of Reconstructed and Exact Temperature Fields

To demonstrate the accuracy of the estimated parameters obtained in the inverse method, in Fig. 5.4 we compare the temperature θ distributions computed using the direct method and the inverse method. This comparison corresponds to a measurement error E=2.0. For the selected values of the crossover probability P_c and the mutation probability P_m which in the present study are 0.80 and 0.03, respectively, it is sufficient to compare the temperature θ distribution corresponding to E= 2.0. This is because the case E= 2.0 contains a maximum error in the estimated values as compared to other sets of E. It is observed that the temperature θ distributions computed using the direct method and the inverse method are in excellent agreement with each other.

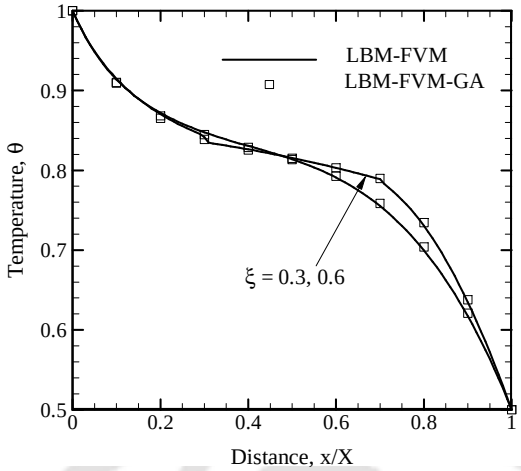

Figure 5.4: Comparison of exact and estimated temperature profiles for measurement error E = 2.0.

5.3.3 Comparison of Computational Time

The comparison of CPU times involved in the direct method as well as the inverse method is presented in Table 5.4. This comparison corresponds to time $\xi = 0.60$ and $\omega = 0.80$, and for four different cases of measurement errors, viz., E=0.0, 0.5, 1.0 and 2.0. All runs were carried out on 2.8 GHz, CPU (Pentium (R) 4 with 248 MB RAM).

Table 5.4: Comparison of the CPU(s) times required in the LBM-FVM and the LBM-FVM-GA for $\xi = 0.60$; $\omega = 0.8$, $\varepsilon_1 = \varepsilon_2 = 1.0$, $\theta_1 = 1.0$ and $\theta_2 = 0.5$.

(N, β)	E	CPU time (s)		Ratio of CPU times $\left(\frac{\text{LBM-FVM-GA}}{\text{LBM-FVM}}\right)$
		LBM-FVM	LBM-FVM-GA	
(0.01, 0.50)	0.0	0.766	1033	1348.56
	0.50	0.766	1159	1513.05
	1.0	0.766	1261	1646.21
	2.0	0.766	1408	1838.12

It is seen that the inverse method requires CPU time approximately 1300-1800 times than that required by the direct method.

5.3.4 Variation of Estimated Parameters

To demonstrate the variation of the estimated parameters with generations, in Fig. 5.5, we present a comparison for the simultaneous estimation of the conduction-radiation parameter, N and the extinction coefficient, β. The comparison has been done for the case without measurement error $E = 0.0$. For this comparison, the population size considered is 100 and the crossover and the mutation probabilities are 0.80 and 0.03, respectively. For this study, the boundary emissivities considered are $\varepsilon_E = \varepsilon_W = 1$ and the

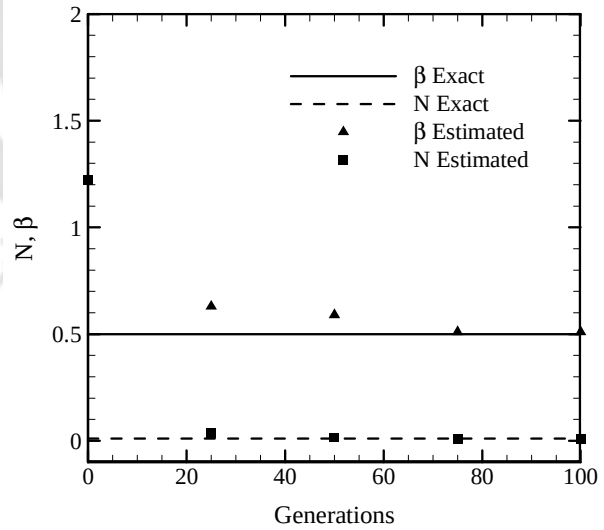

Figure 5.5: Comparison of estimated and the exact values of the parameters with generations. (Range: $(N, \beta) = (0.0 - 5.0)$)

scattering albedo $\omega = 0.80$. It is observed from the figure that the initial values of the two unknown parameters, viz., the conduction-radiation parameter, N and the extinction coefficient, β are the same and between 70-80 generations, both agree very well with their corresponding exact values. In the following pages, we carry out an inverse analysis for a transient conduction-radiation heat transfer problem with variable thermal conductivity.

5.4 Formulation of an Inverse Transient Conduction-Radiation Problem with Variable Thermal Conductivity

For investigating an inverse problem considering the effect of variable thermal conductivity, we assume the thermal conductivity to vary according to the following relationship:

$$k = k_0 + \gamma'(T - T_W) \tag{5.12}$$

where γ' is the variation of thermal conductivity. For the problem under consideration, the governing energy equation is given by

$$\rho C_p \frac{\partial T}{\partial t} = -\frac{\partial}{\partial x}\left(-k\frac{\partial T}{\partial x}\right) - \left(\frac{\partial q_R}{\partial x}\right) \tag{5.13}$$

Substitution of k from Eq. (5.12) in Eq. (5.13) gives the following expression

$$\rho C_p \frac{\partial T}{\partial t} = [k_0 + \gamma'(T - T_W)]\frac{\partial^2 T}{\partial x^2} + \gamma'\left(\frac{\partial T}{\partial x}\right)^2 - \left(\frac{\partial q_R}{\partial x}\right) \tag{5.14}$$

In non-dimensional form, Eq. (5.14) is rewritten as,

$$\frac{\partial\theta}{\partial\xi}=\left(1+\frac{\gamma(\theta-1)}{N}\right)\frac{\partial^2\theta}{\partial x^{*2}}+\frac{\gamma}{N}\left(\frac{\partial\theta}{\partial x^*}\right)^2-\frac{1}{4N}\frac{\partial\Psi_R}{\partial x^*} \tag{5.15}$$

where, γ' is the coefficient of variation of thermal conductivity in non-dimensional form and it is given by,

$$\gamma=\frac{\gamma' T_W N}{k_0} \tag{5.16}$$

Other non-dimensional terms in Eq. (5.15) are already described in the previous chapters and hence they are not repeated here. The FVM formulation to obtain the radiative information remains the same as described in Chapter 2 and the same are not discussed in this section.

Due to temperature dependence of the thermal conductivity, the modified dimensional form of the relaxation time in the lattice Boltzmann equation takes the following form,

$$\begin{aligned}\tau&=\frac{k/\rho c_p}{|c_i|^2}+\frac{\Delta t}{2}=\frac{k_0+\gamma'(T-T_W)}{\rho c_p|c_i|^2}+\frac{\Delta t}{2}\\&=\frac{k_0}{\rho c_p|c_i|^2}+\frac{\gamma'}{\rho c_p|c_i|^2}(T-T_W)+\frac{\Delta t}{2}\end{aligned} \tag{5.17}$$

For generalization, we carry out non-dimensionalization in the following manner,

$$\begin{aligned}&\xi=\alpha\beta^2 t, x^*=\beta x, \theta=\frac{T}{T_W}, \Psi_{\mathrm{R}}=\frac{q_{\mathrm{R}}}{\sigma T_W^4}, \gamma=\frac{\gamma' T_W N}{k_0}\\&N=\frac{k_0\beta}{4\sigma T_W^3}, G^*=\frac{G}{\sigma T_W^4/\pi}\end{aligned} \tag{5.18}$$

The non-dimensional form of the relaxation time in the LBM gets modified to the following,

$$\tau^* = \frac{1}{\left(\Delta x^* / \Delta\xi\right)^2} + \frac{\gamma}{\left(\Delta x^* / \Delta\xi\right)^2}\left(\theta - \theta_w\right) + \frac{\Delta\xi}{2} \tag{5.19}$$

Therefore, for the problem under consideration, the non-dimensional form of the energy equation in the LBM is given by the following equation,

$$f_i^*\left(\vec{x}^* + \vec{c}_i^*\Delta\xi, \xi + \Delta\xi\right) = f_i^*\left(\vec{x}^*, \xi\right) - \frac{\Delta\xi}{\tau^*}\left[f_i\left(\vec{x}^*, \xi\right) - f_i^{*(0)}\left(\vec{x}^*, \xi\right)\right] - \frac{\Delta\xi w_i}{4N}\frac{\partial\Psi_R}{\partial x^*} \tag{5.20}$$

The determination of temperature distributions θ, the construction of the objective function and the solution of the inverse problem are carried out in the same manner as done in the previous chapters. In the following pages, we present the results based on the investigations carried out for the present problem. In the present problem we simultaneously estimate any two parameters such as the conduction-radiation parameter, the extinction coefficient and the scattering albedo. For the case corresponding to the estimation of conduction-radiation parameter and the extinction coefficient, the scattering albedo and the emissivity are fixed. In the simultaneous estimation of the conduction-radiation parameter and the scattering albedo, the emissivity and the extinction coefficient are fixed. Whereas, for the estimation of the extinction coefficient and the scattering albeo, the conduction-radiation parameter and the emissivity are fixed.

5.5 Results and Discussion on Inverse Problem involving Variable Thermal Conductivity

In the following pages, we provide results of the inverse analysis for the simultaneous retrieval of parameters. Initially, the entire system is at a temperature $\theta\left(x^*,0\right)=0.5$. For time $\xi>0$, the east boundary is kept at the same initial temperature $\left(\theta_E=0.5\right)$ and the west boundary is maintained at a higher temperature $\theta_W=2\theta_E=1.0$. In the energy equation, the non-dimensional time step $\Delta\xi=0.0001$ was considered. The steady-state

Table 5.5: Effect of number of lattices/control volumes in the direct method (LBM-FVM) and number of directions in the FVM on the variation of steady state (SS) temperature θ; $\varepsilon_E=\varepsilon_W=1.0$, $\beta=1.0, \omega=0.5, N=0.01, \gamma=0.50$.

Control volumes/ lattices	Number of directions M_δ	Non-dimensional location		
		$x^*=0.20$	$x^*=0.40$	$x^*=0.80$
Effect of control volumes/lattices				
25	12	0.9019	0.8247	0.6439
50	12	0.8928	0.8401	0.6937
100	12	0.8905	0.8550	0.7392
200	12	0.8900	0.8596	0.7486
Effect of number of directions M_δ				
100	6	0.8377	0.8036	0.7023
100	12	0.8905	0.8550	0.7392
100	24	0.9045	0.8643	0.7429

(SS) conditions were assumed to have been attained when the temperature difference between two consecutive time levels at each lattice center did not exceed 1.0×10^{-6}.

In Table 5.5, we study the effect of lattices/control volumes and number of rays on the SS temperature θ distribution. For this, both the boundaries are assumed black. The comparison corresponds to the extinction coefficient $\beta=1.0$, the scattering albedo $\omega=0.5$, the conduction-radiation parameter N = 0.01 and the coefficient of variation of thermal conductivity $\gamma=0.5$. It is observed from Table 5.5 that beyond 100 control volumes and 12 rays, there is no significant change in the temperature θ distributions. Therefore, in the present work, we have provided the results considering 100 control volumes and 12 rays. It is to be noted that in the LBM, the number of lattices remains one more than the number of control volumes.

For checking the accuracy of the direct method, in Fig. 5.6, we compare the SS temperature θ distributions with that given in reference [69]. The cold/east boundary is assumed to be black and the emissivity of the hot/west boundary $\varepsilon_w = 0.5$. For extinction coefficient $\beta=0.1$, the scattering albedo $\omega=0.5$ and the conduction-radiation parameter N = 0.5, this comparison has been shown for three values of thermal conductivity parameter $\gamma=-1.0,-0.50$ and 0.0. It is observed from Fig. 5.6 that the SS temperature θ distributions obtained from the direct method compare very well with those given in the literature where FDM [69] involving implicit scheme and the DTM were used [69].

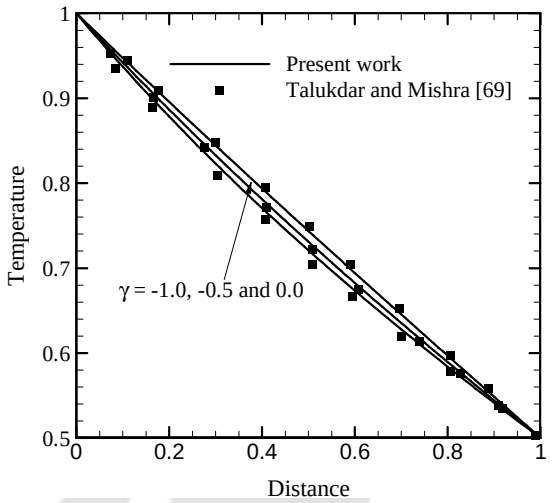

Figure 5.6: Comparison of the temperature θ distributions at different locations for different variable thermal conductivity parameter γ with Talukdar and Mishra [69]

In the following pages, we present results for the inverse analysis using the LBM-FVM in conjunction with the GA. For this analysis, at time $\xi > 0.0$, we maintain the non-dimensional temperatures of the west and the east boundaries at $\theta_W = 1.0$ and $\theta_E = 0.5,$ respectively. For the set of parameters considered in Table 5.5, with the SS temperature θ distributions available from the direct method, in the inverse method, we simultaneously estimate two parameters, viz., (β, N), (ω, N) and (β, ω).

5.5.1 Effects of GA Parameters

To demonstrate the workability of the LBM-FVM-GA in the inverse method, for a population size of 100, in Table 5.6, we study the effect of the crossover probability P_c and the mutation probability P_m on the accuracy of the simultaneous estimation of the

extinction coefficient β and the conduction-radiation parameter N. For measurement errors E in the range 0-2, the effect has been studied for two cases of P_c and P_m, viz.,

(a) lower value of the crossover probability $(P_c = 0.30)$ with a higher value of the mutation probability $(P_m = 0.30)$ and (b) higher value of the crossover probability $(P_c = 0.80)$ with a much lower value of the mutation probability $(P_m = 0.03)$. It is observed from Table 5.6 that for the present study, a higher value of the crossover probability $(P_c = 0.80)$ with a much lower value of the mutation probability $(P_m = 0.03)$ is desirable. Thus, in the present work, we select the $P_c = 0.80$ and $P_m = 0.03$ for simultaneous estimation of other sets of parameters, viz. (β, N), (ω, N) and (β, ω).

Table-5.6: Effect of crossover and mutation probabilities on the simultaneous retrieval of parameters for a population size of 100; $\varepsilon_E = \varepsilon_W = 1.0, \gamma = 0.50$. (Range: $(N, \beta) = (0.0 - 5.0); (N, \omega) = (0 - 5, 0 - 1); (\beta, \omega) = (0 - 5, 0 - 1)$)

Exact Values	(P_c, P_m)	E	Estimated Values	% Error
$(N, \beta) = (0.01, 1.0)$ $\omega = 0.50$	$(0.3, 0.3)$	0.0	(0.0124, 1.1935)	(24.0, 19.35)
		1.0	(0.0067, 0.7938)	(-33.0, 20.62)
		2.0	(0.0157, 1.3259)	(57.0, 32.59)
	$(0.8, 0.03)$	0.0	(0.0105, 1.0581)	(5.0, 5.81)
		1.0	(0.0011, 0.9011)	(11.0, -9.89)
		2.0	(0.0082, 0.8584)	(-18.0, -14.16)
$(N, \omega) = (0.01, 0.5)$ $\beta = 1.0$	$(0.8, 0.03)$	0.0	(0.0097, 0.5481)	(-3.0, 9.62)
		1.0	(0.0081, 0.6039)	(-19.0, 20.78)
		2.0	(0.0128, 0.3673)	(28.0, -26.54)
$(\beta, \omega) = (1.0, 0.5)$ $N = 0.01$	$(0.8, 0.03)$	0.0	(0.9673, 0.4705)	(-3.27, -5.90)
		1.0	(0.8903, 0.5806)	(-10.97, 16.12)
		2.0	(1.2932, 0.3890)	(29.32, -22.2)

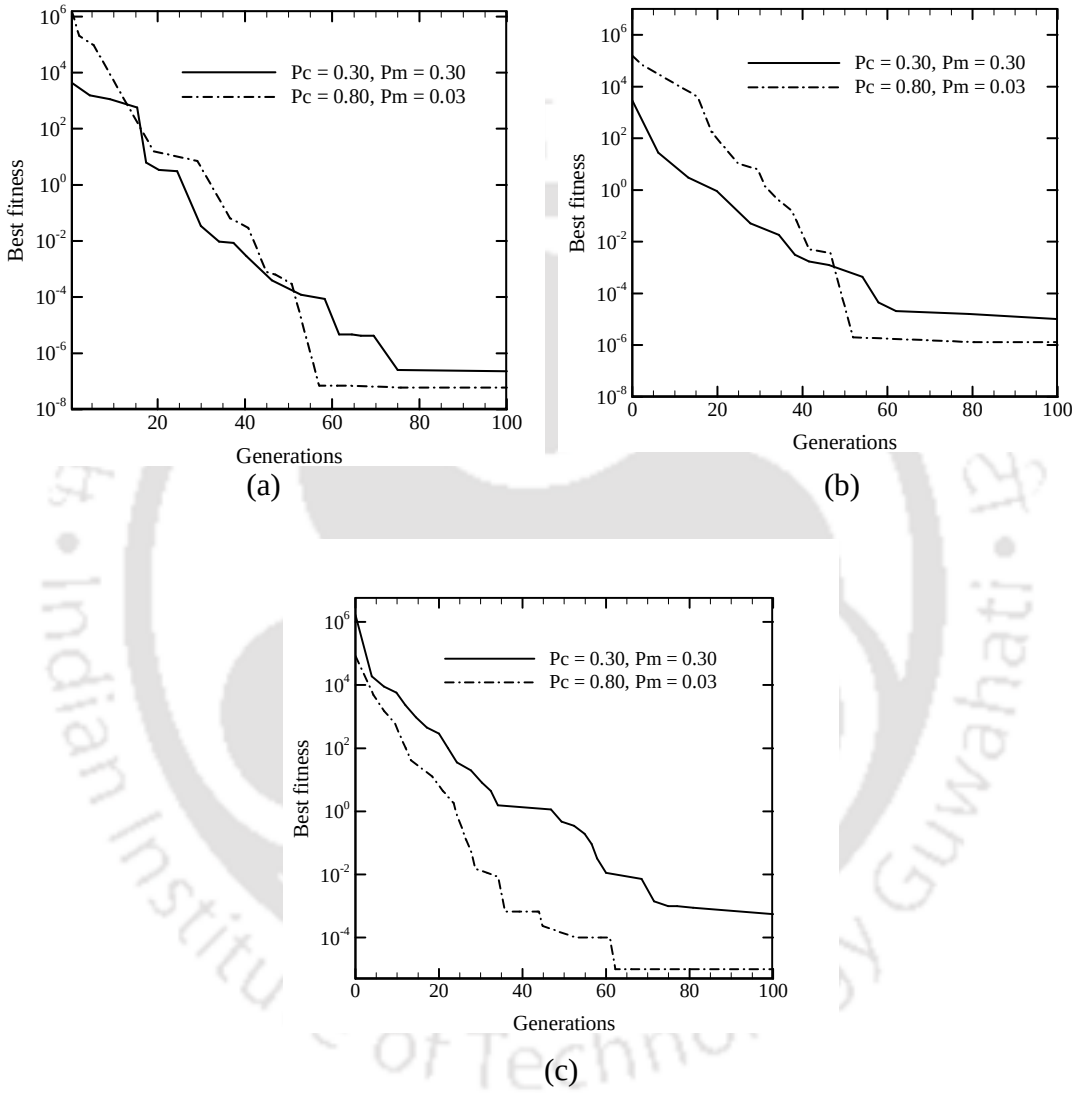

Figure 5.7: Comparison of the effect of crossover probability P_c and mutation probability P_m on the variation of the best fitness and number of generations for different measurement errors, (a) $E=0.0$ (b) $E=1.0$ and (c) $E=2.0$; $N=0.01, \beta=1.0, \varepsilon=1.0, \gamma=0.50$ and $\omega=0.50$, (Estimated values: N and β).

From Table 5.6, it is also seen that with $P_c = 0.80$ and $P_m = 0.03$, the estimated values of the set of parameters (β, N), (ω, N) and (β, ω) are in good agreement with the exact ones. It is also noticed from the table that in the simultaneous estimation of (N, β) as well as (N, ω), at higher measurement errors $(E = 1.0, 2.0)$, estimation of the conduction-radiation parameter N is more difficult than the extinction coefficient β and the scattering albedo ω. However, for the case of without measurement $(E = 0.0)$ both sets of estimated parameters possess reasonably good accuracy with respect to their exact values.

For parameters considered in Table 5.6, to study the effects of the crossover probability P_c and the mutation probability P_m on the convergence rate of the best fitness and their effects on the number of generations required for the convergence, we present a comparison in Fig. 5.7. For simultaneous estimation of the extinction coefficient β and the conduction-radiation parameter N, the comparison has been done for the three different measurement errors, viz., E= 0.0, 1.0 and 2.0 It can be observed that for all measurement errors E, a crossover probability $P_c = 0.8$ and a mutation probability $P_m = 0.03$ provide a minimum value of the best fitness as compared to the other combination of the crossover probability P_c and the mutation probability P_m i.e. $(P_c = 0.30, P_m = 0.30)$. Further, it can be noticed that in case of $(P_c, P_m) = (0.8, 0.03)$, the attainment of the convergence is faster. However, for other combination of P_c and P_m i.e. $(P_c = 0.30, P_m = 0.30)$, it is also observed that there is no significant change in the variation of the best fitness beyond 100 generations. Thus in the

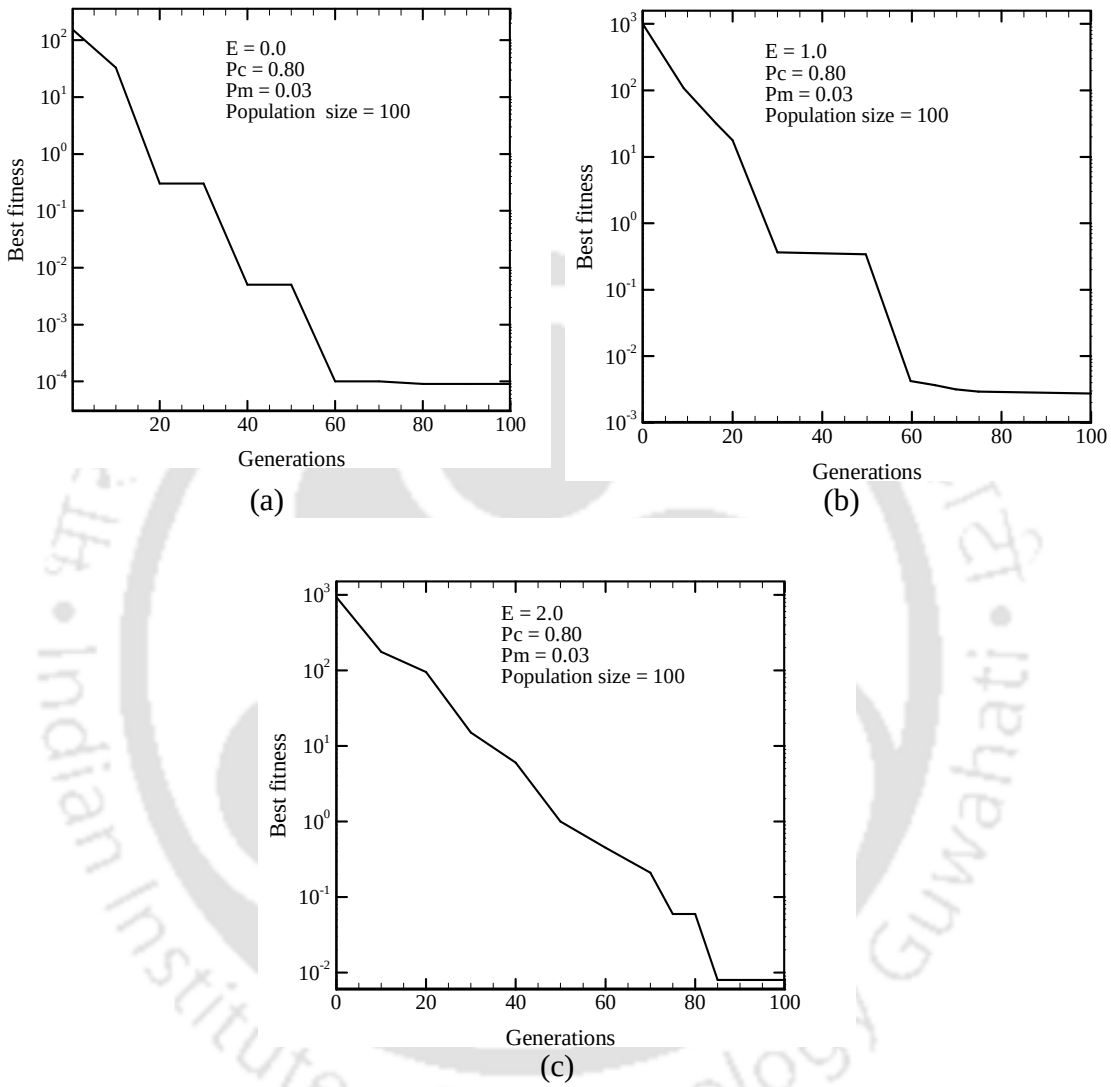

Figure 5.8: Comparison of the variation of the best fitness and number of generations for different measurement errors, (a) $E=0.0$ (b) $E=1.0$ and (c) $E=2.0$; $(P_c, P_m)=(0.80, 0.03)$, $N=0.01, \gamma=0.50, \beta=1.0, \varepsilon=1.0$ and $\omega=0.50$, (Estimated values: N and ω).

present work, the analysis has been done for a maximum of 100 generations. In Fig. 5.8, we present the variation of the best fitness with the number of generations for the simultaneous retrieval of the conduction-radiation parameter N and the scattering albedo ω. The study has been done for three measurement errors E= 0.0, 1.0 and 2.0It is observed that the value of the best fitness increases with measurement errors for a fixed number of generations (100 for the present study). It is also noticed that the convergence rate is faster for the case involving least measurement error, i.e., E= 0.0. This can be explained in the following manner. When the initial population contains large error, the probability that the GA needs large number of generations for tuning the population towards the minimum value becomes more. On the other hand, with the least measurement error, the probability that the population contains more number of fit individuals is high. Thus, the convergence rate is faster and less number of generations is

Table 5.7: Effect of the population size on the estimation accuracy of simultaneous retrieval of parameters; $\varepsilon_E = \varepsilon_W = 1.0, \gamma = 0.50$.
(Range: $(N,\beta)=(0.0-5.0);(N,\omega)=(0-5,0-1);(\beta,\omega)=(0-5,0-1)$)

Exact Values	Population size	E	Estimated Values	% Error
$(N,\beta)=(0.01,1.0)$ $\omega=0.50$	25	0.0	(0.0161, 1.3617)	(61.0, 36.17)
		1.0	(0.0022, 1.4321)	(-78.0, 43.21)
		2.0	(0.0014, 0.4803)	(-86.0, -51.97)
	100	0.0	(0.0105, 1.0581)	(5.0, 5.81)
		1.0	(0.0011, 0.9011)	(11.0, -9.89)
		2.0	(0.0082, 0.8584)	(-18.0, -14.16)
$(N,\omega)=(0.01,0.50)$ $\beta=1.0$	100	0.0	(0.0097, 0.5481)	(-3.0, 9.62)
		1.0	(0.0081, 0.6039)	(-19.0, 20.78)
		2.0	(0.0128, 0.3673)	(28.0, -26.54)
$(\beta,\omega)=(1.0,0.50)$ $N=0.01$	100	0.0	(0.9673, 0.4705)	(-3.27, -5.90)
		1.0	(0.8903, 0.5806)	(-10.97, 16.12)
		2.0	(1.2932, 0.3890)	(29.32, -22.2)

required. For the parameters considered in Table 5.6, we present the variation of the best fitness with number of generations for the simultaneous retrieval of the extinction coefficient β and the scattering albedo ω in Fig. 5.9. It is observed that for all measurement errors *E*, the variation is similar to the one observed in Fig. 5.8. Thus, a similar justification can be provided for the present case also.

To study the effect of population size on the accuracy of the estimated parameters in the inverse method, we present a comparison in Table 5.7. For simultaneous estimation of the extinction coefficient β and the conduction-radiation parameter N, the study has been made for two different population sizes of 25 and 100. For different measurement errors *E*, the crossover probability P_c and the mutation probability P_m have been taken as 0.80 and 0.03, respectively because this combination appears to perform better as observed from Table 5.6 and Figs. 5.7-5.9. It is observed from Table 5.7 that a higher population size gives a more accurate value of the retrieved parameter. This is because, the higher the population size, the higher the probability of obtaining better individuals in the population. The estimated values of the other set of parameters viz., the scattering albedo ω with the conduction-radiation parameter N, and the extinction coefficient β with the scattering albedo ω agree well with that of exact ones for a population size of 100 as observed from Table 5.7.

To study the effect of the population size on the variation of the best fitness with number of generations, we present a comparison in Fig. 5.10. For this comparison, the same set of parameters as assumed in Table 5.7 is taken. It is observed from Fig. 5.10 that for a

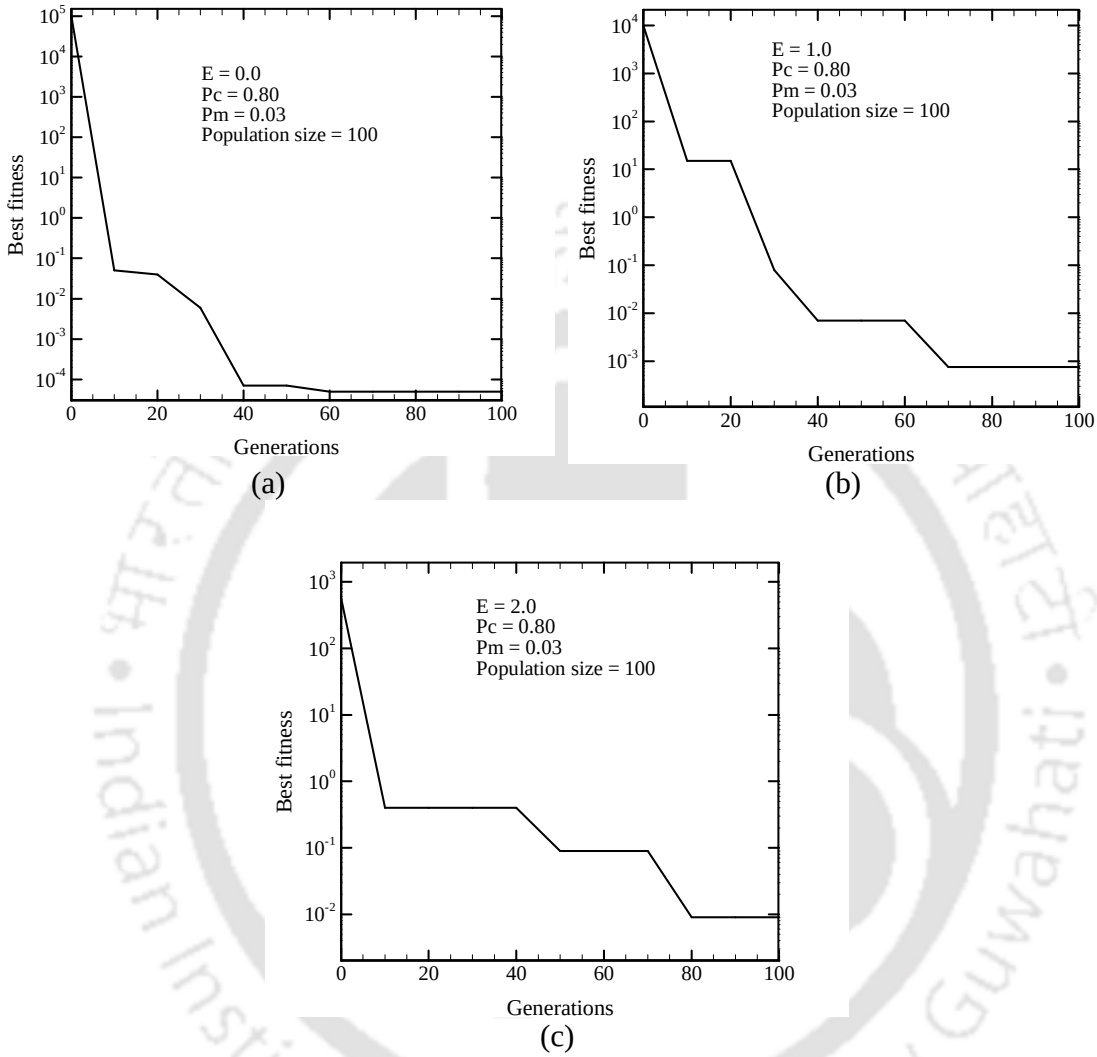

Figure 5.9: Comparison of the variation of the best fitness and number of generations for different measurement errors, (a) $E=0.0$ (b) $E=1.0$ and (c) $E=2.0$; $(P_c, P_m)=(0.80, 0.03), N=0.01, \beta=1.0, \varepsilon=1.0, \gamma=0.50$ and $\omega=0.50$, (Estimated values: ω and β).

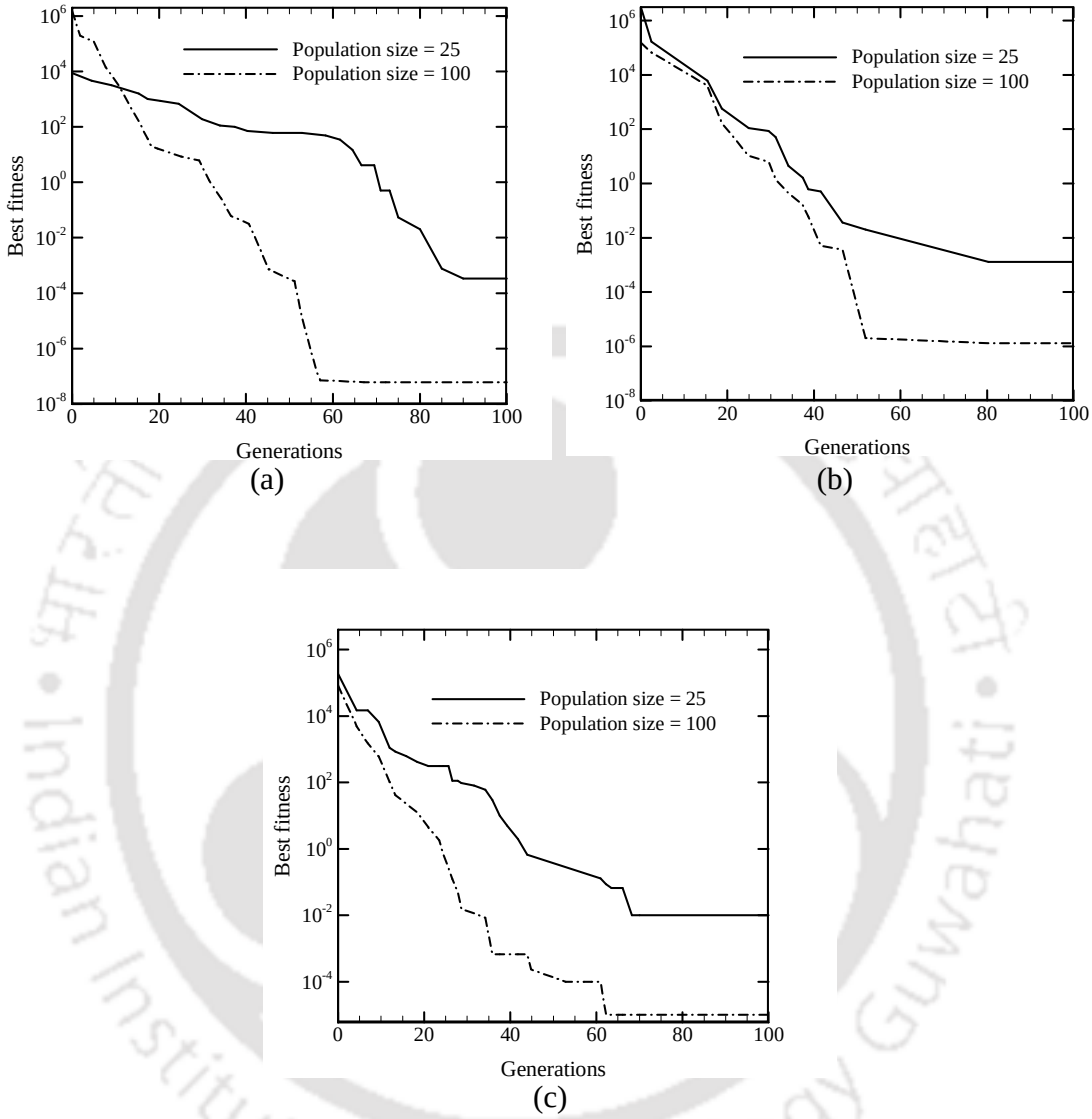

Figure 5.10: Comparison of the effect of the population size on the best fitness and number of generations for different measurement errors, (a) $E=0.0$ (b) $E=1.0$ and (c) $E=2.0$; $(P_c, P_m)=(0.80, 0.03)$, $N=0.01, \beta=1.0,\ \varepsilon=1.0, \gamma=0.50$ and $\omega=0.50$, (Estimated values: N and β).

higher population size, the attainment of the convergence is faster i.e., it requires less number of generations for the convergence. However, it is also noticed that the value of the best fitness is considerably less for a greater population size. This establishes the fact that, if more number of good individuals are present in the population, then the estimation accuracy also improves. It is also noticed from Fig. 5.10 that for all measurement errors, there is no change in the value of the best fitness beyond 100 generations. For different measurement errors E = 0.0, 1.0 and 2.0 the variation of the best fitness with the number of generations for a population size of 100 and $(P_c, P_m)=(0.80, 0.03)$ in case of the simultaneous estimation of the scattering albedo ω along with the conduction-radiation parameter N and for the simultaneous estimation of the extinction coefficient β and the scattering albedo ω has already been shown in Figs. 5.8 and 5.9 respectively. Thus, the details of the same are not repeated here.

5.5.2 Comparison of Reconstructed and Exact Temperature Fields

To demonstrate the accuracy of the estimated parameters obtained in the inverse method, in Fig. 5.11, we compare the temperature θ distributions computed using the direct method and the inverse method. This comparison corresponds to a measurement error E= 2.0. For the selected values of the crossover probability P_c and the mutation probability P_m which in the present study are 0.80 and 0.03, respectively, it is sufficient to compare the temperature θ distribution corresponding to E= 2.0. This is because the case E= 2.0 contains a maximum error in the estimated values as compared to other sets

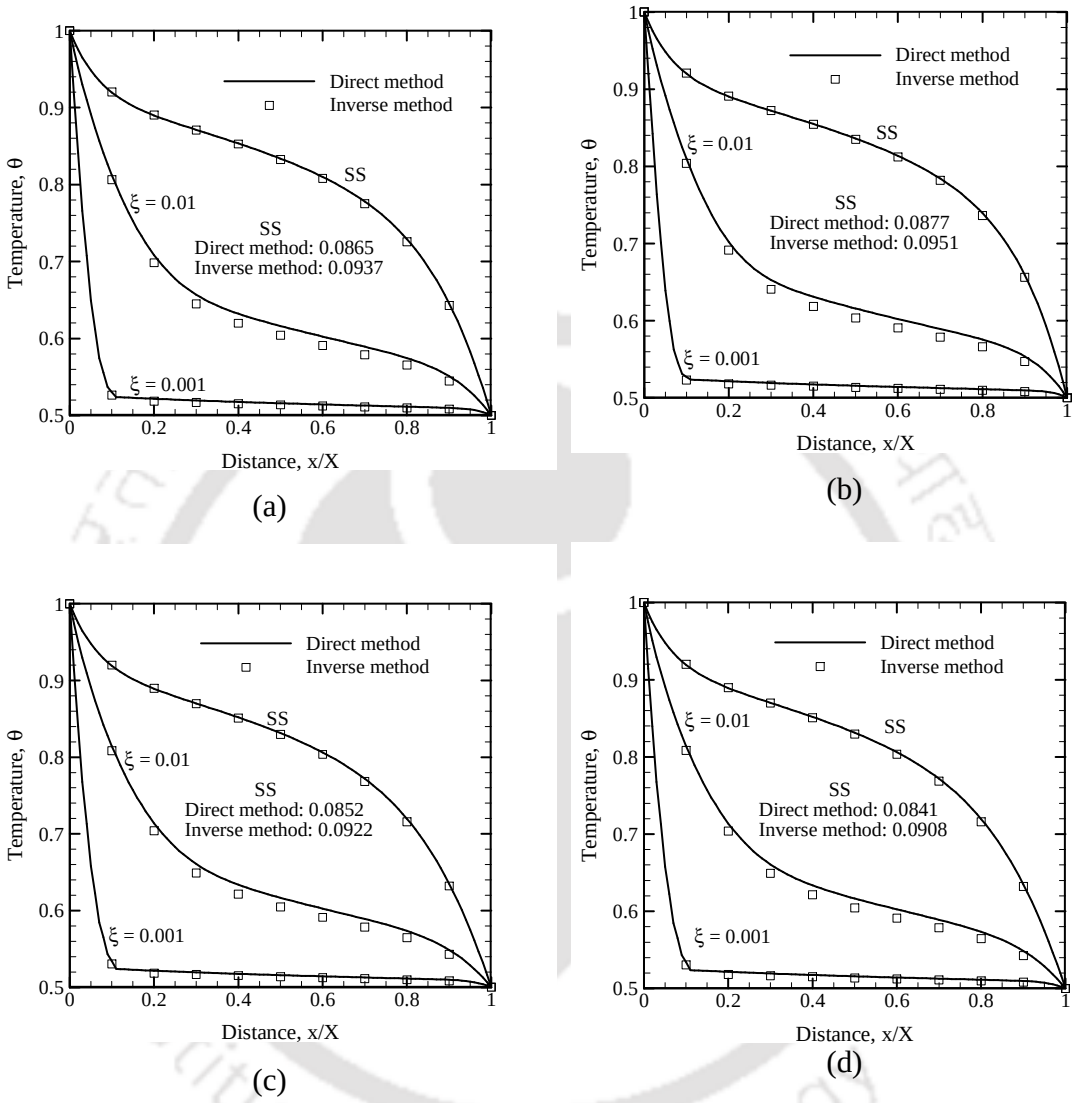

Figure 5.11: Comparison of the temperature θ distributions obtained from the direct method and the inverse method with a measurement error, $E=2.0$ for (a) $\gamma=0.0$ (b) $\gamma=0.5$ (c) $\gamma=-0.5$ and (d) $\gamma=-1.0$; $\varepsilon=1.0, \beta=1.0, \omega=0.5, \gamma=0.50$ and $N=0.01$, (Estimated values are N and ω).

of E= 2.0. It is observed that the temperature θ distributions computed using the direct method and the inverse method are in excellent agreement with each other.

Table 5.8: Comparison of CPU times required in the direct and the inverse method for population size of 100 and $(P_c, P_m)=(0.80, 0.03)$ for SS temperature θ; $\omega=0.50, \varepsilon_E=\varepsilon_W=1.0, \gamma=0.50$.

Exact values	Estimated values	E	CPU time (s)		Ratio of CPU times
			Direct method	Inverse Method	
$(N, \beta)=(0.01,1.0)$	(0.0105, 1.0581)	0.0	9.781	14799	1513.03
	(0.0011, 0.9011)	1.0		15012	1534.81
	(0.0082, 0.8584)	2.0		15758	1611.08

5.5.3 Comparison of Computational Time

To study the effect of the CPU time involved in the direct method and the inverse method, we present a comparison in Table 5.8. The comparison has been done for three different measurement errors, viz., *E*= 0.0, 1.0 and 2.0. All runs were carried out on 2.8 GHz CPU (Pentium (R) 4 with 248 MB RAM). It is evident from the Table 5.8 that the inverse method requires CPU time which is approximately more than 1500 times than that required in the direct method. This is due to the reason that in the inverse method, the GA starts with a random generation of the initial population. The values of the estimated parameters corresponding to this initial population deviates greatly with respect to the actual ones. Thus, to attain the converged solution, the algorithm has to undergo a series of generations and for a particular generation, in the GA loop, there are a number of processes involved. Therefore, in the inverse method, the CPU time is considerably larger than the direct method.

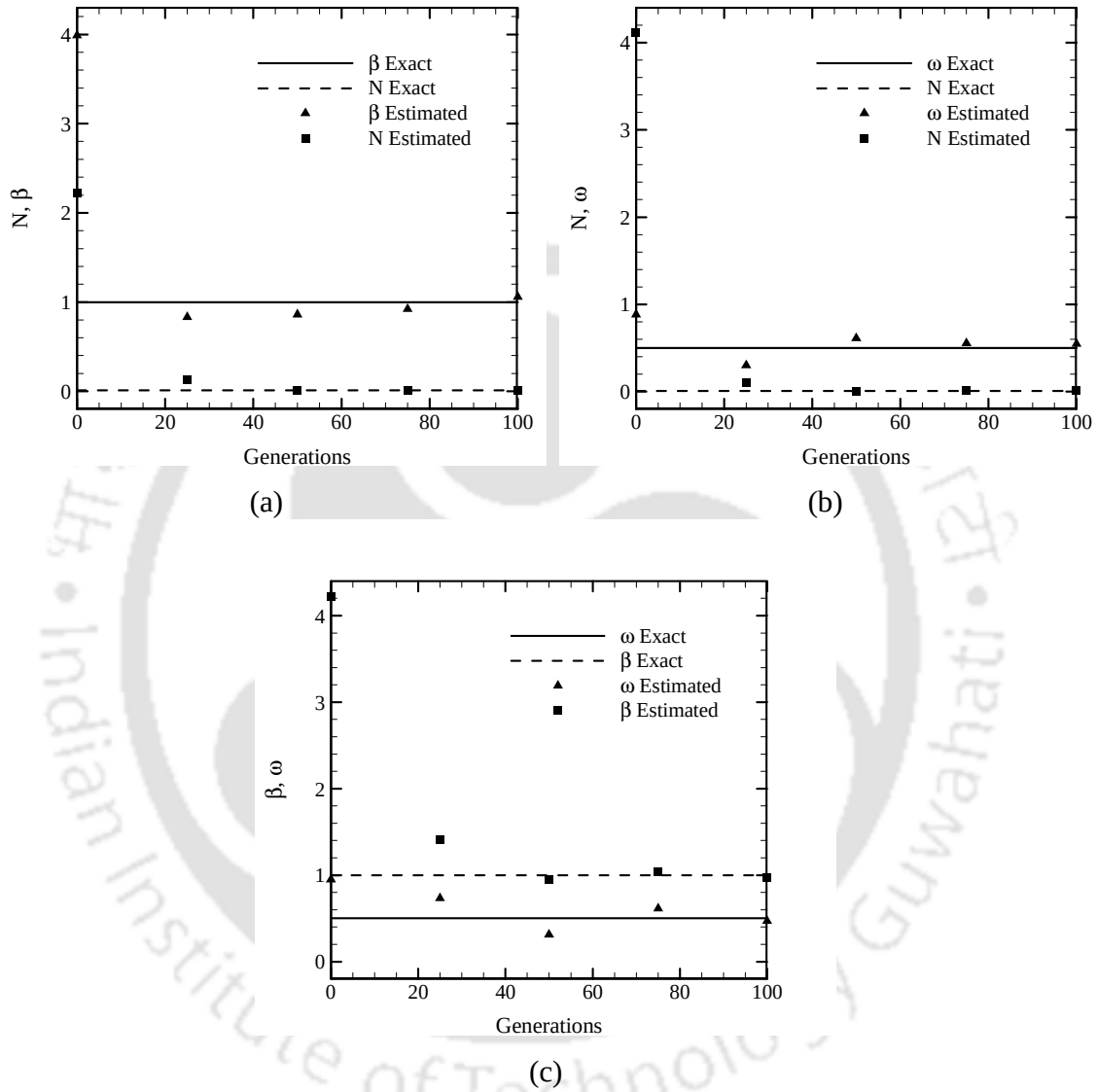

Figure 5.12: Comparison of the estimated parameters with number of generations with the exact ones, for (a) $(N,\beta)=(0.01,1.0)$, (b) $(N,\omega)=(0.01,0.50)$ and (c) $(\beta,\omega)=(1.0,0.50)$; $\gamma=0.5$.

(Range: $(N,\beta)=(0.0-5.0);(N,\omega)=(0-5,0-1);(\beta,\omega)=(0-5,0-1)$)

5.5.4 Variation of Estimated Parameters

In Fig. 5.12, we present the variation of estimated parameters with the number of generations for different sets of combination of parameters considered in Table 5.7. This study has been carried out for the case E= 0.0 and $\gamma = 0.5$. It is observed that the initial values of the estimated parameters are considerably offset from the exact ones and they undergo gradual refinements in successive generations.

5.6 Formulation of an Inverse Transient Conduction-Radiation Problem with Mixed Boundary Condition

In this section, the application of the LBM is extended to the mixed boundary condition problem where the hot boundary is provided with a constant heat flux and the other boundary is kept at constant temperature. Fig. 5.13 shows the 1-D planar medium with its west boundary subjected to a prescribed heat flux. Energy balance over the half-lattice on the west boundary is also shown.

In this chapter, simultaneous estimation of two parameters such as the hot boundary heat flux and the emissivity has been done using the LBM-FVM in conjunction with the GA. In this case too, the FVM is used for the computation of the radiative information and the LBM is employed to solve the energy equation. In the inverse analysis, the GA has been used as the optimization tool. In the following pages, we provide a brief formulation of the solution of mixed boundary condition problem which is followed by the formulation

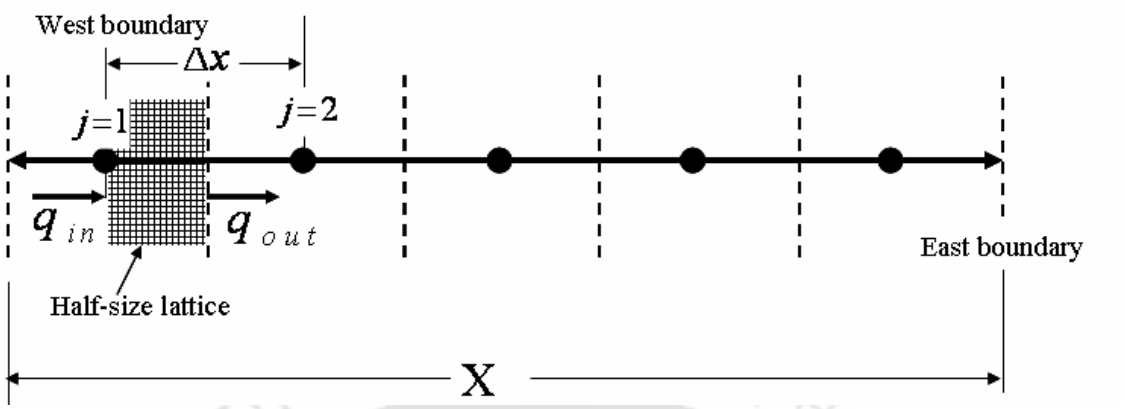

Figure 5.13: 1-D planar medium with D1Q2 lattice subjected to heat flux at its west boundary. The initial and boundary conditions are $\xi = 0 : T_E = T_W = 0.5$, $\xi > 0 : T_E = 0.5$, $\Psi_W = 0.4$, and 1.0

of the inverse problem. This is followed by results and discussions and conclusions are made at the end. Consider a planar homogenous participating medium (Fig. 5.13) in which the east boundary is subjected to a constant temperature and the west boundary is provided with a constant heat flux. Below we briefly discuss the procedure for the treatment of the mixed boundary condition type problem.

In implementation of the boundary condition in the LBM, the conservation of energy is applied to the half size boundary lattice. This conservation of energy over time Δt to the half size lattice at the west boundary yields the following,

$$\rho c_p \int_0^{\left(\frac{\Delta x}{2}\right)} \left(\int_t^{t+\Delta t} \frac{\partial T}{\partial t} dt \right) dx = \int_t^{t+\Delta t} (q_{in} - q_{out}) dt \tag{5.21}$$

where q_{in} is the prescribed heat flux at the west boundary and $q_{out} = q_C + q_R$ is the flux leaving the half size boundary lattice. Using Fourier's law for q_C and after discretization of terms in Eq. (5.21), we get the following equation

$$\rho c_p \left(T_j^{k+1} - T_j^k\right)\frac{\Delta x}{2} = \int_t^{t+\Delta t}\left(\left(q_{in} - q_R\right) - k\left[\frac{T_j^k - T_{j+1}^k}{\Delta x}\right]\right)dt \tag{5.22}$$

where, k and $k+1$ represent the time levels at t and $t+\Delta t$, respectively. Using an explicit scheme for the time discretization on the right hand side of the Eq. (5.21), we obtain the following,

$$T_j^{k+1} = (1-F)T_j^k + FT_{j+1}^k + H\left(q_{in} - q_R\right) \tag{5.23}$$

where, $F = \dfrac{2\alpha\Delta t}{(\Delta x)^2}$ and $H = \dfrac{2\Delta t}{\rho c_p \Delta x}$. Once, the temperature T_j^{k+1} at the boundary is known in terms of the prescribed heat flux q_{in}, the unknown particle distribution function f_i at the boundary can be calculated by using the procedure described in Chapter 2 for the constant temperature boundary condition.

In this case too, the radiative information is obtained using the FVM which is already explained in Chapter 2. The implementation of the LBM scheme for solving the transient energy equation also remains the same as provided in Chapter 2 and thus the same are not reproduced here.

Once the temperature field at different time levels ξ are obtained from the direct method, in the inverse method, we simultaneously estimate the west boundary heat flux Ψ_W and boundary emissivity ε_W. To minimize the objective function represented by square of the

difference between the guessed and exact temperature fields, we have used the GA. The methodology of the construction of the objective function is similar to the one mentioned in Chapter 2. Therefore, these are not explained in this section. In the present work two parameters which are simultaneously retrieved are the boundary heat flux and the emissivity. The extinction coefficient and the conduction-radiation parameter are fixed.

5.7 Results and Discussions on the Inverse Transient Conduction-Radiation Problem with Mixed Boundary Condition

Consider the planar participating medium shown in Fig. 5.13. Initially, the medium is at temperature, T_E, and for time $t > 0$, its west boundary is maintained at temperature $T_N > T_E$. The medium is absorbing emitting and isotropically scattering. Its boundaries are diffuse gray.

From the grid and ray independent tests it is observed that no significant change occurs beyond 100 lattices/control volumes and 16 rays. In this case too, a non-dimensional time step of $\Delta\xi = 1.0\times10^{-4}$ was used and steady state condition was assumed when the temperature θ distributions between two consecutive time steps did not exceed 1.0×10^{-6}. Thus, in the present work, the investigation is carried out by considering 100 control volumes and 16 ray directions. It is noted that the number of lattices is always one more than the number of control volumes. Thus the number of lattices considered in the present work becomes 101.

Table 5.9: Comparison of temperature θ distributions for $\beta = 1.0, \omega = 0.5, \varepsilon_E = \varepsilon_W = 0.5$ and $N = 0.05$.

	Temperature θ at					
$\Psi_{T,W}$	$\frac{x}{X} = 0.0$			$\frac{x}{X} = 0.5$		
	$N = 0.05$					
	[99]	[100]	Present work	[99]	[100]	Present work
0.2	0.701	0.701	0.702	0.439	0.439	0.439
0.4	0.919	0.919	0.921	0.610	0.611	0.612
0.6	1.054	1.055	1.056	0.732	0.733	0.734
0.8	1.155	1.157	1.158	0.828	0.830	0.831

Fernandes and Francis [99] and Lin and Tsai [100]. From Table 5.9, a good comparison is observed.

Table 5.9 presents the steady-state temperature θ distributions for $\beta = 1.0, \omega = 0.5, \varepsilon_E = \varepsilon_W = 0.5$ and $N = 0.05$. This comparison is done for two different locations $\frac{x}{X} = 0.0$, $\frac{x}{X} = 0.5$ and four different cases of west boundary heat flux, viz., $\Psi_{T,W}$ = 0.2, 0.4, 0.6 and 0.8. The results are then compared with those available in

5.7.1 Estimation of Parameter and Unknown Boundary Condition

Table 5.10 presents the estimated and the exact values of the heat flux and hot boundary emissivity. This comparison has been done for three different measurement errors, viz., *E* = 0.0, 1.0 and 2.0. For the inverse method, a uniform crossover and mutation probabilities of 0.8 and 0.03 are taken. This comparison is done for a population size of

Table 5.10: Comparison of the estimated and the exact values of hot boundary heat flux and emissivities for different measurement errors. (Range: $(\Psi_{T,W}, \varepsilon_W) = (0.0-5.0, 0.0-1.0)$)

Exact value $(\Psi_{T,W}, \varepsilon_W)$	Measurement Error,	Estimated Value $(\Psi_{T,W}, \varepsilon_W)$	% Error
(1.0, 0.5)	0.0	(1.120, 0.526)	(12.0, 5.2)
	1.0	(0.809, 0.453)	(19.1, -9.4)
	2.0	(0.683, 0.609)	(-31.7, 21.8)
(0.4, 0.5)	0.0	(0.301, 0.570)	(-24.75, 14.0)
	1.0	(0.352, 0.616)	(-12.0, 23.2)
	2.0	(0.554, 0.363)	(38.5, -27.4)

100. It is noticed that although a good agreement between exact and estimated ones are observed at low measurement errors, with increase in measurement errors, the error in the estimated values increase substantially. Moreover, at zero measurement error and even at all measurement errors, the error in the estimated value of the boundary heat flux $\Psi_{T,W}$ is more than that of the emissivity ε_W and it indicates that the estimation of the flux is difficult compared to the emissivity.

5.7.2 Effect of the GA Parameters

Fig. 5.14 presents the variation in the best fitness for two different population sizes of 25 and 100. For each case two different values of boundary heat flux and emissivity, viz., $(\Psi_{T,W}, \varepsilon_W)$ = (1.0, 0.5) and (0.4, 0.5) are investigated. This comparison corresponds to a measurement error of E= 2.0. It is to be noted that for determination of maximum

number of generations, it is sufficient to investigate the case corresponding to the measurement error of E= 2.0, because it contains the largest error which is minimized using the GA. Other cases of measurement error, viz., E= 0.0 and 1.0, contains smaller perturbations and hence, the number of generations required for a particular value of the objective function in those cases will always be less as compared to the case E= 2.0. Moreover, it is also noticed from Fig. 5.14 that a higher population size, i.e., 100 for the present work, is desirable for reasonable minimization of the objective function. This is due to the reason that in a higher population size, the chance of obtaining a good

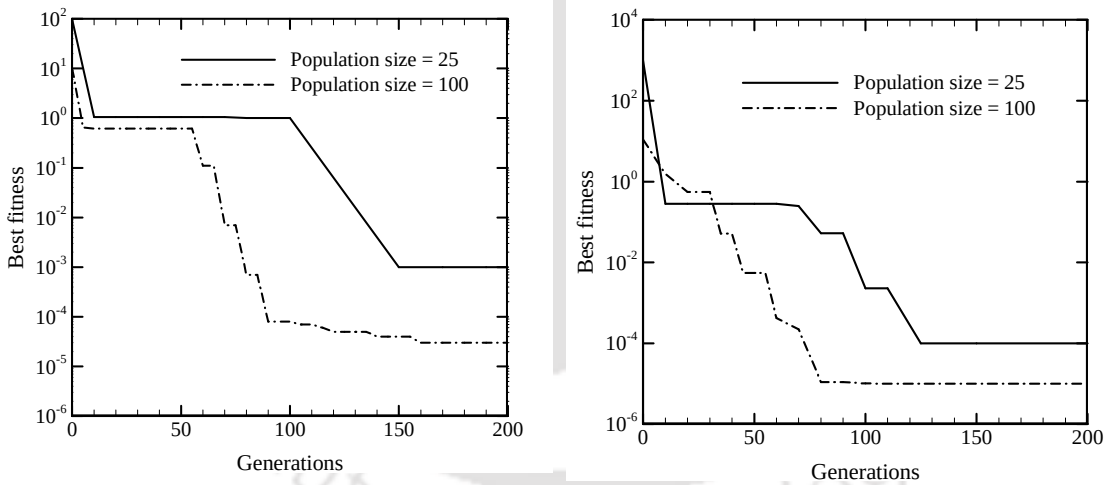

Figure 5.14: Comparison of the best fitness for different population sizes, (a) $\left(\Psi_{T,W}, \varepsilon_W\right)$= (1.0, 0.5) and (b) $\left(\Psi_{T,W}, \varepsilon_W\right)$=(0.4, 0.5); $\beta = 1.0, \omega = 0.5, \varepsilon_E = \varepsilon_W = 0.5$ and $N = 0.05$.

individual is more as compared to a smaller population size. However, it is also noticed that the values of the objective function are lower for any value of generation. For this comparison, a uniform crossover and mutation probabilities of 0.8 and 0.03, respectively have been considered. It is observed that for a population size of 100, no significant change in the value of the best fitness occurs beyond 200 generations. Hence, it is assumed that the convergence has been achieved.

5.7.3 Comparison of Reconstructed and Exact Temperature Fields

Fig. 5.15 shows the reconstructed temperature fields computed using the exact values and estimated ones. For $\beta = 1.0, \omega = 0.5, \varepsilon_E = \varepsilon_W = 0.5$ and $N = 0.05,$ this comparison has been

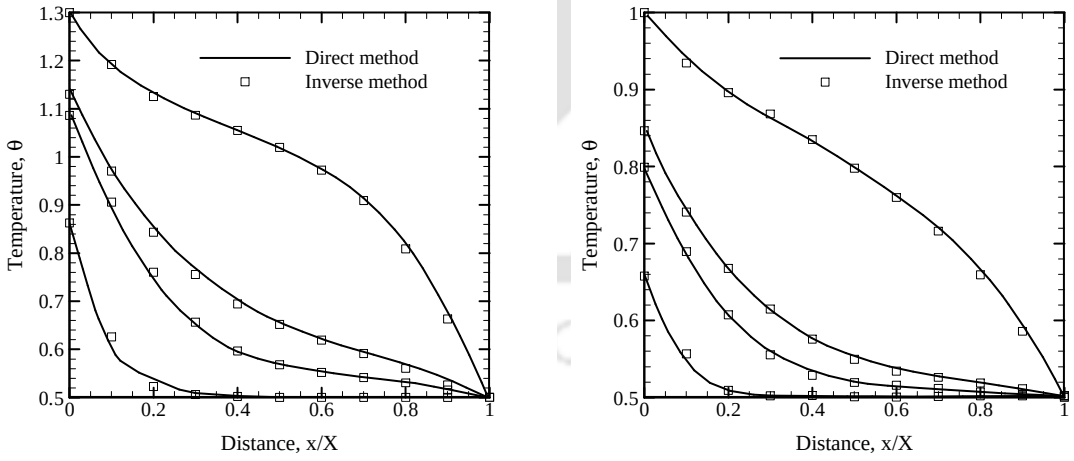

Figure 5.15: Comparison of the exact and estimated temperature θ, (a) $(\Psi_{T,W}, \varepsilon_W)$ = (1.0, 0.5) and (b) $(\Psi_{T,W}, \varepsilon_W)$=(0.4, 0.5); $\beta = 1.0, \omega = 0.5, \varepsilon_E = \varepsilon_W = 0.5$ and $N = 0.05$.

done for two sets of wall heat flux and the boundary emissivities viz. $\left(\Psi_{T,W}, \varepsilon_W\right)$= (1.0, 0.5) and (0.4, 0.5). The comparison has been carried out for the case corresponding to the measurement error *E*= 2.0. A similar justification presented in Fig. 5.14 can be provided for this case too. This comparison is carried out for four different time levels, viz., $\xi = 0.005, 0.03, 0.05$ and the steady-state. A very good agreement between the exact and estimated temperature fields can be observed even though there exists approximately 40% high error in one parameter and 30% low error in the other parameter as observed from Table 5.10. This is due to the reason that parameter dependencies and non uniqueness in the problem could yield different combination of the parameters satisfying a given temperature field. So, the inverse analysis of such kind of heat transfer problems help a designer to carefully design his experimental investigations and obtain the desired choice of parameters.

Table 5.11: Comparison of CPU times involved in the direct method and inverse method

Exact values	Estimated values	*E*	CPU time (s)		Ratio of CPU times
			Direct method	Inverse Method	
$\left(\Psi_{T,W}, \varepsilon_W\right)=(1.0, 0.5)$	(1.120, 0.526)	0.0	11.781	15709	1333.41
	(0.809, 0.453)	1.0		16352	1387.99
	(0.683, 0.609)	2.0		17253	1464.47

5.7.4 Comparison of CPU Time

In Table 5.11, we present the comparison of the CPU times elapsed in the direct method (LBM-FVM) and the inverse method (LBM-FVM-GA). This comparison has been performed for the simultaneous estimation of $\left(\Psi_{T,W}, \varepsilon_W\right)=\left(1.0, 0.5\right)$. The computations were performed on the 2.8 GHz CPU (Pentium (R) 4 with 248 MB RAM). For this comparison, the same set of genetic parameters such as the crossover probability of 0.8 and the mutation rate of 0.03 along with other parameters as considered for comparison in Fig. 5.15 are taken. This comparison has been done for three different values of the measurement errors, viz., E= 0.0, 1.0 and 2.0 are taken. From Table 5.11, it is observed that with increase in the measurement error E, the CPU time required in the direct method remains constant. However, the CPU time required by the GA increases with measurement error. This is due to the reason that calculation of the exact temperature field is obtained from the direct method which in the present work is computed using the LBM-FVM. Once this exact temperature field is obtained, measurement errors have been imposed and the minimization procedure is being carried out using the GA. Thus the GA needs to minimize a larger error when the measurement error increases. Consequently, the CPU time elapsed for the convergence also increases with the measurement error.

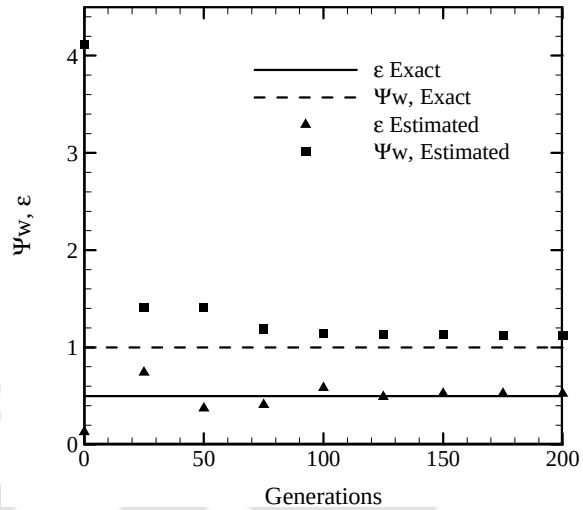

Figure 5.16: Comparison of the estimated and the exact values of the parameters with number of generations. (Range: $\left(\Psi_{T,W}, \varepsilon_W\right) = \left(0.0-5.0, 0.0-1.0\right)$).

5.7.5 Variation of Estimated Parameters

Fig. 5.16 shows the variation of the estimated parameters with number of generations. It is noticed that at around 100 generations, the estimated values matches very well with

that of the exact ones. With further increase in the number of generations, the variation is very small. It is also noticed from Fig. 5.16 that the estimation of west boundary heat flux Ψ_W requires more refinement as compared to the emissivity ε_W indicating a difficult estimation or converging tendency. This is due to the reason that the temperature field which is minimized in the inverse method is contributed by virtue of this heat flux imposed on the west boundary.

5. 8 Summary

Three different types of inverse transient conduction-radiation problem involving different levels of complexities were analyzed. At first, an inverse method was used for simultaneous estimation of parameters in a non-Fourier transient conduction-radiation problem. Two parameters such as the extinction coefficient and the conduction-radiation parameter were simultaneously estimated and they were compared with their exact value. Effects of different genetic parameters such as the crossover and the mutation probabilities, the population size, the number of generations were studied. For the non-Fourier transient conduction-radiation problem, for the crossover probability of 0.80, the mutation probability of 0.03 and a population size of 100, approximately 100 generations were found to be satisfactory. It was observed that at low measurement errors, the estimated values of both the conduction-radiation parameter and the extinction coefficient posses approximately the same accuracy. However, at large measurement error, the estimated accuracy of the conduction-radiation parameter is less than the extinction coefficient. A comparison of CPU times involved in the direct and the inverse method was also done. It was observed that the CPU time required in the inverse method varied approximately between 1400-1800 times than that required in the direct method. The accuracy of the estimated parameters was checked by comparing the temperature distributions obtained using the direct and the inverse method. The estimated results were found to be in reasonably good agreement with the exact ones. The LBM, the FVM and the GA have been found to provide reasonably correct estimates of unknown parameters in a non-Fourier conduction-radiation problem.

Next, an inverse method was used for the simultaneous retrieval of parameters in a transient conduction-radiation problem involving variable thermal conductivity. Different combinations of two parameters such as the extinction coefficient, the scattering albedo and the conduction-radiation parameter were simultaneously estimated and they were compared with their exact values. Effects of different genetic parameters such as the crossover and the mutation probabilities, the population size, number of generations were studied in this case too. In this problem too, for the crossover probability of 0.80, the mutation probability of 0.03 and a population size of 100, approximately 100 generations were found to be satisfactory. Effect of measurement errors on the accuracy of the retrieved parameters was also investigated. It was observed that in the simultaneous estimation of the conduction-radiation parameter and the extinction coefficient, error in estimation of the conduction-radiation parameter was more compared to the extinction coefficient. In case of the simultaneous estimation of the conduction-radiation parameter and the scattering albedo, at low measurement error, the error in the estimation of the scattering albedo was more than the conduction-radiation parameter. However, in the simultaneous estimation of the extinction coefficient and the scattering albedo, at lower measurement errors, the estimated error in the scattering albedo was more and vice versa. A comparison of the CPU times involved in the direct and the inverse method was also done. In this case the CPU times required in the inverse method were found to vary between 1500-1600 times than those required in the direct method. The accuracy of the estimated parameters was checked by comparing the temperature distributions obtained using the direct and the inverse method. The LBM and the FVM in conjunction with the

GA have been found to provide fairly good estimates for the unknown parameters in a transient conduction-radiation problem involving temperature dependent thermal conductivity.

Lastly, an inverse method for the reconstruction of temperature fields and estimation of boundary heat flux and emissivity subjected to a transient mixed boundary condition was analyzed. The problem was solved using the LBM and the FVM in conjunction with the GA. The estimated parameters were studied for the effect of measurement errors and genetic parameters such as the population size and number of generations. In the present problem, for the crossover probability of 0.80, the mutation probability of 0.03 and a population size of 100, approximately 200 generations were found to be satisfactory. In most of the cases, the error in the estimated values of the heat flux was found to be more as compared to the boundary emissivity. The ratio of CPU times required in the inverse method to the direct method was found to vary between 1300-1400 times. The reconstruction of the transient temperature field is also done by using the inverse method and the same was compared with the exact one. From the present investigation, it is found that for the inverse analysis, a good estimation of the unknown parameters is obtained using the LBM, the FVM and the GA. In the next chapter, we carry out an inverse analysis in a cylindrical geometry involving transient conduction and radiative heat transfer.

CHAPTER 6

Simultaneous Reconstruction of Thermal Field and Retrieval of Parameters in a Cylindrical Enclosure

6.1 Introduction

In the previous chapters, inverse analyses have been done to retrieve unknown medium properties and/or boundary conditions of transient conduction-radiation problems in 1-D planar and 2-D rectangular geometry. Problems of varying complexities were considered. The suitability of the LBM as a solver for the energy equations, the usage of the FVM for the computation of radiative information and the application of the GA as an optimization tool were successfully demonstrated by simultaneously retrieving either two or three unknown parameters. Because of the changing area in the radial direction, compared to a planar and a rectangular geometry, a cylindrical geometry brings additional difficulties. Computation of radiative information is much more difficult as unlike a 1-D planar medium, in case of a 1-D cylindrical geometry, the azimuthal symmetry does not exist. The cylindrical geometry finds plenty of applications in engineering devices. In the present chapter, we do the inverse analyses of transient heat conduction and radiative heat transfer in a concentric cylindrical enclosure. The LBM and the GA have been used for the inverse analysis of the transient heat conduction

problem. Since in the concentric cylindrical enclosure the DTM formulation is more simpler for the radiative heat transfer problem, the same has been done using the DTM and the GA. For the conduction problem, the unknown radius ratio that would yield a desired temperature distribution has been estimated. While in the radiative transfer problem, two parameters, viz., the extinction coefficient and the radius ratio that would provide a desired heat flux distribution in the medium have been simultaneously estimated. The accuracies of the estimated parameters are studied for the effects of measurement errors and the genetic variables. The CPU times disbursed in the direct method and the inverse method have also been compared. Below we provide the LBM formulation for the conduction heat transfer and the DTM formulation for the computation of radiative heat transfer in a cylindrical geometry.

6.2 Formulation of an Inverse Problem in a Cylindrical Geometry

6.2.1 LBM Formulation for Conduction Problem in a Cylindrical Geometry

In the macroscopic form, the general form of the generalized energy equation for a transient conduction problem applicable for a 1-D planar/cylindrical/spherical geometry can be written as

$$\rho c_p \frac{\partial T}{\partial t} = k \frac{\partial}{\partial r}\left(\frac{1}{r^n} \frac{\partial T}{\partial r} \right) \tag{6.1}$$

where for a planar medium, the exponent $n = 0$ and for a cylindrical medium, $n = 1$ and for a spherical medium $n = 2$. For a cylindrical geometry, Eq. (6.1) becomes

$$\rho c_p \frac{\partial T}{\partial t} = k \frac{\partial^2 T}{\partial r^2} + \frac{k}{r} \frac{\partial T}{\partial r} \tag{6.2}$$

The second term on the right hand side of Eq. (6.2) accounts for the effect of variable area in the cylindrical geometry, which in case of the planar geometry is absent. In the LBM, this term is accounted by modifying the discrete Boltzmann equation given in Chapter 2 as below:

$$\begin{aligned} f_i\left(\vec{r}+\vec{c}_i\Delta t, t+\Delta t\right) = f_i\left(\vec{r},t\right) - \frac{\Delta t}{\tau}\left[f_i\left(\vec{r},t\right) - f_i^{(0)}\left(\vec{r},t\right)\right] \\ + \frac{\Delta t}{\vec{r}\left(\vec{c}_i\Delta t\right)}\left[f_i\left(\vec{r}+\vec{c}_i\Delta t, t\right) - f_i\left(\vec{r},t\right)\right] \end{aligned} \tag{6.3}$$

Equation (6.3) is the LBM formulation of the transient heat conduction in a cylindrical medium. For a conduction-radiation problem in a planar geometry, this procedure has been shown in Mishra and Lankadasu [117].

The procedure of implementing prescribed temperature and/or heat flux boundary conditions in the cylindrical geometry remains the same as that for a Cartesian geometry and the same has been given in Chapter 2. Below we provide a brief formulation of the DTM to compute the radiative information.

6.2.2 Formulation for Radiative Transfer Problem

The radiative transfer equation as derived in Chapter 2 is given by the following equation,

$$\frac{dI}{ds} = -\beta I + S \tag{6.4}$$

The above equation being an ordinary differential equation can be easily solved in which the integrating factor is given by $\exp(-\beta ds)$

In the DTM, with the source term S_{av} assumed to be known from the previous iteration as an average of the source term values at the upstream S_u and the downstream S_d points, intensity at any radial location $\vec{r}$ in any direction (δ, ϕ) is found from the following [103, 118]:

$$I_d = I_u \exp(-\beta ds) + S_{av}\left[1 - \exp(-\beta ds)\right] \tag{6.5}$$

where I_d and I_u are the intensities at the downstream and the upstream points which are separated by a geometric distance ds and optical distance βds. The average source function $S_{av} = \frac{S_u + S_d}{2}$ is taken as the value in the middle of the path-leg.

For an absorbing, emitting and isotropically scattering medium, the source term is given by [118],

$$S = (1-\omega)\frac{\sigma T^4}{\pi} + \frac{\omega}{4\pi} G \tag{6.6}$$

where ω is the scattering albedo and G is the incident radiation which is given by and numerically computed from the following [118],

$$G = \int_{\phi=0}^{2\pi} \int_{\delta=0}^{\pi} I(\delta, \phi) \sin\delta \, d\delta \, d\phi \approx \sum_{k=1}^{M_\phi} \sum_{l=1}^{M_\delta} I^j(\delta_l^j, \phi_k^j) 2 \sin\delta_l^j \sin\left(\frac{\Delta\delta}{2}\right) \Delta\phi \tag{6.7}$$

where δ is the polar angle and ϕ is the azimuthal angle. With intensity distributions known, the radiative heat flux q_R is computed from the following [118]:

$$\begin{aligned} q_R &= \int_{\phi=0}^{2\pi} \int_{\delta=0}^{\pi} I(\delta,\phi)\cos\delta\sin\delta\, d\delta\, d\phi \\ &\approx \sum_{k=1}^{M_\phi} \sum_{l=1}^{M_\delta} I^j(\delta_l^j,\phi_k^j)\sin\delta_l^j\cos\delta_l^j\sin(\Delta\delta)\Delta\phi \end{aligned} \tag{6.8}$$

where M_δ and M_ϕ are the number of discrete points considered over the complete span of the polar angle $(0 \le \delta \le \pi)$ and azimuthal angle $(0 \le \phi \le 2\pi)$, respectively. Therefore, $M_\delta \times M_\phi$ constitute the number of discrete directions in which intensities are considered at any point.

While marching from either boundary of the inner cylinder or the outer cylinder, evaluation of Eq. (6.7) requires knowledge of the boundary intensity. For a diffuse-gray boundary having temperature T_b and emissivity ε_b, the boundary intensity I_b is computed from [118],

$$I_b = \frac{\varepsilon_b \sigma T_b^4}{\pi} + \left(\frac{1-\varepsilon_b}{\pi}\right) \sum_{k=1}^{M_\phi} \sum_{l=1}^{M_\delta/2} I^j\left(\delta_l^j,\phi_k^j\right)\sin\delta_l^j\cos\delta_l^j\sin\Delta\delta\Delta\phi \tag{6.9}$$

In Eq. (6.8), the first and the second terms represent the emitted and the reflected components of the boundary intensity, respectively.

Using the procedure described above, we evaluate the transient temperature profiles for the conduction problem and obtain the heat flux distribution for the radiation problem. In the inverse method we construct the objective function in the same manner as described

in the Chapter 2 and the same are not reproduced in this section. The only difference is that, in the conduction problem, we minimize the objective function represented by the square of the exact and the guessed temperature fields whereas in the radiative transfer problem, we minimize the heat flux profiles. In the estimation of the radius ratio and the extinction coefficient, the boundary emissivity was kept fixed at 1.0 and the medium was considered non-scattering, i.e., the scattering albedo was taken as 0.0. Being purely a radiative transfer problem, the conduction-radiation parameter assumes the value 0.0.

6.3 Results and Discussions

The following problems are considered:

- A concentric solid cylinder having inner and outer radii r_1 and r_2, respectively (Fig. 6.1) is initially at temperature $\theta = 0.1$ and for time $\xi \left(= \frac{\alpha t}{r_2^2} \right) > 0.0$, its inner boundary is raised to temperature $\theta_2 = 1.0$. The objective of the inverse analysis using LBM in conjunction with the GA is to reconstruct the temperature θ profile and estimate the radius ratio $\frac{r_1}{r_2}$.

- The concentric cylinder having inner and outer radii r_1 and r_2 (Fig. 6.1), respectively is filled with an absorbing and emitting participating isothermal medium. The cylinder boundaries are cold and are black. The objective of the inverse analysis in this problem is to reconstruct the flux Ψ profile and to

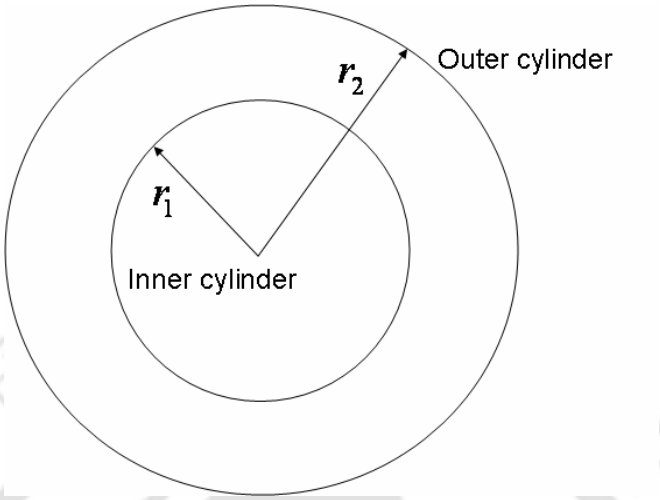

Figure 6.1: Physical geometry of the problem; initial condition and boundary conditions are $\theta = 0.1;\ \xi > 0 : \theta_1 = 0.1, \theta_2 = 1.0$

simultaneously estimate the extinction coefficient β and the radius ratio $\frac{r_1}{r_2}$. In this case, the DTM in conjunction with the GA is used in the inverse analysis.

In the following pages we provide the results for the simultaneous estimation of the temperature profile and radius ratio $\left(r_1 / r_2\right)$ in a conduction problem and estimation of extinction coefficient β and radius ratio $\left(r_1 / r_2\right)$ in a non-radiative equilibrium problem.

From grid and ray independency tests it is observed that 100 nodes in the DTM and 101 lattices in the LBM along with 16 rays in δ direction and 32 rays in ϕ direction are sufficient to obtain independent solutions. In Table 6.1, we compare the steady-state heat

Table 6.1: Comparison of the hot/inner boundary heat flux for different extinction coefficient computed using the DTM with those available in [101].

Extinction coefficient	Hot/Inner boundary heat flux	
	Modest [101]	Present work-DTM
0.1	0.1770	0.1767
0.2	0.3172	0.3161
0.3	0.4299	0.4280
0.4	0.5213	0.5186
0.5	0.5960	0.5928
0.6	0.6573	0.6537
0.7	0.7080	0.7041
0.8	0.7500	0.7460
0.9	0.7850	0.7809
1.0	0.8143	0.8102
1.5	0.9047	0.9008
2.0	0.9458	0.9425
2.5	0.9662	0.9636
3.0	0.9772	0.9752
3.5	0.9836	0.9823
4.0	0.9877	0.9869
4.5	0.9904	0.9901
5.0	0.9923	0.9924

flux $\Psi = \frac{q_R}{\sigma T_{\text{ref}}^4 / \pi}$ distribution for a non-radiative equilibrium problem computed in the present work with those available in Modest [101]. It is observed that a good agreement is attained between the present results and those available [101].

In order to establish the accuracy of the LBM for the application in concentric cylindrical media, in Fig. 6.2 we compare the results of the same with that obtained using the FDM and also that obtained analytically. For this comparison, a concentric cylindrical enclosure with radius ratio $\left(r_1 / r_2\right) = 0.5$ is considered. The hot and cold boundaries are

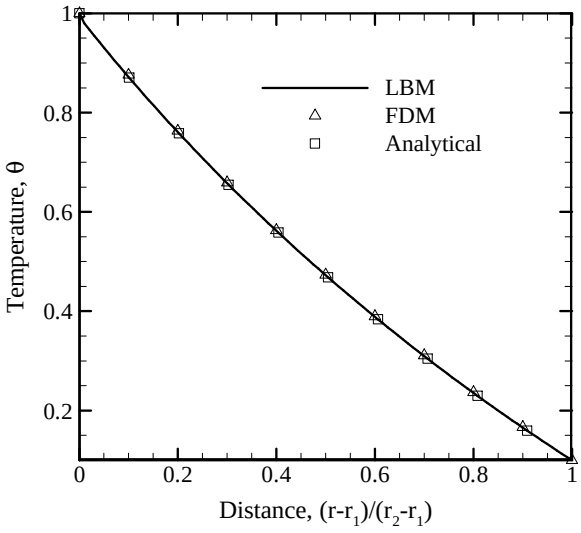

Figure 6.2: Comparison of the steady state temperature distribution computed using the LBM with that obtained analytically and by the FDM.

maintained at temperatures $\theta_1 = 1.0$ and $\theta_2 = 0.1$, respectively. An excellent agreement can be observed from Fig. 6.2.

Table-6.2 Comparison of the estimated and the exact values of the radius ratio along with measurement error. (Range: $\left(r_1/r_2 = 0.0 - 1.0\right)$

Exact value	Measurement error	Estimated Value	% Error
0.1	0.0	0.1072	7.2
	1.0	0.0801	-19.9
	2.0	0.1202	20.2
0.5	0.0	0.4603	-7.9
	1.0	0.4535	-9.3
	2.0	0.5814	16.2
0.9	0.0	0.8793	-2.3
	1.0	0.9402	4.4
	2.0	0.7805	-13.2

6.3.1 Effects of the GA Parameters

In Table 6.2, we compare the exact and the estimated values of the radius ratio for a conduction problem in a concentric cylindrical media. The tests have been shown for three different values of the radius ratios, viz., $\left(r_1/r_2\right)$ = 0.1, 0.5 and 0.9. For a particular value of the radius ratio, three different measurement errors E = 0.0, 1.0 and 2.0, have been considered. It is observed from Table 6.2 that the estimated results agree fairly well for the small measurement errors. With large estimation error E = 2.0, the maximum error in the estimated value is 20.2 %.

In order to study the effect of the population size on the value of the best fitness, a comparison is shown in Fig. 6.3. The test corresponds to two different population sizes of 25 and 100, respectively. For this study, the probability of the crossover and the mutation probabilities have been taken as P_c =0.8 and P_m =0.03. The results are shown for the case corresponding to the large measurement error i.e. E=2.0. It is seen that the values of the best fitness are more when the population size is small. This is because in a smaller population size, the availability of good solution or good individuals is less. Therefore, for a particular generation, the corresponding values of the objective function or the best fitness are comparetively larger as compared to those with larger population size. Moreover, 200 generations are found sufficient for a population size of 100. Thus, the results in this case are also in line with those obtained in previous investigations.

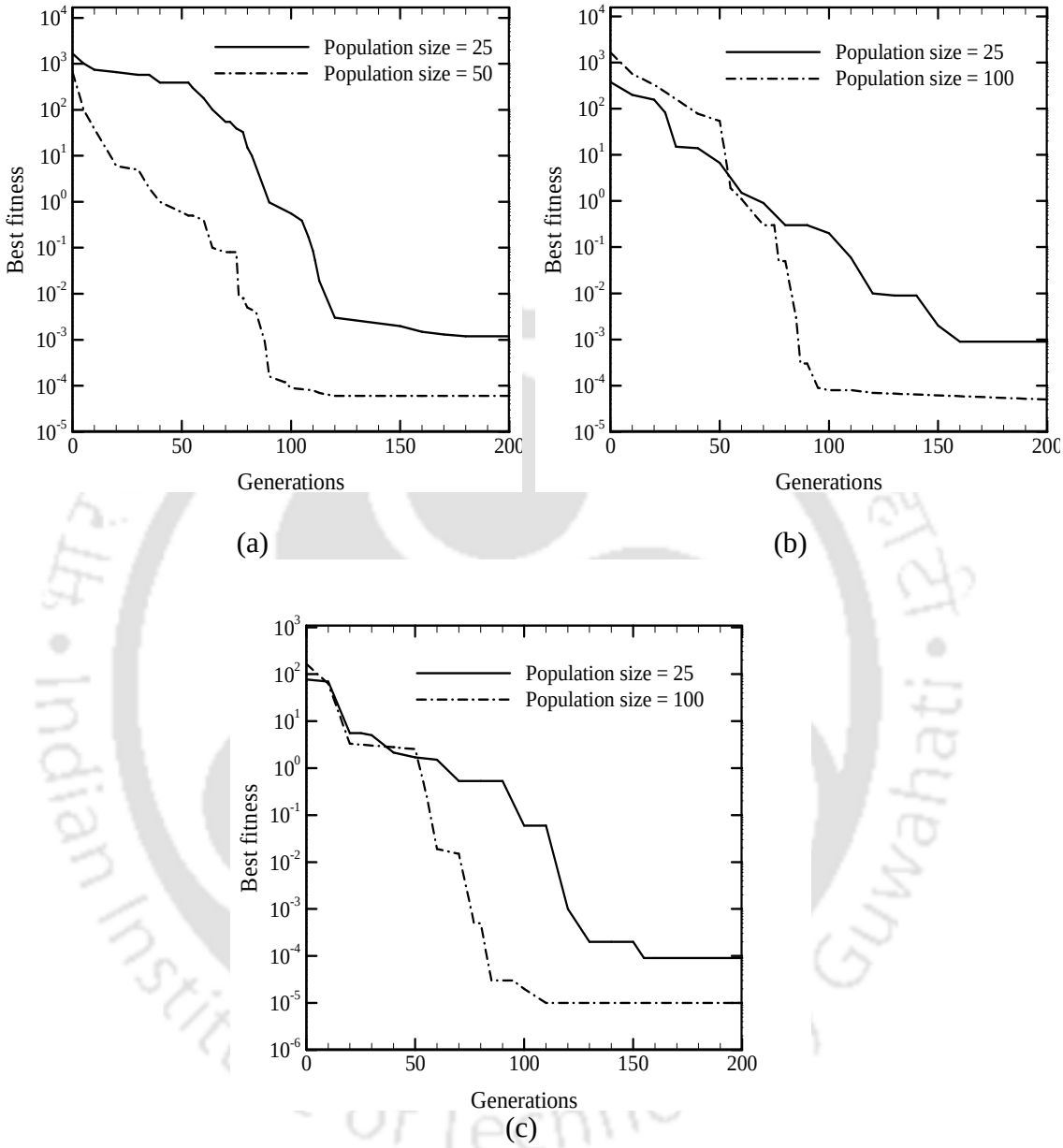

Figure 6.3: Variation of the best fitness for the estimation in radius ratio (a) $\left(r_1/r_2\right)$ = 0.1, (b) $\left(r_1/r_2\right)$=0.5 and (c) $\left(r_1/r_2\right)$=0.9

Table 6.3 shows the estimation of parameters for radiative transfer problems subjected to different measurement errors. In this case, simultaneous estimation of two parameters, viz., the extinction coefficient β and the radius ratio r_1/r_2 have been done. It is observed that in most of the cases, the estimation accuracy of the radius ratio is better than the extinction coefficient. This is because, in the estimation of the radius ratio, the search is performed for a narrower range of 0.0 and 1.0. However, in other cases too, the difference in the estimation accuracy between the extinction coefficient and the radius ratio is within 9%.

Table-6.3 Comparison of the exact and estimated values of $\left(\beta, r_1/r_2\right)$ for different measurement errors (Range: $\left(\beta, r_1/r_2\right) = \left(0.0-10, 0.0-1.0\right)$)

Exact value $\left(\beta, r_1/r_2\right)$	Measurement error	Estimated Value	% Error
(1,0.5)	0.0	(1.011, 0.513)	(1.1, 2.6)
	1.0	(0.953, 0.544)	(-4.7, 8.8)
	2.0	(0.879, 0.399)	(-12.1, -20.2)
(5,0.5)	0.0	(4.617, 0.495)	(-7.6, -1.0)
	1.0	(5.703, 0.561)	(14.0, 12.2)
	2.0	(4.203, 0.602)	(-15.9, 20.4)
(5,0.001)	0.0	(4.79, 0.001)	(-4.2, 0.0)
	1.0	(4.533, 0.001)	(-9.3, 0.0)
	2.0	(4.381, 0.001)	(-12.3, 0.0)

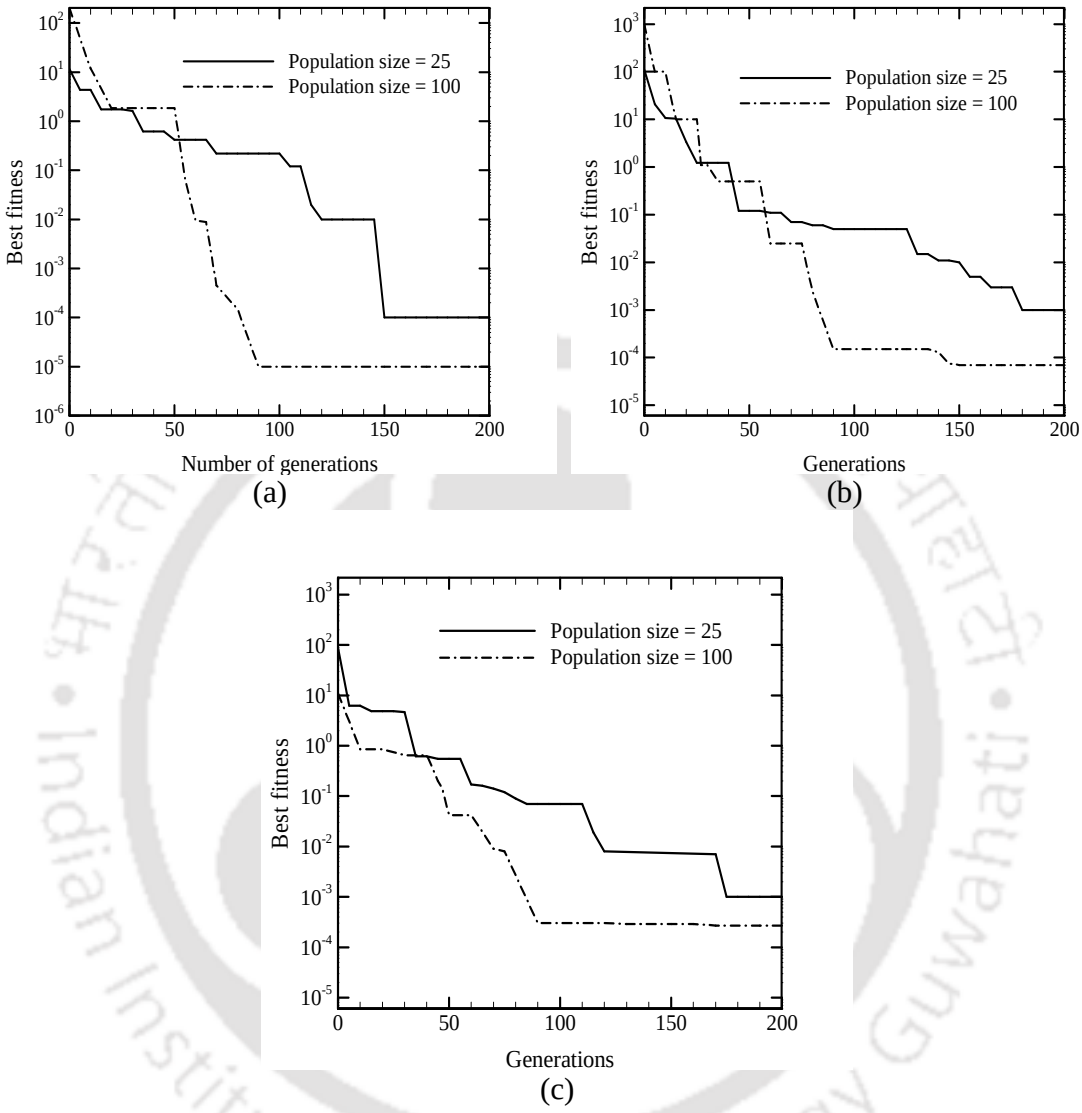

Figure 6.4: Variation of the best fitness for the estimation in radius ratio (a) β =1.0, $\left(r_1/r_2\right)$ = 0.5, (b) β =5.0, $\left(r_1/r_2\right)$=0.5 and (c) β =5.0, $\left(r_1/r_2\right)$=0.0.

In order to investigate the variation in best fitness against two different population sizes of 25 and 100, for the set of parameters considered in Table 6.3, we present a comparison in Fig. 6.4. The same trend as observed for the conduction problem is observed in this case too.

6.3.2 Comparison of Reconstructed and Exact Thermal Fields

In order to verify the temperature profiles at transient as well as steady-state, the exact and estimated temperature profiles are presented in Fig. 6.5. The results are shown for the case corresponding to the largest measurement error E=2.0. It is observed that the estimated results match very well with that of the exact ones at all time levels. However, it is also noticed from the figure that at lower value of the radius ratio, the attainment of the steady-state is relatively slower than those having higher radius ratio. Moreover, at particular location, the steady-state temperatures are also lesser than those with higher values of the radius ratio. This is because at lower values of the radius ratio, the hot and the cold cylindrical surfaces are at a larger distance. Therefore, the thermal disturbance propagates through a larger distance and thus consumes more time. Therefore, the attainment of the steady-state is delayed. A lower value of the radius ratio also means a less temperature availability at the colder boundary. Thus, the temperatures are generally less for lower radius ratios. On the other hand, when the cold and the hot surfaces are at close proximity, the rate of energy exchange is also faster and, therefore, the steady-state times are less and a higher temperature distribution is obtained.

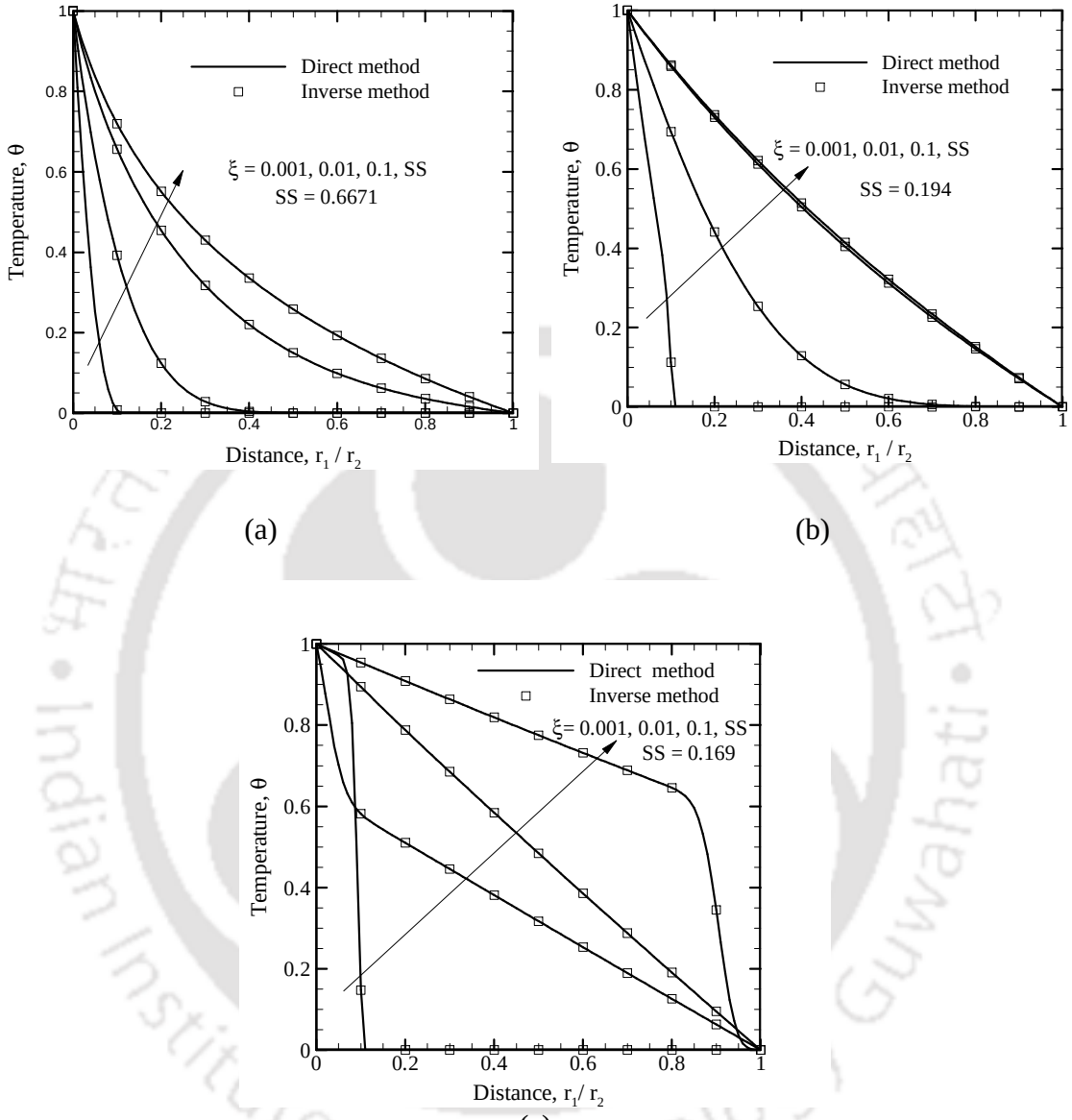

Figure 6.5: Comparison of the estimated and exact temperature profiles (a) radius ratio=0.1, (b) radius ratio=0.5 and (c) radius ratio=0.9.

Thus it is observed that the method involving LBM-GA is well capable for simultaneous estimation of the temperature profile and the radius ratio. In the following pages, we present the results of simultaneous estimation of extinction coefficient and radius ratio in

a non-radiative equilibrium problem. The comparison of the estimated values of the heat flux, Ψ distributions at different radial locations are shown in Fig. 6.6. This has been carried out for different sets of radius ratios and extinction coefficients. It is observed that the local heat flux distributions shift to lower values with increase in extinction coefficient due to loss of radiative information. Further, it is also noticed from Fig. 6.6 that at a given value of the extinction coefficient, the local heat flux are lower when the radius ratio decreases due to slower energy exchange and more loss of the radiative energy. An excellent comparison is observed between the exact and the estimated radiative heat flux profiles.

6.3.3 Variation of Estimated Parameters

For measurement error, E=0.0, Figs. 6.7a and 6.7b represent variations of the estimated parameters in the conduction and the radiative transfer problems, respectively. It is observed that initially the process starts with a values of the estimated parameter which deviates considerably from the actual value and successively undergoes refinements until the convergence or satisfactory values close enough to the actual ones are obtained. It is observed that at approximately 200 numbers of generations, the exact and the estimated values are in excellent match with each other. This indicates the requirement of an optimization algorithm which must be robust enough to perform the desired task.

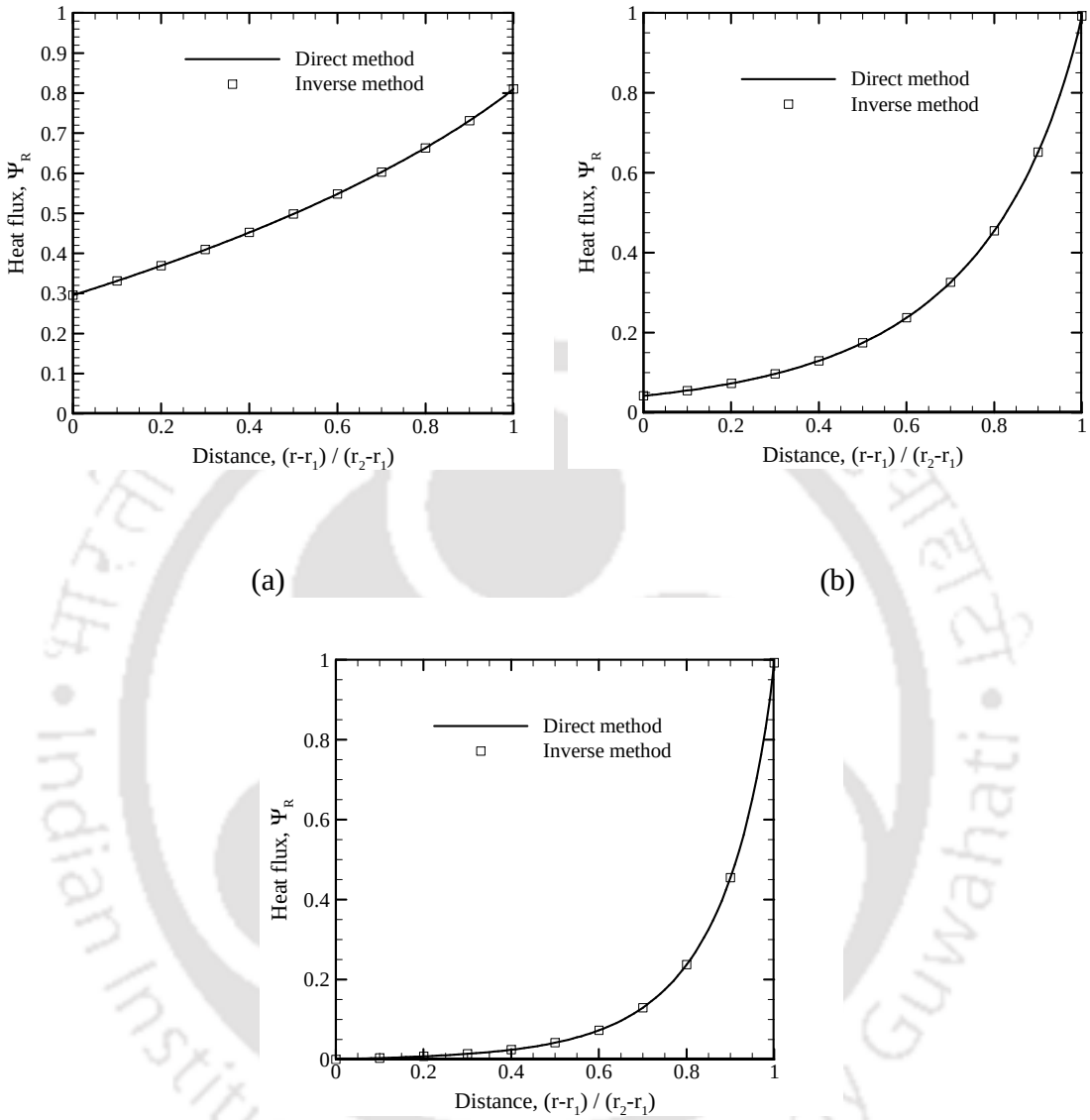

Figure 6.6: Comparison of the estimated and exact heat fluxes (a) β =1.0, $\left(r_1/r_2\right)$ = 0.5, (b) β =5.0, $\left(r_1/r_2\right)$=0.5 and (c) β =5.0, $\left(r_1/r_2\right)$=0.0.

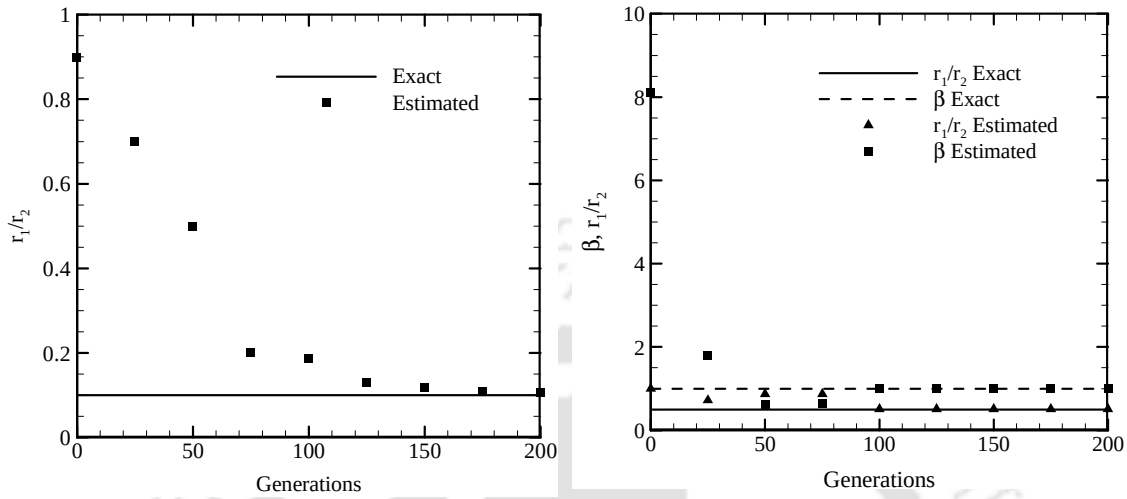

(a) (b)

Figure 6.7: Comparison of the exact and the estimated values of parameters with generations for (a) conduction problem and (b) radiative transfer problem.

6.3.4 Comparison of CPU Time

In order to compare the CPU times disbursed in the direct as well as inverse methods, we present a comparison in Tables. 6.4 and 6.5 for the conduction and the radiation problems, respectively.

From Table 6.4, it is observed that the attainment of the steady-state is faster for a concentric cylinder having a larger radius ratio $\frac{r_1}{r_2}$. This is due to the reason that when the radius ratio $\frac{r_1}{r_2}$ is more, the two boundaries are in close proximity. Therefore, the rate of heat exchange is faster and consequently the attainment of the steady-state is faster. For a smaller radius ratio, the CPU time disbursed in the inverse method is approximately 70

times more than that expended in the direct method. However, for a larger radius ratio, the CPU time required in the inverse method is almost 3500 times more than that required in the direct method. It is also observed from Table 6.4 that the CPU time required in the inverse method does not vary considerably with the increase in the radius ratio $\frac{r_1}{r_2}$. This is due to the reason that in both the direct and the inverse problems, the solution of the energy equation to solve for the temperature field is not computationally intensive. Since the GA consumes more time in the minimization process, the CPU time in the inverse method is more than the direct method. The major difference in the CPU time owing to the solution of the energy equation does not get reflected in the inverse analysis.

From Table 6.5, it is noticed that for the reconstruction of the heat flux Ψ field and for simultaneously estimating the extinction coefficient β and the radius ratio $\frac{r_1}{r_2}$, CPU times required in the inverse method is almost 1700 times more than those required in the direct method. Moreover, as observed in Table 6.4, it is noticed that the CPU times required in the inverse method do not vary considerably in this case too.

Table 6.4: Comparison of CPU times in the direct and inverse methods for the conduction problem.

Exact value of $\frac{r_1}{r_2}$	CPU time required (s)		Ratio of CPU time in direct and Inverse method
	Direct method	Inverse method	
0.1	43.662	2279	71.11
0.5	7.661	1838	230.18
0.9	0.515	1826	3545.63

Table 6.5: Comparison of CPU times in the direct and inverse methods for the radiation problem.

Exact value of $\left(\beta, \frac{r_1}{r_2}\right)$	CPU time required (s)		Ratio of CPU time in direct and Inverse method
	Direct method	Inverse method	
(5.0, 0.0)	1.047	1776	1696.27
(5.0, 0.5)	0.906	1639	1809.05
(1.0, 0.5)	0.890	1597	1794.38

6.4 Summary

An inverse method was used for the reconstruction of temperature and heat flux profiles and for parameter estimation in a transient conduction and radiation problem in a concentric cylindrical enclosure. In the conduction problem, the radius ratio was estimated using an inverse analysis involving the LBM and the GA. Effects of different genetic parameters such as the population size and the number of generations were studied. Effect of measurement errors on the accuracy of the retrieved parameters was also investigated. It was observed that the estimated error in the radius ratio did not exceed beyond 9%. The temperature fields obtained using the direct method and those obtained using the estimated value of the unknown parameter in the inverse method were also compared and found to be in good agreement. For all the estimated range of the radius ratio, the ratio of CPU times involved in the direct method to the inverse method approximately varied between 71 -3545. In the radiative transfer problem, simultaneous estimation of two parameters viz., the extinction coefficient and the radius ratio was done

by an inverse analysis involving the DTM and the GA. The effect of various GA parameters was also studied in the present problem. It was observed that, for all measurement errors, the maximum estimated error in the radius ratio and the extinction coefficient did not exceed 21% and 16%, respectively. The accuracy of the estimated parameters was checked by comparing the heat flux fields obtained using the direct and the inverse method. In this case, the ratio of CPU times involved in the direct method and the inverse method approximately varied between 1700 - 1800. The DTM in conjunction with the GA was found suitable to accurately reconstruct the heat flux fields and also in estimating the parameters even with data containing measurement errors.

CHAPTER 7

Conclusions and Scope for Future Work

This dissertation dealt with the analysis of inverse transient conduction-radiation heat transfer problems in 1-D planar, 2-D rectangular and 1-D cylindrical geometry. The aim of the work is to propose a methodology to retrieve various thermophysical properties, surface properties, geometric properties and boundary conditions from the knowledge of temperature distributions in the medium in transient conduction-radiation heat transfer problems. Different types of estimation of unknown parameters such as the conduction-radiation parameter, the extinction coefficient, scattering albedo, boundary emissivity as well as unknown boundary conditions was carried out. Different types of conduction-radiation problems involving varying complexities and involving different geometric configurations were studied. The governing energy equation was solved using the LBM and the FVM was used to compute the radiative information. However, the DTM was used for the solution of radiative transfer problem in a 1-D concentric cylindrical geometry. In the inverse analysis, the GA was used as an optimization tool. The usage of the LBM, the FVM or the DTM and the GA was studied for the simultaneous estimation of various unknown properties and/or unknown boundary conditions. The quality of the estimated values of the unknown parameters was studied for the effect of different optimization/GA parameters and measurement errors. The CPU times involved in the direct method and those required in the inverse method were also compared. Inverse

analysis was carried out for a total of six problems. In the following pages conclusions of the study made in this work are presented and scope for the future work are enumerated.

7.1 Conclusions

The work starts with a transient conduction-radiation problem and the effect of parameters such as the scattering albedo, the conduction-radiation parameter and the boundary emissivity on the temperature distribution and simultaneous estimation of combination of two parameters is done in a 1-D planar medium. The conclusions are as mentioned below:

- The local temperature distributions are higher for lower value of the scattering albedo, the conduction-radiation parameter and higher value of emissivity.
- The solution accuracy was found to dependent upon the GA parameters and measurement error.
- The maximum error in the estimated values of the conduction-radiation parameter, the scattering albedo and the emissivity were +38%, +37% and -28.5%, respectively. These high errors indicate that the high values of mutation probabilities are undesirable.

The second problem undertaken in the present study was a transient conduction-radiation problem in a 2-D Cartesian enclosure. In this chapter, in addition to the investigation of medium and boundary properties, simultaneous estimation of three

parameters such as the conduction-radiation parameter, the scattering albedo and the boundary emissivity was done for different ranges of parameters. The conclusions derived from the study are as mentioned below:

- The local temperature distributions are higher for lower value of the scattering albedo, the conduction-radiation parameter and higher value of emissivity.
- Crossover probability of 0.80 and mutation probability of 0.03, population size of 100 and 200 generations were found to yield the most accurate estimation.
- At maximum measurement error, the maximum error in the conduction-radiation parameter, the scattering albedo and the emissivity was found to be +11%, -0.9% and -12%, respectively.
- Mere attainment of minimum value of the objective function does not always guarantee correct estimation of parameters. In other words, many combinations of the estimated parameters can provide a given temperature field.

Next, three problems containing different level of non-linearites and boundary conditions were investigated. The problems considered are non-Fourier, variable thermal conductivity and mixed boundary condition type of conduction-radiation problems. The main conclusions derived from the study are the following:

- In the non-Fourier problem, with most suitable value of the GA parameters (crossover probability of 0.80 and mutation probability of 0.03) at a measurement error of E= 2.0, the accuracy in the estimation of the conduction-

radiation parameter and the extinction coefficient were -14% and +5%, respectively. Population size and generation size of 100 were found to be satisfactory.

- The effect of variable thermal conductivity is observed to have very insignificant effect in radiation dominant situation.
- In the variable thermal conductivity problem, with best combination of the GA parameters, the accuracy in the simultaneous estimation of the conduction-radiation parameter and the extinction coefficient were -18% and -14%, respectively. In the estimation of the conduction-radiation parameter and the scattering albedo this was found to be +28% and -26%, respectively. Whereas, in the estimation of the extinction coefficient and the scattering albedo, the accuracy was +29% and -22%, respectively.
- Crossover and mutation probabilities of 0.80 and 0.03 provide better results. Population and generation size of 100 each was found to yield satisfactory solutions for the variable thermal conductivity problem.
- In the conduction-radiation problem involving variable thermal conductivity, the estimation of boundary heat flux was found relatively difficult than the boundary emissivity due a non-linear dependency of the temperature field on the total heat flux. At highest level of measurement error, the error in the estimation of the boundary heat flux and the emissivity were found to be +38% and -27%, respectively.
- In the conduction-radiation problem involving mixed boundary condition, a higher value of boundary heat flux gives higher local temperatures.

- Crossover and mutation probabilities of 0.80 and 0.03, respectively and population and generation size of 100 and 200, respectively were found to provide better solutions in the mixed boundary condition problem.

In the last problem, the study of conduction and radiation problem in a concentric cylindrical enclosure was carried out. The following conclusions were derived from the analysis:

- As radius ratio increases, the local temperature in the medium also rises significantly.
- For a given value of radius ratio, the local heat flux distributions shift to lower values with increase in extinction coefficient due to loss of radiative information.
- Estimated error in the radius ratio did not excced +20% even at a measurement error of E = 2.0.
- In the simultaneous estimation of the extinction coefficient and the radius ration, for all measurement errors, the maximum estimated error in the radius ratio and the extinction coefficient did not exceed 21% and 16%, respectively .

Therefore from the study it can be concluded that in the estimation of unknown parameters involving transient conduction-radiation, the LBM-FVM-GA can be successfully applied. However, proper care needs to be taken in the selection of GA parameters which could significantly affect the solution quality. Furthermore, it should be noted that mere attainment of a desired thermal field doesnot always guarantee correct estimation because of the availability of a number of possible combinations of

the unknown parameters satisfying a given temperature field. This happens when the retrieved parameters are interrelated and the temperature field possess non-linearities especially when the involvement of thermal radiation becomes appreciable especially at high temperatures. Therefore such kind of inverse analysis are useful in the design of high temperature heating enclosures and combustion chambers involving high temperature heating.

Further, a comparison of CPU times for different inverse problems show that the problems involving different complexities could be solved without significant variation in CPU times. For example, 1-D Fourier conduction-radiation problem, variable thermal conductivity problem and the mixed boundary condition type problem comsumes approximately same amount of CPU time. This is possibly due to the ability of LBM to absorb non-linearities into its own framework and don't allow the enhancement of CPU times drastically. On the other hand, non-Fourier conduction–radiation problem and the cylindrical geometry problem consumes even lesser time. Thus the usage of LBM in such cases is very helpful when problems in different geometries and involving different non-linerities exist.

7.2 Scope for the Future Work

In the present work, unknown parameters in transient conduction and radiation heat transfer problems were estimated using the inverse analyses. Energy equations of all problems were formulated using the LBM. For the 1-D planar and the 2-D rectangular

geometry, the radiative information were obtained using the FVM, while in case of a 1-D cylindrical enclosure, the DTM was used to compute the radiative information. In all cases, optimizations of the objective functions were done using the GA. The present analyses have resulted in some important findings as summarized above. However, this study has also paved way for further work in the area of inverse analysis, and applications of the methods, viz., the LBM, the FVM, the DTM and the GA used in such problems. With reference to these accomplishments, scopes for the future work are enumerated below:

- Inverse analyses of volumetric radiation in the presence of conduction and convection need to be explored for simple as well complex geometry. This analysis can be done for the estimation of different parameters such as the Prandtl number, Grashof number, Rayleigh number, etc.
- Estimation of heater powers in a multi-dimensional heating chamber can be investigated. In this problem, walls of a heating chamber can have a finite number of panel heaters and their powers can be different. For a specified temperature or heat flux distributions along the design object located inside the chamber, the required heater powers need to be estimated.
- Inverse problems involving pulsed radiation can be studied to estimate the inhomogenity contained inside the medium. This can effectively be used in cancer treatment applications.

- The above problems can be investigated using the LBM, the FVM and the GA and by solving the same problems using other methods, a recommendation can be made on usage of these methods for more general problems.
- By keeping the solver for the energy equation, such as the LBM and the method for calculation of the radiative information, such as the FVM, as the same, usages of different optimization algorithm viz., the GA, the CGM, the particle swarm method, the tabu search method, the ant colony method, etc., can be compared and a suitable recommendation about an optimization method can be made.
- A comparison of the combination of evolutionary and deterministic methods can be made.

References

1. J. Hadamard, *The Psychology of Invention in the Mathematical Field* Princeton University Press, Princeton, NJ, 1945.
2. M.N. Ozisik and H.R.B Orlande, *Inverse Heat Transfer: Fundamentals and Applications*, Taylor & Francis, New York, 2000.
3. M.T. Chahine, Inverse Problems in Radiative Transfer: Determination of Atmospheric Parameters, *J. Atmospheric Sciences*, Vol. 27, pp. 960-967, 1970.
4. F. Caparrini, F. Castelli and D. Entekhabi, Mapping of Land-Atmosphere Heat Fluxes and Surface Parameters with Remote Sensing Data, *Boundary Layer Meteorology*, Vol. 107, pp. 605-633, 2004.
5. E.A. Ustinov, The Inverse Problem of Multi-scattering Theory and the Interpolation of Measurements of Scattered Radiation in the Cloud Layer of Venus, *Cosmic Res.* ,Vol. 15, pp. 667-672, 1977.
6. T. Schmugge, S.J. Hook and C. Coll, Recovering Surface Temperature and Emissivity from Thermal Infrared Multispectral Data - Physical Principles and Inverse Modeling, *Remote Sensing of Environment*, Vol. 65, pp. 121-131, 1998.
7. M.A. Katz and B. Rubinsky, An Inverse Finite-Element Technique to Determine the Change of Phase Interface Location in One-Dimensional Melting Problems, *Numer. Heat Transfer, A*, Vol. 7, pp. 269-283, 1984.

8. M.A. Martorano and J.D.T. Capocchi, Heat Transfer Coefficient at the Metal-Mould Interface in the Unidirectional Solidification of Cu-8%Sn Alloys, *Int. J. Heat Mass Transfer*, Vol. 43, pp. 2541-2552, 2000.

9. D.-S. Kwag, I-S Park and W-S. Kim, Inverse Geometry Problem of Estimating the Phase Front Motion of Ice in a Thermal Storage System, *Inverse Prob. Sci. Eng.*, Vol. 12, pp. 1-15, 2004.

10. S.K. Kim, B.S. Jung, H.J. Kim and W. Lee, Inverse Estimation of Thermophysical Properties for Anisotropic Composite, *Experimental Thermal and Fluid Science*, Vol. 27, pp. 697–704, 2003.

11. A.S. Milani and J.A. Nemes, An Intelligent Inverse Method for Characterization of Textile Reinforced Thermoplastic Composites using a Hyperelastic Constitutive Model, *Composite Science and Technology*, Vol. 64, pp. 1565-1576, 2004.

12. R. Koker, Reliability-Based Approach to the Inverse Kinematics Solution of Robots using Elman's Networks, *Engineering Applications of Artificial Intelligence*, Vol. 18, pp. 685-693, 2005.

13. C-H. Huang and H.-C. Lo, A Three-Dimensional Inverse Problem in Predicting the Heat Fluxes Distribution in the Cutting Tools, *Numer. Heat Transfer, A*, Vol. 48, pp. 1009-1034, 2005.

14. H.J. Kim, N.K. Kim and J.S. Kwak, Heat Flux Distribution Model by Sequential Algorithm of Inverse Heat Transfer for Determining Workpiece Temperature in Creep Feed Grinding, *Int. J. Machine Tools and Manufacture*, Vol. 46, pp. 2086-2093, 2006.

15. S. Mroz, A. Stefanik and H. Dyja, The Application of the Inverse Method for Determination of Slitting Criterion Parameter during the Multi Slit Rolling (MSR) Process, *J. Materials Processing Technology*, Vol. 177, pp. 493-496, 2006.

16. J. Pujana, P.J. Arrazola, R. M'Saoubi and H. Chandrasekaran, Analysis of the Inverse Identification of Constitutive Equations Applied in Orthogonal Cutting Process, *Int. J. Machine Tools and Manufacture*, Vol. 47, pp. 2153-2161, 2007.

17. Y.C. Yang, W.J. Chang , T.H. Fang and S.C. Fang, Modelling of Thermal Conductance during Microthermal Machining with Scanning Thermal Microscope using an Inverse Methodology, *Physics Letters, A*, Vol. 372, pp. 519-523, 2008.

18. C. Guo and S. Malkin, Inverse Heat Transfer Analysis of Grinding, Part I: Method, *ASME J. Eng. Ind.* ,Vol. 118, pp. 137–142, 1996.

19. P. Lair, J. Dumoulin and P. Millon, Inverse Method for Flux Characterization using Infrared Thermography in Die Forging, *Numer. Heat Transfer, A*, Vol. 33, pp. 267-277, 1998.

20. C.H. Huang and M.N. Ozisik, Direct Integration Approach for Simultaneously Estimating Temperature Dependent Thermal Conductivity and Heat Capacity, *Numer. Heat Transfer, A*, Vol. 20, pp. 95-110, 1991.

21. C.H. Huang and M.N. Ozisik, Inverse Problem of Determining Unknown Wall Heat Flux in Laminar Flow through a Parallel Plate Duct, *Numer. Heat Transfer, A*, Vol. 21, pp. 55-70, 1992.

22. H.Y. Li, Estimation of the Temperature Profile in a Cylindrical Medium by Inverse Analysis, *J. Quant. Spectrosc. Radiat. Transfer*, Vol. 52, pp. 755-764, 1994.

23. S. Garcia, and E. P. Scott, Use of Genetic Algorithms in Thermal Property Estimation: Part I - Experimental Design Optimization, *Numer Heat Transfer, A*, Vol. 33, pp. 135-147, 1998.

24. S. Garcia, J. Guynn, and E.P. Scott, Use of Genetic Algorithms in Thermal Property Estimation: Part II – Simultaneous Estimation of Thermal Properties, *Numer. Heat Transfer, A*, Vol. 33, pp. 149-168, 1998.

25. P.-T. Hsu, C.-K. Chen and Y.-T. Yang, A 2-D Inverse Method for Simultaneous Estimation of the Inlet Temperature and Wall Heat Flux in a Laminar Circular Duct Flow, *Numer. Heat Transfer, A*, Vol. 34, pp. 731-745, 1998.

26. R.S. Banim, M.J. Tierney and P.N. Brett, The Estimation of Fluid Temperatures through an Inverse Heat Conduction Technique, *Numer. Heat Transfer, A*, Vol. 37, pp. 465 –476, 2000.

27. E. Divo, A. Kassab and F. Rodriguez, Characterization of Space Dependent Thermal Conductivity with a BEM-Based Genetic Algorithm, Numer. Heat Transfer, A, Vol. 37, pp. 845 –875, 2000.

28. J. Su and G.F. Hewitt, Inverse Heat Conduction Problem of Estimating Time-Varying Heat Transfer Coefficient, *Numer. Heat Transfer, A*, Vol. 45, pp. 777-789, 2004.

29. C.K. Chen, L.W. Wu and Y.T. Yang, Application of the Inverse Method to the Estimation of Heat Flux and Temperature on the External Surface in Laminar Pipe Flow, *Applied Thermal Engineering*, Volume 26, pp. 1714-1724, 2006.

30. M. A. Iglesias, C. Dawson, The Representer Method for State and Parameter Estimation in Single-Phase Darcy Flow, *Computer Methods in Applied Mechanics and Engineering*, Vol. 196, pp. 4577-4596, 2007.

31. S. Rouquette, J. Guo, P. L. Masson, Estimation of the Parameters of a Gaussian Heat Source by the Levenberg–Marquardt Method: Application to the Electron Beam Welding, *Int. J. Thermal Sci.*, Vol. 46, pp. 128-138, 2007.

32. W.L. Cheng and Y.C. Yang, On the Inverse Heat Convection Problem of the Flow over a Cascade of Rectangular Blades, *Int. J. Heat Mass Transfer*, Vol. 51, pp. 4184-4194, 2008.

33. H. J. Reinhardt and D. N. Hao, A Sequential Conjugate Gradient Method for the Stable Numerical Solution to Inverse Heat Conduction Problems, *Inv. Prob. Sci. Eng.*, Vol. 2, pp. 263-272, 1996.

34. T. F. Chen, S. Lin and J.C. Y. Wang, An Application of Kalman Filter and Finite Difference Scheme to Inverse Heat Conduction Problems, *Inv. Prob. Sci. Eng.*, Vol. 3, pp. 163-175, 1996.

35. O. M. Alifanov and A. V. Nenarokomov, Boundary Inverse Heat Conduction Problem: Algorithm and Error Analysis, *Inv. Prob. Sci. Eng.*, Vol. 9, pp. 619-644, 2001.

36. C. H. Huang, D. M. Wang and H. M. Chen, Prediction of Local Thermal Contact Conductance in Plate Finned-Tube Heat Exchangers, *Inv. Prob. Sci. Eng.*, Vol. 7, pp. 119-141, 1999.

37. H.Y. Li, Estimation of Thermal Properties in Combined Conduction and Radiation, *Int. J. Heat Mass Transfer*, Vol. 42, pp. 565-572, 1999.

38. L.H. Liu, Simultaneous Identification of Temperature Profile and Absorption Coefficient in One-Dimensional Semitransparent Medium by Inverse Radiation Analysis, *Int. Comm. Heat Mass Transfer*, Vol. 27, pp. 635-643, 2000.

39. H.M. Park and T.Y. Yoon, Solution of the Inverse Radiation Problem using a Conjugate Gradient Method, *Int. J. Heat Mass Transfer*, Vol. 43, pp. 1767-1776, 2000.

40. H.M. Park and T.Y. Yoon, Solution of Inverse Radiation Problems using the Karhunen-Loeve Galerkin Procedure, *J. Quant. Spectrosc. Radiat. Transfer*, Vol. 68, pp. 489-506, 2001.

41. H.M. Park and D.H. Yoon, A Multidimensional Inverse Radiation Problem of Estimating the Strength of a Heat Source in Participating Media, *Int. J. Heat Mass Transfer*, Vol. 44, pp. 2949-2956, 2001.

42. H.M. Park and W.J. Lee, The Solution of Inverse Radiation Problems using an Efficient Computational Technique, *J. Quant. Spectrosc. Radiat. Transfer*, Vol. 73, pp. 41-54, 2002.

43. H. Erturk, O.A. Ezekoye and J.R. Howell, The Application of an Inverse Formulation in the Design of Boundary Conditions for Transient Radiative Enclosure, *J. Heat Transfer*, Vol. 124, pp. 1095-1102, 2002.

44. J. R. Shenefelt, R. Luck, R. P. Taylor and J. T. Berry, Solution to Inverse Heat Conduction Problems Employing Singular Value Decomposition and Model-Reduction, *Int. J. Heat Mass Transfer*, Vol. 45, pp. 67-74, 2002.

45. H.T Chen, S.Y Lin, H.R Wang and L.C. Fang, Estimation of Two-Sided Boundary Conditions for Two-Dimensional Inverse Heat Conduction Problems, *Int. J. Heat Mass Transfer*, Vol. 45, pp. 15-23, 2002.

46. S.M.H. Sarvari, S.H. Mansouri and J.R. Howell, Inverse Boundary Design Radiation Problem in Absorbing-Emitting Media with Irregular Geometry, *Numer. Heat Transfer, A*, Vol. 43: 565–584, 2003.

47. S.M.H. Sarvari, J.R. Howell and S.H. Mansouri, Inverse Boundary Design Conduction-Radiation Problem in Irregular Two-Dimensional Domains, *Numer. Heat Transfer, B,* Vol. 44: 209–224, 2003.

48. C.Y. Yang, Estimation of Boundary Conditions in Non-Linear Inverse Heat Conduction Problems, *J. Thermophys. Heat Transfer*, Vol. 17, pp.389-395, 2003.

49. X. Ling, R. G. Keanini , H. P. Cherukuri, A Non-Iterative Finite Element Method for Inverse Heat Conduction Problems, *Int. J. Numer. Method Engg*., Vol. 56, pp. 1315-1334, 2003.

50. P. Ding and W.Q. Tao, An Inverse Analysis for the Estimation of Boundary Heat Flux in a Circular Pipe Employing the Proper Orthogonal

Decomposition, *Progress Computational Fluid Dynamics*, Vol. 9, pp. 231-246, 2009

51. X.T. Xiong, C.L. Fu and H.F. Li, Central Difference Schemes in Time and Error Estimate on a Non–Standard Inverse Heat Conduction Problem, *Appl. Math. Computation*, Vol. 157, pp. 77-91, 2004.
52. K.W. Kim, S.W. Baek, M.Y. Kim and H.S. Ryou, Estimation of Emissivities in a Two-Dimensional Irregular Geometry by Inverse Radiation Analysis using Hybrid Genetic Algorithm, *J. Quant. Spectrosc. Radiat. Transfer*, Vol. 87, pp. 1-14, 2004.
53. S. Znaidia, F. Mzali, L. Sassi, A. Mhimid, A. Jemni, S. Ben Nasrallah and D. Petit, Inverse Problem in a Porous Medium: Estimation of Effective Thermal Properties, *Inv. Prob. Sci. Eng*., volume 13, pp. 581-593, 2005.
54. K.J. Daun and J.R. Howell, Inverse Design Methods for Radiative Transfer Systems, *J. Quant. Spectrosc. Radiat. Transfer*, Vol. 93, pp. 43-60, 2005.
55. J. Wang and N. Zabaras, Using Bayesian Statistics in the Estimation of Heat Source in Radiation, *Int. J. Heat and Mass Transfer*, Vol. 48, pp. 15-29, 2005.
56. M. Deiveegan, C. Balaji and S.P. Venkateshan, Comparison of Various Methods for Simultaneous Retrieval of Surface Emissivities and Gas Properties in Gray Participating Media, *J. Heat Transfer*, Vol. 128, pp. 829-837, 2006.

57. S. Deng and Y. Hwang, Applying Neural Networks to the solution of Forward and Inverse Heat Conduction Problems, *Int. J. Heat Mass Transfer*, Vol. 49, pp. 4732-4750, 2006.

58. F. H. R. Franca and J. R. Howell, Transient Inverse Design of Radiative Enclosures for Thermal Processing of Materials, *Inv. Prob. Sci. Eng.*, vol. 14, pp. 423-436, 2006.

59. K.W. Kim and S.W. Baek, Inverse Radiation-Conduction Design Problem in a Participating Concentric Cylindrical Medium, *Int. J. Heat Mass Transfer*, Vol. 50, pp. 2828-2837, 2007.

60. Wei Cheng, Chu-Li Fu and Zhi Qian, A modified Tikhonov regularization method for a spherically symmetric three-dimensional inverse heat conduction problem, *Math. Computers Simulation*, Vol. 75, pp. 97-112, 2007.

61. S. Verma and C. Balaji, Multi-Parameter Estimation in Combined Conduction-Radiation from a Plane Parallel Participating Medium using Genetic Algorithms, *Int. J. Heat Mass Transfer*, Vol. 50, pp. 1706-1714, 2007.

62. H. Qi, L.M. Ruan, H.C. Zhang, Y.M. Wang and H.P. Tan, Inverse Radiation Analysis of a One-Dimensional Participating Slab by Stochastic Particle Swarm Optimizer Algorithm, *Int. J. Thermal Sci.*, Vol. 46, pp. 649-661, 2007.

63. F.B Liu, A Modified Genetic Algorithm for Solving the Inverse Heat Transfer Problem of Estimating Plan Heat Source, *Int. J. Heat Mass Transfer*, Vol. 51, pp. 3745-3752, 2008.

64. D. Slota, Using Genetic Algorithms for the Determination of an Heat Transfer Coefficient in Three-Phase Inverse Stefan Problem, *Int. Comm. Heat Mass Transfer*, Vol. 35, pp. 149-156, 2008.

65. S. Parthasarathy and C. Balaji, Estimation of Parameters in Multi-Mode Heat Transfer Problems using Bayesian Inference – Effect of Noise and a Priori, *Int. J. Heat Mass Transfer*, Vol. 51, pp. 2313-2334, 2008.

66. W.H. Sutton, A Short Time Solution for Coupled Conduction and Radiation in a Participating Slab Geometry, *J. Heat Transfer*, Vol. 108, pp. 465–466, 1986.

67. J.H. Tsai and J.D. Lin, Transient Combined Conduction and Radiation with Anisotropic Scattering, *J. Thermophys. Heat Transfer*, Vol. 4, pp. 92–97, 1990.

68. P. Talukdar and S.C. Mishra, Analysis of Conduction and Radiation Heat Transfer with Heat Generation in Participating Medium Using the Collapsed Dimension Method, *Numer. Heat Transfer, A*, Vol. 39, pp. 79–100, 2001.

69. P. Talukdar and S. C. Mishra, Transient Conduction and Radiation Heat Transfer with Variable Thermal Conductivity, *Numer. Heat Transfer, A*, Vol. 41, pp. 851-867, 2002.

70. H. S. Chu and C. J. Tseng, Thermal Performance of Ultra-Fine Powder Insulation at High Temperatures, *J. Building Phys.*, Vol. 12, pp. 298-312, 1989.

71. H. S. Chu and C. J. Tseng, Conduction-Radiation Interaction in Absorbing, Emitting, and Scattering Media with Variable Thermal Conductivity, *J. Thermophys. Heat Transfer*, Vol. 6, pp. 537-540, 1992.

72. C.Y. Wu and N.R. Ou, Transient Two-Dimensional Radiative and Conductive Heat Transfer in a Scattering Medium, *Int. J. Heat Mass Transfer*, 37, 2675-2686, 1994.

73. W.W. Yuen and E.E. Takara, Analysis of Combined Conductive-Radiative Heat Transfer in a Two-Dimensional Rectangular Enclosure with a Gray Medium, *J. Heat Transfer*, 110, 468-474, 1988.

74. S.C. Mishra, P. Talukdar, D. Trimis and F. Durst, Computational Efficiency Improvements of the Radiative Transfer Problems with or without Conduction – a Comparison of the Collapsed Dimension Method and the Discrete Transfer Method, *Int. J. Heat Mass Transfer*, 46, 3083-3095, 2003.

75. F. Asllanaj, G. Jeandel, J. R. Roche and D. Lacroix, Transient Combined Radiation and Conduction Heat Transfer in Fibrous Media with Temperature and Flux Boundary Conditions, *Int. J. Thermal Sci.*, Vol. 43, pp. 939-950, 2004.

76. S.C. Mishra, P. Talukdar, D. Trimis, F. Durst, Two-Dimensional Transient Conduction and Radiation Heat Transfer with Temperature Dependent

Thermal Conductivity, *Int. J. Heat Mass Transfer*, Vol. 32, pp. 305-314, 2005.

77. C. Cattaneo, A Form of Heat Conduction Equation which Eliminates the Paradox of Instantaneous Propagation, *Comput Rendus.*, Vol. 431-433, 1958.
78. P. Vernotee, Les Paradoxes de la Theorie Continue de 1 equation del la Chaleur. *Comput Rendus*., Vol. 246, pp. 3154-3155, 1958.
79. M.N. Ozisik, D.Y. Tzou, On the Wave Theory in Heat Conduction. *J. Heat Transfer*, Vol. 116, pp. 526-535, 1994.
80. K. Mitra, S. Kumar, A. Vedavarz, M.K Moallemi., Experimental Evidence of Hyperbolic Heat Conduction in Processed Meat, *J. Heat Transfer*, Vol. 117, pp. 568-573, 1995.
81. Z.S. Deng and J. Liu, Non-Fourier Heat Conduction Effect on Prediction of Temperature Transients and Thermal Stress in Skin Cryopreservation, *J. Therm. Stress*, Vol. 26, pp. 779-798, 2003.
82. P.J. Antaki, New Interpretation of Non-Fourier Heat Conduction in Processed Meat, *J. Heat Transfer*, Vol. 127, pp. 189-2003, 2005.
83. F. Xu, K.A Seffen, T.J. Lu, Non-Fourier Analysis of Skin Biothermomechanics, *Int. J. Heat Mass Transfer*, Vol. 51, pp. 2237-2259, 2008.
84. L.H. Liu, H.P. Tan and T.W. Tong, Non-Fourier Effects on Transient Temperature Response in Semi Transparent Medium caused by Laser Pulse, *Int. J. Heat Mass Transfer*, Vol. 44, pp. 3335-3344, 2001.

85. H.S. Chu, S. Lin, C.H. Lin, On Non-Fourier Heat Conduction with Radiation in an Absorbing, Emitting, and Isotropically Scattering Medium, *J. Quant. Spectrosc. Radiat. Transfer*, Vol. 73, pp. 571-582, 2002.

86. Y. Chou and R.J. Yang, Application of CESE Method to Simulate Non-Fourier Heat Conduction in Finite Medium with Pulse Surface Heating, *Int. J. Heat Mass Transfer*, Vol. 51, pp. 3525-3534, 2008.

87. Y.Po Chang and R.S. Smith Jr., Steady and Transient Heat Transfer by Radiation and Conduction in a Medium Bounded by Two Coaxial Cylindrical Surfaces, Int. *J. Heat Mass Transfer*, Vol. 13, pp. 69-80, 1970.

88. R. Fernandes and J. Francis Combined Conductive and Radiative Heat Transfer in an Absorbing, Emitting, and Scattering Cylinder Medium, *J. Heat Transfer*, Vol. 104, pp. 594–601, 1982.

89. R. Martins S. da Gama, Numerical Simulation of the (Nonlinear) Conduction/Radiation Heat Transfer Process in a Nonconvex and Black Cylindrical Body, *J. Computational Phys*., Vol. 128, pp. 341-350, 1996.

90. C. K. Krishnaprakas, Combined Conduction and Radiation Heat Transfer in a Cylindrical Medium, *J. Thermophys. Heat Transfer*, Vol. 12, pp. 605-608, 1998.

91. D. Rivas, R. Haya, A Conduction–Radiation Model for the Floating-Zone Technique in Monoellipsoidal Mirror Furnaces, *J. Crystal Growth*, Vol. 206, pp. 230-240, 1999.

92. N. Aouled-Dlala, T. Sghaier, E. Seddiki, Numerical Solution of Radiative and Conductive Heat Transfer in Concentric Spherical and Cylindrical Media, *J. Quant. Spectrosc. Radiat. Transfer*, Vol. 107, pp. 443-457, 2007.

93. E.H. Chui, G.D. Raithby and P.M. Hughes, Prediction of Radiative Transfer in Cylindrical Enclosures with the Finite Volume Method. *J. Thermophys. Heat Transfer*, Vol. 6 4, pp. 605–611, 1992.

94. S.W. Baek and M.Y. Kim, Modification of the Discrete Ordinates Method in an Axisymmetric Cylindrical Geometry. *Numer. Heat Transfer, B,* Vol. 31 pp. 313–326, 1997.

95. M. Ben Salah, F. Askri, K. Slimi and S. Ben Nasrallah, Numerical Resolution of the Radiative Transfer Equation in a Cylindrical Enclosure with the Finite-Volume Method, *Int. J. Heat Mass Transfer*, Vol. 47, pp. 2501-2509, 2004.

96. P. Dutta and K N. Seetharamu, Free Convection in a Saturated Porous Medium Adjacent to a Vertical Impermeable Wall subjected to a Non-uniform Heat Flux, *Int. J. Heat Mass Transfer*, Vol. 28, pp. 27-32, 1993.

97. S. Chakraborty, Analytical Solutions of Nusselt Number for Thermally Fully Developed Flow in Microtubes under a Combined action of Electroosmotic Forces and Imposed Pressure Gradients, *Int. J. Heat Mass Transfer*, Vol. 49, pp. 810-813, 2006.

98. C.Hong, Y. Asako, Heat Transfer Characteristics of Gaseous Flows in Microtube with Constant Heat Flux, *Appl. Thermal Eng*., Vol. 28, pp. 1375-1385, 2008.

99. Fernandes and J. Francis, Finite Element Analysis of Planer Conductive and Radiative heat transfer with flux boundary. In Paper No. 82-0910, 3rd AIAA/ASME Joint Thermophysics, Fluids, *Plasma and Heat Transfer Conf*., Saint Louis, MO, June 7-11,1992.

100. J. D. Lin and J. H. Tsai, Radiation-conduction interaction in a planer, anisotropically scattering medium with flux boundary. *Numer. Heat Transfer, A*, Vol. 16, pp. 119-128, 1989.

101. M.F. Modest, *Radiative Heat Transfer*, 2nd ed., Academic Press, New York, 2003.

102. R. Siegel and J.R Howell, *Thermal Radiation Heat Transfer*, 4th ed., Taylor and Francis, 2002.

103. P. J. Coelho and M. G. Carvalho, A Conservative Formulation of the Discrete Transfer Method, *J. Heat Transfer*, Vol. 119, pp. 118–128, 1997.

104. K.A.R Ismail, C.S Salinas, Application of Multidimensional Scheme and the Discrete Ordinate Method to Radiative Heat Transfer in a Two-Dimensional Enclosure with Diffusely Emitting and Reflecting Boundary Walls, *J. Quant. Spectrosc. Radiat. Transfer*, Vol. 88, pp. 407-422, 2004.

105. K. F. Evans, Two-Dimensional Radiative Transfer in Cloudy Atmospheres: The Spherical Harmonic Spatial Grid Method, *J. Atmos. Sci.*, Vol. 50, pp. 3111-3124, 1993.

106. S Wolf, T Henning, B Stecklum, Multidimensional Self-Consistent Radiative Transfer Simulations based on the Monte-Carlo Method, *Astronomy and Astrophys.*, Vol. 349, pp. 839-850, 1999.

107. J.C. Chai and S.V. Patankar, Finite Volume Method for Radiation Heat Transfer, *Adv. Numer. Heat Transfer*, Vol. 2, pp. 110-135, 2000.

108. J. C. Chai, G. Parthasarathy, H. O. Lee, S.V. Patankar, Finite Volume Radiative Heat Transfer Procedure for Irregular Geometries, *J. Thermophys. Heat Transfer*, Vol. 9, pp. 410-415, 1995.

109. G.D. Raithbay and E.H. Chui, A Finite Volume Method for Predicting Radiant Heat Transfer in Enclosures with Participating Media, *J. Heat Transfer*, Vol. 112, pp. 415-423, 1990.

110. J.Y. Murthy and S. R. Mathur, Finite Volume Method for Radiative Heat Transfer using Unstructured Meshes, *J. Thermophys. Heat Transfer*, Vol. 12, pp. 312- 321, 1998.

111. C. K Krishnaprakas, B. K. Narayana, and P. Dutta, Use of GCG Methods for the Efficient Solution of Matrix Problems Arising from the FVM Formulation of Radiative Transfer, *Numerical Heat Transfer, B*, Vol. 40, pp. 515-533, 2001.

112. A.R Mitchell and D.F Griffiths, *The Finite Difference Method in Partial Differential Equations*, Wiley-Interscience Publication, Chichester, Wiley, 1980.

113. C Johnson, *Numerical Solution of Partial Differential Equations by the Finite Element Method*, Cambridge Univ. Press, 1987.

114. S.V. Patankar, *Numerical Heat Transfer, Hemisphere,* Washington DC, 1980.

115. P.L. Bhatanagar, E.P. Gross and M. Krook, A model for Collusion Process in Gases. I. Small Amplitude Processes in Charged and Neutral One-Component Systems, *Phys. Rev.,E*, Vol. 94, pp. 511-525, 1954.

116. S. Succi, *The Lattice Boltzmann Method for Fluid Dynamics and Beyond*, Oxford University Press, New York, 2001.

117. J.R. Ho, C.P. Kuo, W.S Jiaung, C.J. Twu, Lattice Boltzmann Scheme for Hyperbolic Heat Conduction, *Numer. Heat Transfer, B,* vol. 41, pp. 591-607, 2002.

118. S.C. Mishra and A. Lankadasu, Analysis of Transient Conduction and Radiation Heat Transfer using the Lattice Boltzmann Method and the Discrete Transfer Method, *Numer. Heat Transfer, A,* Vol. 47, 935-954, 2005.

119. S.C. Mishra, A. Lankadasu and K. Beronov, Application of the Lattice Boltzmann Method for Solving the Energy Equation of a 2-D Transient Conduction-Radiation Problem, *Int. J. Heat Mass Transfer*, Vol. 48, pp. 3648-3659, 2005.

120. S.C. Mishra and H.K. Roy, Solving Transient Conduction-Radiation Problems using the Lattice Boltzmann Method and the Finite Volume Method, *J. Comput. Phys.*, vol. 223, 89-107, 2007.

121. G.H. Tang, W.Q. Tao and Y.L. He, Thermal Boundary Condition for the Thermal Lattice Boltzmann Equation, *Physical Review, E*, Vol. 72, pp. 016703, 2005.

122. S. Chakraborty and D. Chatterjee, An Enthalpy based Hybrid Lattice Boltzmann Method for Modeling Solid-Liquid Phase Transition in Presence of Convective Transport, *J. Fluid Mechanics*, Vol. 592, 155-175, 2007.

123. S.C. Mishra, T.B. Pavan Kumar and B. Mondal, Lattice Boltzmann Method Applied to the Solution of Energy Equation of a Radiation and Non-Fourier Heat Conduction Problem, *Numer. Heat Transfer, A*, Vol. 54, pp. 798-818, 2008.

124. J.R Ho, C.P Kuo, W.S Jiaung, C.J Twu, Lattice Boltzmann Scheme for Hyperbolic Heat Conduction Equation, *Numer. Heat Transfer, B*, Vol. 41, pp. 591-607, 2002.

125. G.H Tang, W.Q Tao and Y.L He, Lattice Boltzmann Method for Gaseous Microflows using Kinetic Theory Boundary Conditions, *Phys. Fluids*, Vol. 17, pp. 058101, 2005

126. W.S Jiaung and J.R Ho, Lattice Boltzmann Study on Size Effect with Geometrical Bending on Phonon Heat Conduction in a Nanoduct, *J. Applied Phys.*, Vol. 95, pp. 958, 2004

127. C.H Wang, J.R Ho, Lattice Boltzmann Modeling of Bingham Plastics, *Physica A: Stat. Mech. Appl.*, Vol. 387, pp. 4740-4748, 2008.

128. A. Kumar and S. Chakraborty and N. Chakrabarti, Fluid Flow in a Tundish Optimized through Genetic Algorithms, *Steel Research Int.*, Vol. 78, pp. 517-521, 2007.

129. A. Mukherjee, R. Biswas, , K. Deb and A.P. Mathur,. Multi-Objective Evolutionary Algorithms for the Risk-Return Trade-Off in Bank Loan Management. *Int. Trans. Operations Research*, Vol. 9, pp. 583-597, 2002.

130. T. Banerjee, M..K.Singh, A. Khanna, Genetic Algorithm to Estimate Interaction Parameters of Multicomponent Systems for Liquid–Liquid Equilibria, *Computers and Chem. Eng*., Vol.29, pp. 1712-1719, 2005.

131. K. Sivakumar, N. G. R. Iyengar, and K. Deb, Optimum Design of Laminated Composite Plates with Cutouts Undergoing Large Amplitude Oscillation, *Adv. Composite Materials*, Vol. 8, pp. 295-316, 1999.

132. K. Deb, and A. Kumar, Real-Coded Genetic Algorithms with Simulated Binary Crossover, Studies on Multimodal and Multiobjective Problems, *Complex Sys.*, Vol. 9, pp. 431-454.

133. D. E. Goldberg, B. Korb, and K. Deb, Messy Genetic Algorithms: Motivation, Analysis and First Results, *Complex Sys.*, Vol. 3, pp. 493-530, 1989.

134. A. Corana, M. Marchesi, C. Martini, S. Ridella, Minimizing Multimodal Functions of Continuous Variables with the “Simulated Annealing” Algorithm, *ACM Transactions on Mathematical Software* (TOMS), Vol. 13, pp. 262-280, 1987.

135. H. Czu, Fast Simulated Annealing, *AIP Conference Proceedings*, Vol. 151, pp. 420-425, 1986.

136. A. El-Bouri, N. Azizi, and S. Zolfaghar**,** A Comparative Study of a New Heuristic based on Adaptive Memory Programming and Simulated Annealing: The case of Job Shop Scheduling, *European J. Operation Research*, Vol. 177, pp. 1894-1910, 2007.

137. F.-D Chou, H. M Wang, P.C. Chang, A Simulated Annealing Approach with Probability Matrix for Semiconductor Dynamic Scheduling Problem, *Expert Systems with Applications*, Vol. 35, pp. 1889-1898, 2008.

138. S. Sitarz, Ant Algorithms and Simulated Annealing for Multicriteria Dynamic Programming, *Computers & Operations Research*, Vol.36, pp. 433-441, 2009.

139. Y. Shi and R. C. Eberhart, Parameter Selection in Particle Swarm Optimization, *Lecture Notes in Comp. Sc.*,Vol. 1447, pp. 591-600, 2006.

140. F. van den Bergh and A.P. Engelbrecht, Effects of Swarm Size on Cooperative Particle Swarm Optimizers, Proceedings of the Genetic and *Evolutionary Computation*, 2001.

141. F. van den Bergh and A.P. Engelbrecht, A Cooperative Approach to Particle Swarm Optimization, *Evolutionary Computation*, Vol. 8, pp. 225-239, 2004.

142. J. Kennedy, Stereotyping: Improving Particle Swarm Performance with Cluster Analysis, Proceedings of the 2000 Congress on Evolutionary Computation, Ja Jolla, CA, USA, Vol. 2, pp. 1507-1512, 2000.

143. L. S. Coelho, C. A. Sierakowski, A Software Tool for Teaching of Particle Swarm Optimization Fundamentals, *Adv. Eng. Software*, Vol. 39, pp. 877-887, 2008.

144. A.A. El-Ela, T. Fetouh, M.A. Bishr, R.A.F. Saleh, Power Systems Operation using Particle Swarm Optimization Technique, *Electric Power Systems Research*, Vol. 78, pp. 1906-1913, 2008.

145. D.S. Liu, K.C. Tan, S.Y. Huang, C.K. Goh, W.K. Ho, On Solving Multiobjective Bin Packing Problems using Evolutionary Particle Swarm Optimization, *European J. Operational Research*, Vol. 190, pp. 357-382, 2008.

146. R. Battiti, G. Tecchiolli, Training Neural Nets with the Reactive Tabu Search, *IEEE Transactions on Neural Networks*, Vol. 6, pp. 1185-1200, 1995.

147. B. Lin, DC Miller, Solving Heat Exchanger Network Synthesis Problems with Tabu Search, *Computers and Chemical Engineering*, Vol. 28, pp. 1451-1464, 2004.

148. L. Cavin, U. Fischer, F. Glover and K. Hungerbühler**,** Multi-Objective Process Design in Multi-Purpose Batch Plants using a Tabu Search Optimization Algorithm, *Computers and Chemical Engineering*, Vol.28, pp. 459-478, 2004.

149. D.E Glass, M.N Ozisik, D.S McRae, Hyperbolic Heat Conduction with Radiation in an Absorbing and Emitting Medium, *Numer. Heat Transfer, A*, Vol. 12, pp. 321-333, 1987.

150. S. H. Jacobson, L. A. McLay, Applying Statistical Tests to Empirically Compare Tabu Search Parameters for MAX 3-SATISFIABILITY: A Case Study, *Omega*, Vol. 37, pp. 522-534, 2009.

151. R.A. Walker II, C. J. Colbourn, Tabu Search for Covering Arrays using Permutation Vectors, *J. Statistical Planning Inference*, Vol. 139, pp. 69-80, 2009.

152. T.l Öncan, J.F Cordeau, G. Laporte, A Tabu Search Heuristic for the Generalized Minimum Spanning Tree Problem, *European J. Operational Research*, Vol. 191, pp. 306-319, 2008.

153. H.S. Wang, A Two-Phase Ant Colony Algorithm for Multi-Echelon Defective Supply Chain Network Design, *European J. Operational Research*, Vol.192, pp. 243-252, 2009.

154. C. Solnon, Combining Two Pheromone Structures for Solving the Car Sequencing Problem with Ant Colony Optimization, *E. J. Operational Research*, Vol. 191, pp. 1043-1055, 2008.

155. W.H. Liao, Y.Kao, C.M. Fan, Data Aggregation in Wireless Sensor Networks using Ant colony Algorithm, J. *Network Computer Applications*, Vol. 31, pp. 387-401, 2008.

156. K. C. Abbaspour, R. Schulin, M. Th. Genuchten, Estimating Unsaturated Soil Hydraulic Parameters using Ant Colony Optimization, *Advances in Water Resources*, Vol. 24, pp. 827-841, 2001.

157. R.P. Souto, H. F. Campos Velho, S. Stephany, Reconstruction of Vertical Profiles of the Absorption and Scattering Coefficients from Multispectral Radiances, *Math. Computers in Simulation*, Vol. 73, pp. 255-267, 2006.

158. P. Talukdar, *Combined radiation, Conduction and/or Convection Heat Transfer in Participating Media*, PhD thesis, Indian Institute of Technology Guwahati, India, 2004.

159. S. Rooseland, *Theoretical Astrophysics; Atomic Theory and the Analysis of Steller Atmosphere and Envelopes*, Clarendon Press, Oxford, 1936.

160. H.C. Hottel and E.S. Cohen, Radiant Heat Exchange in a Gas Filled Enclosure: Allowance for Non-Uniformity of Gas Temperature, *AIChE Journal*, Vol. 4, pp. 3-14, 1958.

161. J. A. Fleck, The Calculation of Non-Linear Radiation Transport by a Monte Carlo Method: Statistical Physics, *Methods in Comput. Phys*., Vol. 1, pp. 43-65, 1961.

162. T. M. Shih and Y.N. Chen, A Discretized Intensity Method proposed for Two-dimensional Systems enclosing Radiative and Conductive Media, *Numer. Heat Transfer, A*, Vol. 6, pp. 117-134, 1983.

163. F.A. Milne, *Thermodynamics of Stars, Handbook of Astrophysics*, Springer-Verlag, OHG, Berlin, pp. 65-225, 1930.

164. V. Kourganoff, *Basic Methods in Transfer Problems*, Dover Publications, New York, 1963.

165. J. C. Chai, H. S. Lee, S. V. Patankar, Treatment of Irregular Geometries using a Cartesian Coordinates Finite-Volume Radiation Heat Transfer Procedure, *Numer. Heat Transfer, B,* Vol. 26, pp. 225-235, 1994.

166. B. Mondal, *Application of the Lattice Boltzmann Method in Solving Energy Equations of Heat Transfer Problems involving Thermal Radiation*, PhD thesis, Indian Institute of Technology Guwahati, India, 2008.

167. P. Mahanta and S.C. Mishra, Collapsed Dimension Method applied to Radiative Transfer Problems in Complex Enclosures with Participating Medium, *Numer. Heat Transfer, B,* Vol. 42, pp. 367-380, 2002.

LIST OF PUBLICATIONS FROM THE WORK

International Journals:

1. R. Das, S.C. Mishra and R. Uppaluri, Multi-parameter estimation in a transient conduction-radiation problem using the lattice Boltzmann method and the finite volume method coupled with the genetic algorithms, *Numerical Heat Transfer, Part A, 53, 1321-1338, 2008.*

2. R. Das, S.C. Mishra, M. Ajith and R. Uppaluri, An inverse analysis of a transient 2-D conduction-radiation problem using the lattice Boltzmann method and the finite volume method coupled with the genetic algorithm, *Journal of Quantitative Spectroscopy and Radiative Transfer, 109, 2060-2077, 2008.*

3. R. Das, S.C. Mishra and R. Uppaluri, Simultaneous reconstruction of thermal field and retrieval of parameters in a cylindrical enclosure, *Numerical Heat Transfer, Part A, 54, 983-998, 2008.*

4. R. Das, S.C. Mishra and R. Uppaluri, Retrieval of thermal properties in a transient conduction-radiation problem with variable thermal conductivity, *International Journal of Heat and Mass Transfer, 52, 2749-2758, 2009.*

5. S.C. Mishra, M.Y. Kim, R. Das, M. Ajith and R. Uppaluri, Lattice Boltzmann method applied to the analysis of transient conduction-radiation problem in a cylindrical medium, *Numerical Heat Transfer, Part A, 56, 42-59, 2009.*

6. R. Das, S.C. Mishra and R. Uppaluri, Inverse analysis applied to retrieval of parameters and reconstruction of temperature field in a transient conduction-radiation heat transfer problem involving mixed boundary conditions, *International Communications in Heat and Mass Transfer, 37, 52 – 57, 2010.*

7. M. Ajith, R. Das, R. Uppaluri and S.C. Mishra, Optimization of heat fluxes on the heater and the design surfaces of a radiating-conducting medium, *Numerical Heat Transfer, Part A, 56, 846 – 860.*

8. R. Das, S. C. Mishra, T.B. Pavan Kumar and R. Uppaluri, An Inverse analysis for parameter estimation applied to a non-Fourier conduction-radiation problem, *Heat Transfer Engineering (revised manuscript submitted), 2010.*